QUALITATIVE AND QUANTITATIVE TECHNICAL CRITERIA FOR DETERMINING THE MINIMUM MISCIBILITY PRESSURES FROM FOUR EXPERIMENTAL METHODS

A Thesis
Submitted to the Faculty of Graduate Studies and Research
In Partial Fulfillment of the Requirements
For the Degree of

Master of Applied Science
in
Petroleum Systems Engineering
University of Regina

By
Kaiqiang Zhang
Regina, Saskatchewan
April 2016

UNIVERSITY OF REGINA

FACULTY OF GRADUATE STUDIES AND RESEARCH

SUPERVISORY AND EXAMINING COMMITTEE

Kaiqiang Zhang, candidate for the degree of Master of Applied Science in Petroleum Systems Engineering**,** has presented a thesis titled, ***Qualitative and Quantitative Technical Criteria for Determining the Minimum Miscibility Pressures from Four Experimental Methods,*** in an oral examination held on April 7, 2016. The following committee members have found the thesis acceptable in form and content, and that the candidate demonstrated satisfactory knowledge of the subject material.

External Examiner:	Dr. Amr Henni, Industrial Systens Engineering
Supervisor:	Dr. Yongan Gu, Petroleum Systems Engineering
Committee Member:	Dr. Fanhua Zeng, Petroleum Systems Engineering
Committee Member:	Dr. Amy Veawab, Environmental Systems Engineering
Chair of Defense:	Dr. Nader Mobed, Department of Physics

ABSTRACT

In this study, several qualitative and quantitative technical criteria are examined/developed and applied to determine the minimum miscibility pressures (MMPs) of different light crude oil–CO_2 systems from four experimental methods, i.e., the slim-tube tests, coreflood tests, rising-bubble apparatus (RBA), and vanishing interfacial tension (VIT) technique.

First, five slim-tube tests with the live light crude oil–CO_2 system and five coreflood tests with the dead light crude oil–CO_2 system are conducted at different injection pressures and the actual reservoir temperature of T_{res} = 53.0°C. It is found that different MMPs can be obtained from the same measured oil recovery factor (ORF) vs. injection pressure data if different MMP criteria, regression methods, and threshold values or intersection options are adopted. Thus the determined MMP is better given in a small pressure range than specified as a definitive pressure value. By means of the ORF and break-over pressure (BOP) criteria, two MMP ranges of the live and dead light crude oil–CO_2 systems are determined to be 15.2–15.4 MPa from the slim-tube tests and 12.4–12.9 MPa from the coreflood tests at T_{res} = 53.0°C, respectively.

Second, two separate series of pure and impure CO_2-bubble tests in a light crude oil column with the RBA are conducted at six different test pressures and T_{res} = 53.0°C. The MMPs of the light crude oil–pure and impure CO_2 systems are estimated and compared by using four existing (i.e., the bubble shape, size, colour, and rising height) and new bubble break-up (BBU) qualitative criteria with the RBA. It is found that the BBU criterion is consistent with the four existing qualitative criteria for estimating the MMPs. Furthermore, by means of newly developed bubble-rising height (BRH) and bubble-

rising velocity (BRV) quantitative criteria, two respective MMP ranges of the light crude oil–pure and impure CO_2 systems are found to be 11.7–12.4 MPa and 23.4–23.5 MPa at T_{res} = 53.0°C.

Third, six series of the dynamic interfacial tension (IFT) tests for the dead and live light crude oil–CO_2 systems are conducted under different test conditions. Two new linear correlation coefficient (LCC) and critical interfacial thickness (CIT) technical criteria are developed to determine the MMP when the LCC is smaller than 0.990 or the interfacial thickness is smaller than 1.0 nm for the first time. The determined MMPs of 12.9 MPa and 13.2 MPa for the dead and live light crude oil–CO_2 systems from the VIT technique by using the two new criteria agree well with 12.4–12.9 MPa for the former system from the coreflood tests but poorly with 15.2−15.4 MPa for the latter system from the slim-tube tests. In addition, the specific effects of three important experimental factors on the determined MMPs are studied by using the two new technical criteria: the initial vs. equilibrium IFTs, oil composition, and initial gas−oil ratio (GOR) in volume. It is found that the measured initial rather than equilibrium IFTs are accurate enough to determine the MMP from the VIT technique. The live light crude oil pre-saturated with CH_4-dominated hydrocarbons has a slightly increased MMP, in comparison with the dead light crude oil. Moreover, the initial GOR effect on the MMP is found to be negligible in a lower GOR range (1:1−10:1 in volume) or in a large CO_2 concentration range (31.76–94.69 mol.%). It becomes pronounced in a higher GOR range (200:1–4000:1 in volume) or in an extremely small range of high CO_2 concentrations (98.79–99.99 mol.%).

ACKNOWLEDGMENTS

I wish to acknowledge the following individuals and organizations:

- Dr. Yongan (Peter) Gu, my academic advisor, for his excellent guidance, valuable advice, strong support, and continuous encouragement throughout the course of this study;
- My past and present research group members for their useful technical discussions and assistances during my Master's program;
- My thesis defense committee members;
- PennWest Exploration for the industrial Research and Development (R&D) fund to Dr. Yongan (Peter) Gu;
- Petroleum Technology Research Centre (PTRC) for the Innovation Fund to Dr. Yongan (Peter) Gu;
- Natural Sciences and Engineering Research Council (NSERC) of Canada for the Discovery Grant and the Collaborative Research and Development (CRD) Grant to Dr. Yongan (Peter) Gu;
- Faculty of Graduate Studies and Research (FGSR) at the University of Regina for awarding the Graduate Studies Scholarships;
- Saskatchewan Research Council (SRC) for conducting five slim-tube tests; Ms. Meng Cao for conducting five coreflood tests and three pressure-volume-temperature (PVT) tests; Mr. Tyson Affleck, Mr. Bryan Ruther, and Mr. Weiguo Luo for conducting two series of the rising-bubble apparatus (RBA) tests; Mr. Pengcheng Hou and Mr. Weiguo Luo for conducting one series of the dynamic interfacial tension (IFT) tests (Test #6) at the University of Regina.

DEDICATIONS

To my parents and wife, for their unconditional love, caring, and support.

TABLE OF CONTENTS

LIST OF TABLES

LIST OF FIGURES

NOMENCLATURE

Notations

d	Diameter of the slim tube, cm
D	Diameter of the core plugs, in
k	Permeability, mD
L	Length of the composite reservoir core plugs, in
L	Length of the slim tube or flat glass tube, cm
MMP	Minimum miscibility pressure, MPa
MW	Molecular weight, g/mol
MW_{oil}	Molecular weight of the original dead light crude oil, g/mol
ORF	Oil recovery factor, %
P	Test pressure, MPa
P_{CH_4}	CH_4 injection pressure, MPa
P_{CO_2}	CO_2 injection pressure, MPa
P_{inj}	Injection pressure of the slim-tube and coreflood tests, MPa
P_{max}	Maximum operating pressure, MPa
P_{mix}	Mixture pressure, MPa
P_{sat}	Saturation pressure, MPa
q_{brine}	Brine injection rate, cm^3/min
q_{CO_2}	CO_2 injection rate, cm^3/min
q_{oil}	Oil injection rate, cm^3/min

R^2	Linear correlation coefficient
R_c^2	Critical value of the linear correlation coefficient
S_{oi}	Residual oil saturation, %
S_{wc}	Connate water saturation, %
SF	Oil-swelling factor
t	Time, s
T	Temperature, °C
T_{lab}	Laboratory temperature, °C
T_{res}	Reservoir temperature, °C
v_m	Mass-based specific volume, cm^3/g
V_{oil}	Oil volume at 1 atm and a pre-specified temperature, cm^3
w_{asp}	Asphaltene content (*n*-pentane insoluble), wt.%
z_{CO_2}	CO_2 concentration, mol.%

Greek letters

ΔP	Differential pressure between the inlet and outlet of the slim tube/coreholder during the oil injection process prior to CO_2 flooding, MPa
Δt	Time difference, s
γ	Dynamic Interfacial tension between the light crude oil drop and CO_2, mJ/m^2
γ_{eq}	Equilibrium interfacial tension between the light crude oil drop and CO_2, mJ/m^2

γ_{in}	Initial interfacial tension between the light crude oil drop and CO_2, mJ/m^2
μ_{oil}	Viscosity of the original dead crude oil, cP
ρ_{CO_2}	Density of CO_2, g/cm^3
ρ_{oil}	Density of the original dead crude oil, g/cm^3
ϕ	Porosity, %
χ_{CO_2}	CO_2 solubility in the original dead crude oil, wt.%
δ	Interfacial thickness, nm
δ_c	Critical interfacial thickness, nm
ω	Pitzer acentric factor

Subscripts

asp	Asphaltenes
brine	Brine
c	Critical
cell	IFT cell
CH_4	Methane
C_2H_6	Ethane
C_3H_8	Propane
C_8H_{18}	Octane
$C_{10}H_{22}$	Decane
$C_{18}H_{38}$	Octadecane
CO_2	Carbon dioxide
eq	Equilibrium

gas	Gas
HC	Hydrocarbon
in	Initial
inj	Injection
lab	Laboratory
m	Mass
max	Maximum
N_2	Nitrogen
oi	Initial oil
oil	Oil
res	Reservoir
sat	Saturation
w	Water
wc	Connate water

Acronyms

ADSA	Axisymmetric drop shape analysis
BBU	Bubble break-up
BOP	Break-over pressure
BOPD	Barrel of oil per day
BPR	Back-pressure regulator
BRH	Bubble-rising height
BRV	Bubble-rising velocity

BT	Breakthrough
CIT	Critical interfacial thickness
CMG	Computer modelling group
EOR	Enhanced oil recovery
EOS	Equation of state
FCM	First-contact miscibility
FGSR	Faculty of Graduate Studies & Research
GC	Gas chromatography
GOR	Gas–oil ratio
HC	Hydrocarbon
IEA	International Energy Agency
IFT	Interfacial tension
LCC	Linear correlation coefficient
MCM	Multi-contact miscibility
MMP	Minimum miscibility pressure
NSERC	Natural Sciences and Engineering Council of Canada
OOIP	Original oil-in-place
ORF	Oil recovery factor
P-1-D	Poly (1-decane)
P–R	Peng–Robinson
PTRC	Petroleum Technology Research Centre
PV	Pore volume
PVEE	Poly (vinyl ethyl ether)

PVT	Pressure–volume–temperature
RBA	Rising-bubble apparatus
R&D	Research and Development
SG	Specific gravity
SRC	Saskatchewan Research Council
TDS	Total dissolved solids
USA	United States of America
VIT	Vanishing interfacial tension

CHAPTER 1 INTRODUCTION

1.1 CO_2-Enhanced Oil Recovery (CO_2-EOR)

Enhanced oil recovery (EOR) processes have become increasingly important to the oil industry [Watkins and Sharp, 1985; Cao, 2012]. After the primary and secondary oil recovery, a typical residual oil saturation in a light or medium oil reservoir is still in the range of 50–60% of the original oil-in-place (OOIP) [Moritis, 2006]. Since the 1950s [Whorton *et al.*, 1952], a number of laboratory [Holm and Josendal, 1974; Yellig and Metcalfe, 1980] and field [Brock and Bryan, 1989; Christensen, *et al.*, 2001] studies have shown that CO_2 can be an efficient oil-displacing and oil-extracting agent under reservoir conditions. For example, a laboratory study shows that the ultimate oil recovery factor (ORF) of a CO_2 secondary flood is over 60% of the OOIP, which is substantially higher than the average ORF of 44% of the OOIP for a secondary water flood [Chung *et al*., 1988]. The major CO_2-EOR mechanisms include the miscible or immiscible displacement, interfacial tension (IFT) reduction, oil viscosity reduction, oil-swelling effect, and light-hydrocarbons (HCs) extraction by CO_2 [Stalkup, 1983; Green and Willhite, 1998; Li, 2014]. In particular, miscible CO_2 flooding has long been proven to be one of the most commonly-used and effective CO_2-EOR methods for exploiting the light and medium oil reservoirs [Folden, 1987; Ali and Thomas, 1996]. There were a total of 114 miscible and 9 immiscible ongoing CO_2-EOR projects in the USA [Kuuskraa, 2012]. In Canada, there are two commercial and ongoing miscible CO_2-EOR projects and at least four CO_2-EOR pilot tests in Alberta and Saskatchewan [Koottungal, 2012]. In 2014, the miscible CO_2-EOR processes produced 292,735 barrels of oil per day (BOPD), which

accounted for 38% of the total daily oil production of all the EOR methods and surpassed the daily oil production of any other EOR methods altogether in the USA [ABI/INFORM Global, 2014]. It is worthwhile to mention that CO_2-EOR projects not only recover the crude oil but also mitigate the greenhouse gas emissions by storing CO_2 underground [Aycaguer *et al.*, 2001]. It is estimated that CO_2-EOR projects have the potentials to recover 1.07 trillion barrels of oil and store 320 billion tonnes of CO_2 in many basins worldwide [Godec *et al.*, 2011].

1.2 Miscibility and Minimum Miscibility Pressure (MMP)

Gas injection, such as CO_2 injection [Martin and Taber, 1992], has been proven to be an effective EOR method through both laboratory [Holm and Josendal, 1974; Cao and Gu, 2013] and numerical [*et al*., 1990; Torabi *et al*., 2012] studies and also applied to many oilfields [Pyo *et al*., 2003]. The miscibility between the residual oil and the injected gas, which means that the oil and gas can be mixed together into one phase at any portions, is desired for a gas injection project [Rao and Lee, 2003]. Usually, the injected CO_2 cannot immediately achieve the so-called first-contact miscibility (FCM) with the reservoir crude oil [Stalkup, 1983]. However, it can gradually develop the so-called dynamic miscibility through the multiple contacts under the actual reservoir conditions, which is also referred to as the multi-contact miscibility (MCM) [Green and Willhite, 1998]. Correspondingly, the minimum miscibility pressure (MMP) is defined as the lowest operating pressure at which the oil and gas phases can become miscible in any portions through a dynamic MCM process at an oil reservoir temperature [Teklu *et al*., 2014].

1.3 Experimental Methods for the MMP Determinations

Accurate determination of the MMP for a given crude oil–gas (e.g., CO_2) system is required for a gas injection EOR project in an oilfield. In the literature, a number of theoretical models [Wang and Orr Jr., 1997; Jessen *et al*., 1998; Fazlali *et al*., 2013a; Fazlali *et al*., 2013b; Shorkrollahi *et al*., 2013], numerical simulations [Høier and Whitson, 2001], and experimental methods [Ayirala and Rao, 2011; Naseri *et al*., 2015] have been developed to determine the MMPs of various crude oil–CO_2 systems. In general, the experimental methods are considered to be the most accurate and reliable. There are four commonly used experimental methods to determine the MMP between the crude oil and CO_2, which include the slim-tube tests, coreflood tests, rising-bubble apparatus (RBA), and vanishing interfacial tension (VIT) technique.

The slim-tube tests have been widely accepted and used by the petroleum industry as a standard method for the MMP measurement [Yellig and Metcalfe, 1980; Dong *et al*., 2001]. The major component of the experimental setup for the slim-tube tests is a long (L = 2–40 m) but small (d = 0.1–1 cm) coiled tubing, which is packed with proper particulate materials (e.g., the Ottawa sands or glass beads) and saturated with the crude oil to be tested [Flock and Nouar, 1984]. The solvent (e.g., CO_2) is injected at different test pressures and the actual oil reservoir temperature through the long coiled slim tube to model the crude oil–gas two-phase flow through the porous medium by effectively eliminating the viscous fingering and entrance effect [Ekundayo and Ghedan, 2013]. However, the slim-tube tests are extremely expensive and time-consuming. Moreover, the measured ORFs of the slim-tube tests are also affected by several experimental factors, such as the slim-tube length and diameter, packing material, and gas injection rate, to

different extents [Ekundayo and Ghedan, 2013; Randall and Bennion, 1989]. Although the slim-tube tests have long been recognized as the petroleum industry standard method, no standard experimental design, no standard operating procedure, and no standard MMP criterion are commonly accepted and used to determine the MMP from these well-controlled idealized laboratory 1-D displacement tests [Elsharkawy *et al*, 1996]. In the literature, it was also suggested that a series of high-pressure CO_2 coreflood tests [Huang, 1992] can be conducted and used to determine the MMP, similar to the slim-tube tests. It should be noted that the actual reservoir core plugs are often used and more importantly, the connate water saturation is achieved prior to CO_2 flooding in the coreflood tests [Cao and Gu, 2013].

The RBA was invented by Christiansen and co-workers for the MMP determinations in the middle 1980s [Christiansen and Kim, 1986; Christiansen and Haines, 1987] and subsequently applied by other researchers [Mihcakan and Poettmann, 1994; Huang and Dyer, 1993]. By means of the RBA, the MMP is inferred by properly interpreting the dynamic appearance or behaviour of a gas (e.g., CO_2) bubble as it rises through a thin oil column at various test pressures and the actual reservoir temperature [Christiansen and Haines, 1987]. More recently, the VIT technique was first proposed for the MMP determination in 1997 by Rao (1997) and subsequently applied by several researchers [Rao and Lee, 2002; Wang *et al*., 2010; Naseri *et al*, 2015]. In this method, the equilibrium IFTs between the crude oil and CO_2 are accurately measured at different test pressures and the actual reservoir temperature, for example, by applying the axisymmetric drop shape analysis (ADSA) technique for the pendant drop case. Then the VIT technique is used to determine the MMP of the crude oil–CO_2 system by linearly

regressing and extrapolating the measured equilibrium IFTs vs. test pressure data to zero IFT [Rao, 1997]. Neither the RBA nor the VIT technique has porous media so that it is free from the reservoir plugging problem, though asphaltene precipitation may still occur in both methods [Elsharkawy *et al*, 1996; Rao and Lee, 2002]. Two bulk gas and oil phases are allowed to contact and interact with each other directly in the RBA or IFT test, which can be observed at any time. In comparison with the traditional slim-tube and coreflood tests, both the RBA and the VIT technique have some common distinct merits, such as the time-saving advantage, low capital and operating costs, small gas and oil sample requirements, and direct visual observations [Thomas *et al*., 1994; Ayirala and Rao, 2006].

1.4 Purpose and Scope of This Study

The purpose of this study is to systematically examine and develop several qualitative and quantitative technical criteria for determining the MMPs from the slim-tube tests, coreflood tests, RBA tests, and VIT technique. The specific research objectives and the overall scope of this study are listed as follows:

1. To conduct a series of slim-tube tests for the live light crude oil–CO_2 system terminated at certain pore volume (PV) of injected CO_2 and measure the ORFs at different injection pressures and the actual reservoir temperature;
2. To examine the quantitative ORF and break-over pressure (BOP) technical criteria based on the measured ORF vs. injection pressure data for determining the MMPs of the live light crude oil–CO_2 system from the slim-tube tests;

3. To conduct a series of coreflood tests for the dead light crude oil–CO_2 system terminated at a large PV of injected CO_2 and measure the ORFs at different injection pressures and the actual reservoir temperature;
4. With the measured ORF vs. injection pressure data, to apply the quantitative ORF and BOP technical criteria for determining the MMPs of the dead light crude oil–CO_2 system from the coreflood tests;
5. To conduct two respective series of the RBA tests at different test pressures and the actual reservoir temperature for the light crude oil–pure and impure CO_2 systems and study four CO_2-bubble appearances, i.e., bubble shape, size, colour, and rising height;
6. To propose a novel qualitative technical criterion and interpret the miscibility developments and estimate the MMPs with the RBA by means of the new and four existing qualitative criteria on the basis of the overall bubble appearance;
7. To develop some new quantitative technical criteria, properly interpret the miscibility developments, and accurately determine the MMPs of the light crude oil–pure and impure CO_2 systems with the RBA;
8. To conduct several series of the dynamic IFT tests for the dead and live light crude oil–CO_2 systems at different initial gas–oil ratios (GORs) in volume and T_{res} = 53.0°C and measure the initial and equilibrium IFT vs. test pressure data by using the advanced axisymmetric drop shape analysis (ADSA) technique for the pendant drop case;
9. To develop some new quantitative technical criteria for determining the MMPs from the VIT technique; and

10. To study the specific effects of the following three important experimental factors on the determined MMPs from the VIT technique by using the new quantitative technical criteria: the initial vs. equilibrium IFTs, oil composition, and initial GOR in volume.

1.5 Outline of the Thesis

This thesis consists of eight chapters. Specifically, Chapter 1 gives an introduction to the thesis topic along with the purpose and the scope of this study. Chapter 2 presents an updated literature review on the CO_2-EOR mechanisms and projects, MCM development between the crude oil and CO_2, and different existing technical criteria for determining the MMPs from the slim-tube tests, coreflood tests, RBA tests, and VIT technique. At the end of this chapter, the problem statement of this thesis is provided. Chapter 3 gives the experimental details, which include the gas chromatography (GC) compositional analysis of the original dead light crude oil, preparations of the live light crude oil and impure CO_2 samples, experimental preparations and procedures for the slim-tube tests, coreflood tests, RBA tests, and IFT tests. In Chapter 4, the ORF vs. injection pressure data are obtained by conducting five slim-tube tests. Two quantitative ORF and BOP criteria are analyzed and applied to determine the MMPs of the live light crude oil–CO_2 system. Chapter 5 describes the applications of the ORF and BOP criteria for determining the MMPs of the dead light crude oil–CO_2 system from the coreflood tests. In Chapter 6, two series of the RBA tests are conducted for the light crude oil–pure and impure CO_2 systems. A novel bubble break-up (BBU) qualitative criterion is proposed and used to interpret the miscibility developments and estimate the MMPs. Moreover, two new quantitative

technical criteria, namely, the bubble-rising height (BRH) and bubble-rising velocity (BRV), are developed and applied to properly interpret the miscibility developments and accurately determine the MMPs of the two light crude oil–CO_2 systems. In Chapter 7, six series of the dynamic IFT tests for the dead and live light crude oil–CO_2 systems are conducted under different test conditions. Two new quantitative technical criteria, namely, the linear correlation coefficient (LCC) and critical interfacial thickness (CIT), are developed and used to determine the MMPs from the VIT technique. Chapter 8 summarizes major scientific findings of this study and makes several technical recommendations for future studies.

CHAPTER 2 LITERATURE REVIEW

2.1 CO_2-EOR Mechanisms and Projects

The commonly-recognized enhanced oil recovery (EOR) mechanisms for CO_2 flooding include the oil viscosity reduction, oil-swelling effect, interfacial tension (IFT) reduction, light-hydrocarbons (HCs) extraction, immiscible and miscible displacements [Holm and Josendal, 1974; Simon and Graue, 1965; Mungan, 1981]. These mechanisms can play more or less important roles, primarily depending on whether the CO_2 displacement is immiscible or miscible. For example, the oil viscosity reduction, IFT reduction and immiscible displacement are more important oil recovery mechanisms for the immiscible CO_2 flooding process, whereas the oil-swelling effect, light-HCs extraction and miscible displacement play more important in the miscible CO_2 flooding process [Martin and Taber, 1992]. A number of experimental studies have been conducted to examine the CO_2 ability to extract some light HCs from the crude oils [Grigg, 1995; Gardner *et al.*, 1981; Holm *et al.*, 1982]. In fact, the colour differences and compositional analyses of the produced oils indicate strong light-HCs extraction into CO_2 phase during CO_2 flooding. Moreover, the experimental results show that the oil recovery factor (ORF) is reduced if C_{5-19} mole fractions in the crude oil are reduced or the asphaltene content is increased [Huang, 1992]. Recently, the ORF is found to be increased when much more intermediate HCs of C_{9-17} and much fewer heavy HCs (C_{30+}) are found in the produced oil [Cao and Gu, 2013].

As early as 1952, Whorotn and Brownscombe applied a patent for an oil recovery method by using carbon dioxide (CO_2) [Whorotn *et al.*, 1952]. CO_2 tertiary or even secondary oil recovery can be used to further exploit the conventional oil reserves. A

recent study of the U.S. oilfields found that about 23% of the oil remaining in 10 U.S. oil-producing regions could be produced by using CO_2 flooding, which could recover almost 14 billion m^3 (89 billion bbl) of oil [Al-Mjeni *et al.*, 2010]. Some laboratory tests and field trials show that after the secondary waterflooding, many light and medium oil reservoirs may be especially suitable for the miscible or even immiscible CO_2 flooding. It has been found in a laboratory study that the ultimate oil recovery factor of a CO_2 secondary flood is over 60% of the original oil-in-place (OOIP), which is substantially higher than the average oil recovery factor of 44% of the OOIP for a secondary water flood [Chung *et al.*, 1988]. Some comprehensive experimental studies on the feasibility of CO_2 miscible flooding for the Weyburn oilfield, Canada, were conducted in the 1990s [Srivastava and Huang, 1997; Srivastava *et al.*, 2000]. It was found that 20–30% of the OOIP could be recovered during CO_2 tertiary coreflood tests. Eventually, the oil recovery factors in the range of 13–19% of the OOIP were expected in the Weyburn oilfield through the miscible CO_2 tertiary flooding [Whittaker *et al.*, 2004]. Another technically and economically successful CO_2 miscible field project has been undertaken in the Joffre Viking pool since 1984. A total of 12–25% of the OOIP has been recovered during the CO_2 tertiary oil recovery process [Pyo *et al.*, 2003]. Generally speaking, a miscible CO_2 tertiary flood can recover 8–25% of the OOIP in the field-scale pilot tests [Duncan, 1994; Pyo *et al.*, 2003]. Recently, experimental studies on the CO_2-thickened polymer flooding in light oil reservoir core plugs were conducted in the laboratory. It was found that two commercial polymers, poly (vinyl ethyl ether) (PVEE) and poly (1-decane) (P-1-D)-thickened CO_2 flooding can further enhance oil recovery after a pure CO_2 breakthrough. The CO_2 breakthrough can be significantly delayed if polymer-thickened CO_2 is injected

directly [Zhang and Gu, 2011]. Also, it is worthwhile to note that CO_2 flooding can not only effectively recover the residual oil but also considerably reduce the greenhouse gas emissions [Aycaguer, 2001].

2.2 Multi-Contact Miscibility (MCM) Development

The multi-contact miscibility (MCM) arises from the crude oil–CO_2 fluid flow [Orr Jr. and Jessen, 2007]. In fact, the two-way mass transfer between the crude oil and CO_2 can be in the forms of the gradual CO_2 dissolution into the crude oil through the molecular diffusion and convective dispersion and the light-HCs extraction from the crude oil to the CO_2 phase with multiple contacts [Yang and Gu, 2005]. This process can be approximately simulated through a series of the experimental tests in the so-called mixing cells [Hutchinson and Braun, 1961; Stalkup, 1983]. More specifically, in the first mixing cell, CO_2 is mixed with the original oil to form a crude oil–CO_2 mixture, which is subsequently split into two equilibrium vapour and liquid phases. Then these two equilibrium phases flow into the second mixing cell to be mixed with the fresh crude oil, while the newly-injected CO_2 is added into the first mixing cell. It should be noted that at this stage, the equilibrium mixture of the fresh oil from the second mixing cell plus the combination of the vapour and liquid phases from the first mixing cell flow out together from the second mixing cell to the next. The MCM is achieved by repeating this process through a large number of the mixing cells. Three different mechanisms of the MCM development have been proposed and studied in terms of the overall fluid composition, which include the vapourizing, condensing, and condensing/vapourizing processes [Zick, 1986].

In general, the injected gaseous solvent with a relatively lean gas (such as CO_2, CH_4, or N_2) is for the vapourizing process, whereas light HCs (such as $C_{2–4}$) are for the condensing process [Green and Willhite, 1998]. As the injected gaseous solvent moves forward, it contacts the crude oil for several times and becomes enriched by vapourizing the light components (i.e., $C_{2–4}$) from the crude oil for the former case, whereas the light components are condensed from the gaseous solvent into the crude oil to make the crude oil lighter for the latter case. The continuation of this process for either case modifies the crude oil to be miscible with the injected gaseous solvent in the reservoir so that the MCM can be achieved at the end.

The condensing/vapourizing process was first proposed in 1986 [Zick, 1986] and verified through the numerical simulations, theoretical, and laboratory studies [Monroe *et al*., 1990; Johns *et al*., 1992]. In the condensing/vapourizing process, the light components of the injected gaseous solvent are condensed into the crude oil to make the crude oil lighter, while the light components (i.e., $C_{2–4}$) are vapourized and the intermediate components (i.e., $C_{5–10}$) are stripped from the crude oil to enrich the injected gaseous solvent. The crude oil in contact with the injected gaseous solvent initially becomes lighter because the light components of the injected gaseous solvent cannot substitute for the stripping of the intermediate components. As the gaseous solvent is continuously injected, there will be no further condensation of light components from the injected gaseous solvent into the crude oil because the crude oil is saturated with the light components, whereas the vaporization of the light components or the stripping of the intermediate components from the crude oil to the injected gaseous solvent still continues. Thus the gaseous solvent is enriched with the ongoing condensing/vapourizing process

and becomes miscible with the crude oil in the reservoir. It should be noted that the condensing process occurs at the leading edge of the gas displacement, while the vapourizing process takes place at the trailing end. There is a two-phase transition zone in between. This mechanism involves the simultaneous counter-current mass transfer between the crude oil and gaseous solvent, which has been proven to be the most-frequently occurring mechanism involved in the miscible gas injection project in the oilfield [Jaubert and Arras, 1998].

2.3 MMP Determinations

2.3.1 Slim-tube tests

Some general MMP determination criteria of the slim-tube tests have been introduced and described in the literature [Wu and Batycky, 1990; Elsharkawy *et al*., 1996], which are based on the measured ORF vs. injection pressure data in the slim-tube tests and called the ORF criterion for the MMP determinations for brevity in this study. In an early publication, the MMP was assumedly reached if the ORF of the OOIP was over 80% at CO_2-breakthrough (CO_2-BT) or 94% at the end of a slim-tube test [Holm and Josendal, 1974]. The MMP is also assumedly achieved when the ORF is equal to 90% or 95% at 1.2 pore volume (PV) of injected gas. Although different high ORFs can be regarded as different threshold values for using the ORF criterion to determine the MMP, 90% or a higher ORF at 1.2 PV of injected gas is commonly accepted to be the threshold ORF and used as an indicator of the dynamic MCM process [Wu and Batycky, 1990]. Then, the pressure at the linear intersection point of the measured ORF vs. injection pressure data in the immiscible and miscible pressure ranges is considered to be the MMP [Deffrene *et al*., 1961]. In case the linear intersection point or break-over point is not sharp enough, the

so-called break-over pressure (BOP) criterion can be applied so that the MMP is determined to be the pressure at which the incremental ORF per incremental injection pressure increase reaches an arbitrarily chosen low threshold slope.

In addition, the ultimate ORFs at any large PVs vs. the so-called enrichment level can be plotted to determine the miscibility [Jerauld, 1998]. Alternatively, the physicochemical properties of the effluent fluids in the slim-tube tests (e.g., the size of the methane bank) were characterized to indicate the miscibility development [Novosad and Costain, 1988]. The visual observations of the effluent fluids [Yellig and Metcalfe, 1980] and/or the accurate measurements of the pressure drops in the slim-tube tests are also helpful to infer the miscibility process [Wu and Batycky, 1990]. In summary, there is no general consensus on which technical criterion (e.g., the ORF or BOP criterion) or which specific choice (e.g., the threshold value or intersection option) should be used to determine the MMP from the slim-tube tests [Orr Jr. *et al*., 1982].

2.3.2 Coreflood tests

The ORF criterion with different threshold ORFs is usually invoked to determine the MMP of a crude oil–CO_2 system from the coreflood tests in a similar manner to the slim-tube tests. Moreover, the produced oil composition becomes an important indicator for the miscibility development from the coreflood tests [Huang, 1992]. Here, the normalized produced oil composition is defined as a ratio of the weight percentage of each HC in the produced oil at any PV to that of this HC in the original oil. The normalized HCs (i.e., C_8, C_{10}, C_{15}, C_{20}, C_{25}, and C_{30}) of the produced oil should be slightly lower than and close to 1.0 during most oil production times but higher than and close to 1.0 near the end in the miscible case. On the other hand, they deviate from 1.0 considerably at the beginning of

the oil production in the immiscible case.

However, the produced oil compositional analysis alone cannot be used to ascertain whether the miscibility is developed. To overcome this shortcoming, more physicochemical properties (e.g., the densities, viscosities, and molecular weights) of the produced oil and gas may be useful to determine the MMP from a series of the CO_2 coreflood tests [Cao and Gu, 2013]. It has been found that under the immiscible condition, the produced oil becomes heavier and more viscous as more CO_2 is injected. Much more light HCs of $C_{3–8}$ are in the produced gas due to the initial quick light-HCs extraction before CO_2-BT. Nevertheless, a relatively lighter oil than the original light crude oil is produced at the end of each CO_2 coreflood test in the near-miscible case. In the miscible case, the original crude oil is produced at the beginning of CO_2 injection due to the volumetric displacement by dense CO_2. Much more intermediate HCs of $C_{9–17}$ and much fewer heavy HCs (C_{30+}) are found in the produced oil at a later time, which becomes much lighter under the miscible condition. Moreover, CO_2 can extract some light to intermediate HCs. The light HCs of $C_{6–8}$ are the dominant components in the produced gas before CO_2-BT and CO_2 becomes the primary component after CO_2-BT.

2.3.3 Rising-bubble apparatus (RBA) tests

In the past, the MMPs have been inferred from the direct visual observations of the rising-bubbles in a thin oil column at different test pressures and a constant test or reservoir temperature with the RBA, in terms of the bubble shape, size, colour [Rao and Lee, 2003], and rising height. The bubble shape was regarded as the primary technical criterion for estimating the MMP when the RBA was first invented in the 1980s [Christiansen and Kim, 1986; Christiansen and Haines, 1987]. More specifically, at a test

pressure below the MMP, the bubble has a spherical or near-spherical shape at its top with the fresh crude oil all the time but its bottom evolves from a spherical to flat shape [Zhou and Orr Jr., 1998]. When the test pressure is equal to or slightly above the MMP, the bubble still has a spherical shape at the top but two tails are gradually formed at its bottom [Dong *et al*., 2001]. Also the bottom crude oil–gas interface becomes fuzzy and the bubble is rapidly dissolved into the crude oil from its bottom to top. At the test pressure far above the MMP, the bubble may disappear almost immediately upon contact with the crude oil so that no shape or interface can be observed in this case. In summary, as the test pressure is increased, the bubble shape gradually evolves from a spherical cap and a flat bottom, to an ellipsoidal cap and two tails at the bottom, and finally to an ellipsoidal cap and a relatively long mixing wake at the bottom. This is referred to as the bubble-shape qualitative criterion for the MMP estimation with the RBA in this study.

Moreover, the bubble size, colour, and rising height have also been studied and used as three additional qualitative technical criteria for the MMP estimation with the RBA. In general, the gas bubble shrinks gradually as it rises through the crude oil column if the test pressure is below the MMP [Srivastava and Huang, 1998; Dong *et al*., 2000]. It is worthwhile to note that such a gradual bubble size reduction or even bubble disappearance is a direct result of the gradual gas dissolution into the oil phase through the molecular diffusion and convective dispersion rather than the miscibility development [Novosad and Costain, 1989]. Once the test pressure is above the MMP and the dynamic MCM is achieved, the bubble size remains almost the same or is slightly increased due to HCs-extraction by CO_2 until the bubble bottom starts to deform and disappear [Christiansen and Haines, 1987]. On the other hand, the bubble cap remains transparent

all the time at the test pressure below the MMP, while the bubble bottom changes gradually from transparent to fuzzy, and finally to transparent again [Elsharkawy *et al*., 1996]. There is a distinct interface between the transparent cap and the fuzzy bottom. As the bubble rises, this interface moves downwards slowly until the entire bubble becomes transparent at the end. When the test pressure approaches or exceeds the MMP, the bubble becomes fuzzier at a higher test pressure and the afore-mentioned interface movement becomes more difficult to observe in the RBA tests [Elsharkawy *et al*., 1996]. In consistent with the bubble size and colour changes, the bubble disappears slowly and may reach the top of the oil column at the test pressure below the MMP. The measured bubble-rising height vs. test pressure curve has a sudden decline once the test pressure is above the MMP [Poettmann *et al*., 1992]. In practice, the above-mentioned four existing qualitative technical criteria, i.e., the bubble shape, size, colour, and rising height, are often applied altogether to best interpret the miscibility development and estimate the MMP with the RBA.

2.3.4 Vanishing interfacial tension (VIT) technique

By means of the vanishing interfacial tension (VIT) technique, the MMP is determined by linearly extrapolating the measured equilibrium IFT vs. test pressure data to zero IFT [Rao, 1997]. In this way, the choice of the lowest equilibrium IFT measured at the highest test pressure may affect the determined MMP. In the past, there have not been any technical criteria for appropriately choosing the lowest equilibrium IFT to be used in the linear extrapolation. In fact, the measured equilibrium IFT vs. test pressure data have been chosen arbitrarily to determine the MMPs [Ayirala and Rao, 2006a]. In general, there may exist two or three distinct pressure ranges for the measured

equilibrium IFT vs. test pressure data [Wang et al., 2010]. The determined MMP from the VIT technique is found to be close to that from the slim-tube tests if the measured equilibrium IFT vs. test pressure data in the first pressure range are linearly extrapolated to zero IFT [Rao and Lee, 2003; Escrochi *et al*., 2013]. However, the MMP determined from the VIT technique is likely to be higher if the lower equilibrium IFTs measured at higher test pressures in the second pressure range are used [Thomas *et al*., 1994; Orr Jr. and Jessen, 2007; Jessen and Orr Jr., 2008]. So far no literature has been found to systematically study any technical criteria for determining the MMP from the VIT technique in terms of the linear extrapolation.

2.4 Problem Statement

As described in the preceding sections of this chapter, the slim-tube tests, coreflood tests, and RBA are the most commonly used experimental methods for determining the MMP and have been made available and improved for several decades. In particular, the slim-tube tests have long been regarded as the petroleum industry standard experimental method for determining the MMP. However, so far no literature has been found to systematically study and quantitatively compare different technical criteria for the MMP determination by using the measured ORF vs. injection test pressure data from the slim-tube or coreflood tests. Moreover, although four qualitative technical criteria (i.e., the bubble shape, size, colour, and rising height) have been suggested and applied to estimate the MMP with the RBA, there is no general consensus on which MMP estimation criterion or criteria should be used in different cases. No fundamental studies can be found in the literature to objectively interpret the miscibility development and quantitatively determine the MMP with the RBA. On the other hand, the VIT technique

was developed almost two decades ago and is often applied because it is quantitative, fast, and economical for the MMP determinations. Unfortunately, so far no literature has been found to specifically study how to determine the MMPs from the VIT technique.

In this study, first, five CO_2 slim-tube tests and five CO_2 coreflood tests are carried out for the live and dead light crude oil–CO_2 systems at different injection pressures and the actual reservoir temperature of T_{res} = 53.0°C, respectively. Two different technical criteria (i.e., the ORF and BOP criteria) with different threshold values or intersection options are applied to determine the respective MMPs of the live and dead light crude oil–CO_2 systems from the slim-tube and coreflood tests. More specifically, the linear and quadratic extrapolation methods as well as the linear intersection method for the ORF criterion and the cubic regression method for the BOP criterion are thoroughly studied and quantitatively compared. Second, two series of the RBA tests are conducted at different test pressures and T_{res} = 53.0°C for the light crude oil–pure and impure CO_2 systems, respectively. One novel qualitative criterion, namely, the bubble break-up (BBU), is proposed and used to interpret the miscibility developments and estimate the MMPs, in comparison with the four existing qualitative criteria (i.e., the bubble shape, size, colour, and rising height). Furthermore, two new quantitative criteria, namely, the bubble-rising height (BRH) and bubble-rising velocity (BRV), are developed and applied to properly interpret the miscibility developments and accurately determine the MMPs of the two light crude oil–CO_2 systems. Third, five series of the dynamic IFT tests for the dead light crude oil–CO_2 system are conducted at five different initial GORs of 1:1, 3:1, 10:1, 200:1, 4000:1 in volume and T_{res} = 53.0°C. One more series of the dynamic IFT tests are performed for the live light crude oil–CO_2 system at the initial GOR of 4000:1 in

volume. Two new quantitative technical criteria, namely, the linear correlation coefficient (LCC) and critical interfacial thickness (CIT), are developed and applied to determine the MMPs from the VIT technique. In addition, the specific effects of the following three important experimental factors on the determined MMPs are studied by using the two new quantitative technical criteria: the initial vs. equilibrium IFTs, oil composition, and initial GOR in volume.

CHAPTER 3 EXPERIMENTAL

3.1 Materials

In this study, the original dead light crude oil was collected from the Pembina Cardium oilfield in Alberta, Canada. The obtained original crude oil was cleaned by using a centrifuge (Allegra X-30 Series, Beckman Coulter, USA) to remove any sands and brine. The density and viscosity of the cleaned light crude oil were measured to be $\rho_{oil} = 842.9\ \mathrm{kg/m^3}$ and $\mu_{oil} = 7.92\ \mathrm{cP}$ at the atmospheric pressure and T_{lab} = 22.0°C. Its molecular weight was measured to be MW_{oil} = 212.2 g/mol by using an automatic high-sensitivity wide-range cryoscope (Model 5009, Precision Systems Inc., USA). The gas chromatography (GC) compositional analysis result of the cleaned light crude oil is given in Table 3.1. As a light crude oil, the Pembina Cardium oil is especially suitable for CO_2-EOR. The asphaltene content of the cleaned light crude oil was measured to be w_{asp} = 0.26 wt.% (*n*-pentane insoluble) by using the standard ASTM D2007-03 method and filter papers (Whatman No. 5, England) with a pore size of 2.5 μm.

The reservoir brine sample was collected from the same oilfield, cleaned, and analyzed. Its detailed physicochemical properties are listed in Table 3.2. A number of tight sandstone reservoir core plugs were collected from several wells located in the Pembina Cardium oilfield at the reservoir depth of 1,600–1,648 m, where the reservoir temperature was equal to T_{res} = 53.0°C. Three pressure–volume–temperature (PVT) tests with three different CO_2 concentrations in the dead light crude oil were conducted at the actual reservoir temperature of T_{res} = 53.0°C and are summarized in Table 3.3. It is noted

Table 3.1 Compositional analysis result of the original light crude oil with the asphaltene content of w_{asp} = 0.26 wt.% (*n*-pentane insoluble).

Carbon No.	mol.%	Carbon No.	mol.%
C_1	0.00	C_{27}	1.07
C_2	0.00	C_{28}	0.94
C_3	0.20	C_{29}	0.89
C_4	1.17	C_{30}	0.64
C_5	3.67	C_{31}	0.68
C_6	5.01	C_{32}	0.59
C_7	10.67	C_{33}	0.46
C_8	7.20	C_{34}	0.38
C_9	7.61	C_{35}	0.54
C_{10}	6.95	C_{36}	0.47
C_{11}	5.75	C_{37}	0.30
C_{12}	5.01	C_{38}	0.27
C_{13}	4.59	C_{39}	0.37
C_{14}	3.97	C_{40}	0.28
C_{15}	3.74	C_{41}	0.27
C_{16}	2.98	C_{42}	0.22
C_{17}	3.08	C_{43}	0.22
C_{18}	3.09	C_{44}	0.20
C_{19}	2.01	C_{45}	0.20
C_{20}	2.07	C_{46}	0.15
C_{21}	1.96	C_{47}	0.14
C_{22}	1.14	C_{48}	0.13
C_{23}	1.55	C_{49}	0.13
C_{24}	1.28	C_{50+}	3.35
C_{25}	1.27	Total	100.00
C_{26}	1.14		

Table 3.2 Physicochemical properties of the cleaned reservoir brine at P = 1 atm (The chemical analyses were contracted to and conducted by the Saskatchewan Research Council).

Temperature (°C)	15	20	40
Density (g/cm^3)	1.003	1.002	0.996
Viscosity (mPa s)	1.17	1.02	0.67
pH at 20.0°C	8.08		
Specific conductivity (μS/cm)	7,250		
Refractive index at 25.0°C	1.3339		
Chloride (mg/L)	1,130		
Sulphate (mg/L)	4.0		
Total dissolved solids (mg/L)	4,323 at 180 °C		
Potassium (mg/L)	17		
Sodium (mg/L)	1,690		
Calcium (mg/L)	17		
Magnesium (mg/L)	11		
Iron (mg/L)	0.021		
Manganese (mg/L)	<0.001		
Barium (mg/L)	9.20		

Table 3.3 Measured saturation pressures, oil-swelling factors (SFs), and CO_2 solubilities of three dead light crude oil–CO_2 systems at the actual reservoir temperature of T_{res} = 53.0°C.

Test no.	x_{CO_2}		P_{sat} (MPa)	SF at P_{sat}	χ_{CO_2} at P_{sat} (g CO_2/100 g oil)
	wt.%	mol.%			
1	10.4	35.9	6.5	1.16	11.6
2	13.4	42.7	7.8	1.20	15.5
3	18.2	51.7	9.6	1.28	22.2

Notes:
- x_{CO_2} : weight or mole percentage of CO_2 in the dead light crude oil
- P_{sat} : saturation pressure
- SF : oil-swelling factor
- χ_{CO_2} : CO_2 solubility in the dead light crude oil

that the measured saturation pressure, oil-swelling factor (*SF*), and CO_2 solubility in the dead light crude oil increase with CO_2 concentration due to CO_2 dissolution. Carbon dioxide was purchased from Praxair (Canada) and *n*-pentane was purchased from VWR International (Canada). Four hydrocarbon (HC) solvents, methane, ethane, propane, and *n*-butane, were all purchased from Praxair (Canada). The purities of these six solvents used in this study are listed in Table 3.4.

3.2 Reconstitution of the Live Light Crude Oil Sample

In this study, the dead light crude oil was the original dead light crude oil sample, which was not pre-saturated with any solvent prior to any experimental test. The live light crude oil sample was reconstituted by pre-saturating the original dead light crude oil sample with the produced HC gas. The actual produced gas composition was provided by PennWest Exploration (Canada) and simplified as the nominal gas composition by lumping the HCs (C_{4+}) and non-HCs together as *n*-C_4. The compositions of the actual, nominal, and laboratory HC gas samples are listed in Table 3.5. The laboratory HC gas sample was prepared by mixing four HC gases (C_1, C_2, C_3, and *n*-C_4) and then used to reconstitute the live light crude oil sample. It is worthwhile to note that there was a minor amount of air (i.e., 0.46 mol.% N_2) in the laboratory prepared HC gas sample probably because the gas sample cylinder was not completely vacuumed prior to the gas reconstitution.

With the prepared laboratory HC gas sample, the live light crude oil sample was reconstituted by using the actual gas–oil ratio (GOR) of 15:1 in volume under the standard conditions [Gu *et al*., 2013]. The experimental procedure for reconstituting the live light crude oil sample is briefly described below. First, a high-pressure transfer

Table 3.4 Purities of six solvents used in this study.

Solvent	Purity (mol.%)
CO_2	99.998
n-C_5H_{12}	99.76
CH_4	99.97
C_2H_6	99.0
C_3H_8	99.5
n-C_4H_{10}	99.5

Table 3.5 Compositions of the actual, nominal, and laboratory hydrocarbon (HC) gas samples.

Component	Actual (mol.%)	Nominal (mol.%)	Laboratory (mol.%)
C_1	66.50	66.50	70.20
C_2	11.41	11.41	10.02
C_3	11.39	11.39	10.26
i-C_4	1.83	–	–
n-C_4	3.90	10.70	9.06
i-C_5	0.68	–	–
n-C_5	0.86	–	–
C_6	0.55	–	–
C_{7+}	0.54	–	–
N_2	1.48	–	0.46
CO_2	0.86	–	–
Total	100.00	100.00	100.00

cylinder with the volume of 1,000 cm^3 (500-10-P-316-2, DBR, Canada) was cleaned and kept inside an air bath at T_{res} = 53.0°C. A total of 500 cm^3 dead light crude oil sample was injected into the transfer cylinder by using a high-pressure positive-displacement pump (PMP-1000-1-10-MB, DBR, Canada). Second, the laboratory HC gas sample was injected into another cleaned and vacuumed transfer cylinder with the volume of 500 cm^3 until the gas pressure inside the transfer cylinder reached 1.5 MPa. This gas pressure was calculated by applying the Peng–Robinson equation of state (P–R EOS) [Peng and Robinson, 1976] so as to reach the actual GOR of 15:1 in volume for the live light crude oil sample under the standard conditions. Third, the laboratory HC gas sample was injected into the oil cylinder to saturate the dead light crude oil sample. The high-pressure transfer cylinder containing the dead light crude oil and laboratory HC gas sample was kept rotating for at least 7 days to fully mix them. The saturation pressure of this live light crude oil sample was calculated to be P_{sat} = 3.2 MPa at T_{res} = 53.0°C by using the CMG WinProp module (Version 2013.20, Computer Modelling Group Limited, Canada) with the P–R EOS.

3.3 Preparation of the Impure CO_2 Sample

In this study, an impure CO_2 sample was prepared by mixing pure CO_2 and pure CH_4 to reach a pre-determined nominal composition of 80 mol.% CO_2 + 20 mol.% CH_4. The specific procedure for preparing the impure CO_2 sample is briefly described below. First, two transfer cylinders with the volume of 1000 cm^3 each were cleaned and vacuumed. Pure CO_2 was injected into one transfer cylinder until P_{CO_2} = 3.1 MPa and pure CH_4 was injected into the other transfer cylinder until P_{CH_4} = 0.7 MPa at the room temperature of

T_{lab} = 22.0°C. These two pressures were calculated by applying the P–R EOS in order to obtain the impure CO_2 sample with the desired composition. Afterward, pure CH_4 was injected into pure CO_2 cylinder, which was then further pressurized to P_{mix} = 10.0 MPa to form a homogeneous supercritical CO_2–CH_4 mixture. The actual composition of the prepared impure CO_2 sample was found to be 74.87 mol.% CO_2 + 25.13 mol.% CH_4 through the GC compositional analysis.

3.4 Slim-Tube Tests

Figure 3.1 shows a schematic diagram of the slim-tube experimental setup used by the Saskatchewan Research Council (SRC) for conducting a series of five well-controlled 1-D displacement tests and measuring the minimum miscibility pressure (MMP) of the live light crude oil–CO_2 system. The slim-tube setup includes a positive-displacement pump, a stainless steel slim tube packed with the Ottawa silica sands, a differential pressure transducer for measuring the pressure drop along the slim tube, a burette for collecting the produced oil, a gas flow meter for continuously measuring the produced gas volume, and an in-line gas chromatographer for analyzing the produced gas composition at any time. The detailed physical properties and experimental conditions of five slim-tube tests are summarized in Table 3.6. The CO_2 flooding was conducted in a 12.2 m long, 0.457 cm ID slim tube packed with the Ottawa silica sands of 75−106 mesh. The long slim tube with a small ID was purposely chosen to minimize the entrance effect and prevent CO_2 viscous fingering. In this study, the pore volume (PV) of each slim-tube test was approximately 81.7 cm^3. The measured average permeability and porosity were equal to 5.8 D and 41.0%, respectively. The pressure drop along the slim tube was low due to a high permeability, which was below 1.0 MPa during each slim-tube test. The

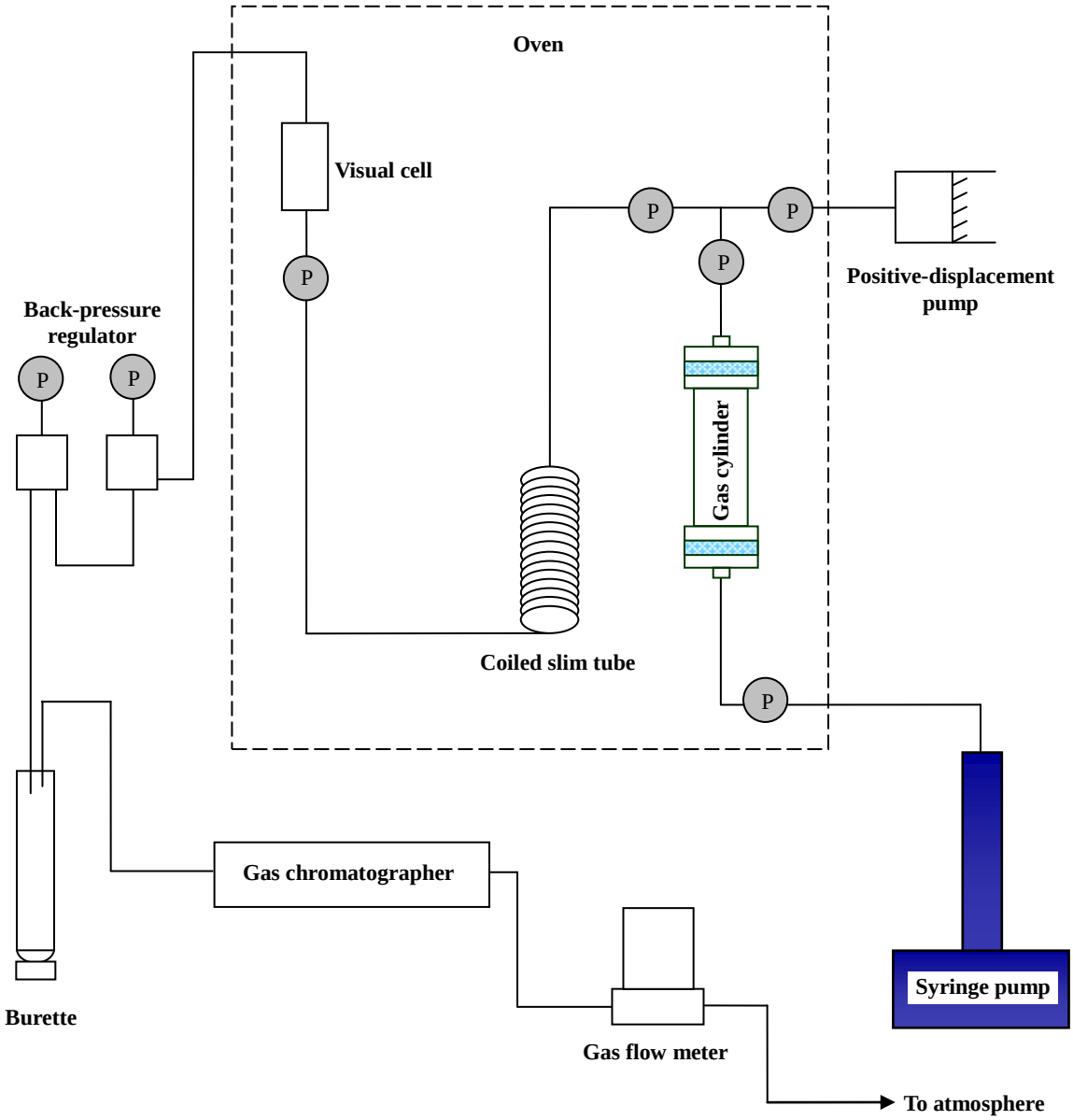

Figure 3.1 Schematic diagram of the slim-tube test setup.

Table 3.6 Physical properties and experimental conditions of five slim-tube tests with the live light crude oil at 1.2 PV of injected pure CO_2 and the actual reservoir temperature of T_{res} = 53.0°C.

Slim-tube material	316 stainless steel
Total length of the slim tube (m)	12.2
ID of the slim tube (cm)	0.457
Packing media	Ottawa silica sands
Mesh size	75–106
Pore volume (cm^3)	81.7
k (D)	5.8
ϕ (%)	41.0

Notes: k: Absolute permeability of the slim tube packed with the Ottawa silica sands of 75–106 mesh

ϕ: Porosity of the slim tube packed with the Ottawa silica sands of 75–106 mesh

GOR of the produced fluids was monitored and measured to ensure that it reached 15:1 in volume for the live light crude oil under the standard conditions. The entire system was placed inside an oven, which was heated to and maintained at the actual reservoir temperature of T_{res} = 53.0°C.

The slim-tube tests were divided into three periods, which were the pre-experimental preparation, experimental execution, and post-experimental clean-up. In preparation of each slim-tube test, the slim tube was cleaned by quickly injecting at least 3.0 PV of toluene through it and dried by purging nitrogen several times. A back-pressure regulator (BPR-50, Temco, USA) was adjusted to the desired production pressure by using a nitrogen cylinder as a back-pressure reservoir. At the beginning of each test, the live light crude oil was pumped into the slim tube to saturate the slim tube packed with the Ottawa silica sands at the given reservoir temperature of T_{res} = 53.0°C. The initial oil saturation was found to be in the range of S_{oi} = 96.7–98.9%, which is equal to the ratio of the volume of the initial oil-in-place to the PV of the sandpacked slim tube. The initial oil saturation could not reach 100% because of the presence of some leftover air. Then CO_2 was injected into the slim tube to recover the live light crude oil by using an automatic positive-displacement pump (PMP-0500-1-10-MB-316-M4-C0, DBR, Canada) at a constant volume flow rate of q_{CO_2} = 0.1 cc/min. The injection and production pressures as well as the differential pressures along the slim tube were continuously monitored and recorded during each slim-tube test. The burette was used to collect and weigh the produced oil under the atmospheric conditions, while the produced gas was in-line analyzed by using the gas chromatographer and its volume was measured by using the gas flow meter. The produced oil weight and gas volume were measured and recorded at

every 0.1 PV. Each slim-tube test was terminated after 1.2 PV of pure CO_2 was injected.

After each test, the entire slim-tube system was blown down and cleaned by injecting 3.0 PV of toluene through it to remove any residual crude oil, leftover CO_2, and precipitated asphaltenes in the porous medium. Typically, one slim-tube test took two days, while another two days was needed to clean the slim tube with toluene and resaturate it with the live light crude oil. Overall, it took about 4 weeks to complete a total of five comprehensive slim-tube tests. It should be noted that the five slim-tube tests at five different test pressures were contracted to and conducted by the SRC.

3.5 Coreflood Tests

Figure 3.2 shows a schematic diagram of the high-pressure CO_2 coreflood apparatus. Prior to each test, the sandstone reservoir core plugs were thoroughly cleaned by using a Dean–Stark extractor (09-556D, Fisher Scientific, Canada) for 4–7 days. An automatic displacement pump was used to displace the crude oil, reservoir brine or CO_2 through the composite reservoir core plugs inside a high-pressure coreholder (RCHR-2.0, Temco, USA). The tap water was pumped by using a programmable syringe pump (100DX, ISCO Inc., USA) to apply the so-called overburden pressure, which was always kept 3.0–5.0 MPa higher than the injection pressure. The composite reservoir core plugs used in the five CO_2 coreflood tests were 8–10″ long (L) and 2″ in diameter (D). Four high-pressure cylinders were used to store and deliver the crude oil, reservoir brine, CO_2, and tap water, respectively. These four transfer cylinders and the coreholder were placed inside an air bath. A thermocouple heating gun (HG 1100, Thankita, USA) and a temperature controller (Standard-89000-00, Cole–Parmer, Canada) were used to heat the air bath and keep it at the constant reservoir temperature of T_{res} = 53.0 ℃. A back-pressure

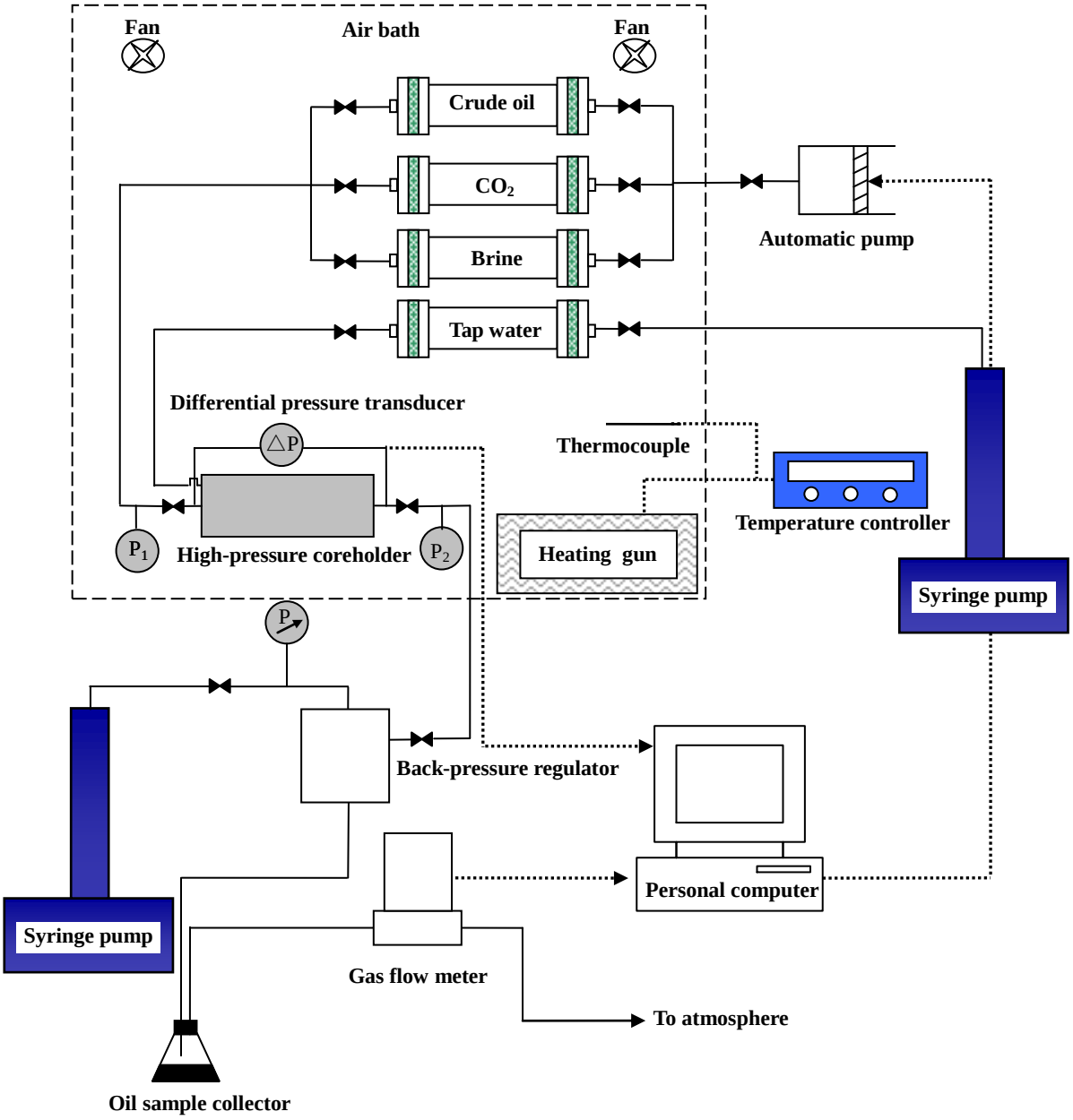

Figure 3.2 Schematic diagram of the high-pressure CO_2 coreflood apparatus.

regulator (BPR-50, Temco, USA) was used to maintain the pre-specified injection pressure during each CO_2 flooding test and the BPR pressure was always set at 0.5–1.0 MPa lower than the injection pressure.

During the reservoir brine, original light crude oil, and CO_2 injection processes, the differential pressure between the inlet and outlet of the coreholder was measured by using a digital differential pressure indicator (Type PM, Heise, USA). A digital video camera was used to record the cumulative volume of the produced oil. The cumulative volume of the produced gas was measured by using a gas flow meter (GFM17, Aalborg, USA). The differential pressure data and cumulative volumes of the produced oil and gas were measured, recorded, and stored automatically in a personal computer at a preset time interval of 10 seconds.

The general procedure for preparing each CO_2 coreflood test is briefly described as follows. Two sandstone reservoir core plugs were placed in series inside the Dean–Stark extractor and cleaned with toluene, methanol, and chloroform in sequence to remove HCs, salts, and clays, respectively. After the two sandstone reservoir core plugs were cleaned and dried, they were assembled in series in the horizontal coreholder and vacuumed for 24 h. Then the cleaned reservoir brine was injected to measure the porosity of the composite reservoir core plugs. Afterwards, the cleaned reservoir brine was injected at different volume flow rates ($q_{\text{brine}} = 0.1 - 0.5\,\text{cm}^3/\text{min}$) to measure the absolute permeability of the composite reservoir core plugs. The measured porosity and absolute permeability were in the ranges of ϕ = 12.7–16.1% and k = 0.8–1.7 mD, respectively. Then, 1.5 PV of the original light crude oil was injected through the initially brine-saturated composite core plugs at a constant flow rate ($q_{\text{oil}} = 0.1\,\text{cm}^3/\text{min}$) until no more

water was produced and the connate water saturation was achieved. It is worthwhile to note that in this study, the composite core plugs were saturated first with the reservoir brine and then with the original crude oil to finally reach the so-called connate water saturation and initial oil saturation at the lab temperature of T_{lab} = 22.0°C. In this way, a high initial oil saturation was obtained purposely so as to model the actual oil reservoir case. The connate water saturation was found to be S_{wc} = 23.3–39.8% and the initial oil saturation was in the range of S_{oi} = 60.2–76.7%.

After the connate water saturation and initial oil saturation were reached, the entire coreflood apparatus was placed inside the air bath, where it was heated to and maintained at the constant reservoir temperature of T_{res} = 53.0°C for at least two days. Then, a total of 3.0 PV of the original light crude oil was injected at $q_{oil} = 0.1\,cm^3/min$ to pressurize the composite core plugs and ensure that the pre-specified injection pressure was reached and that a stable differential pressure between the inlet and outlet of the coreholder was achieved. During CO_2 flooding, a constant volume injection rate of CO_2 ($q_{CO_2} = 0.4\,cm^3/min$) was used at each pre-specified injection pressure and T_{res} = 53.0 ℃. In each coreflood test, CO_2 injection was terminated after a total of 2.0 PV was injected and no more oil was produced. After the produced fluids passed through the BPR, the flashed-off oil was obtained and the digital video camera was used to record the cumulative volume of the produced oil. Meanwhile, the cumulative volume of the produced gas was measured and recorded by using the gas flow meter. In this study, no connate water was produced along with the produced oil in any CO_2 coreflood test. The physical properties and experimental conditions of the five coreflood tests with the dead light crude oil and pure CO_2 at T_{res} = 53.0°C are listed in Table 3.7.

Table 3.7 Physical properties and experimental conditions of five coreflood tests with the dead light crude oil at 2.0 PV of injected pure CO_2 and the actual reservoir temperature of T_{res} = 53.0°C.

Test no.	k (mD)	ϕ (%)	S_{oi} (%)
1	1.7	16.1	63.9
2	1.0	15.9	70.7
3	0.8	14.1	60.2
4	1.5	12.7	76.7
5	1.7	13.0	70.5

Notes: k: Absolute permeability of two composite sandstone reservoir core plugs

ϕ: Porosity of two composite sandstone reservoir core plugs

S_{oi}: Initial oil saturation

3.6 Rising-Bubble Apparatus (RBA)

Figure 3.3 shows a schematic diagram of the RBA used in this study to conduct two separate series of CO_2-bubble tests and determine the MMPs of the light crude oil–pure and impure CO_2 systems at the actual reservoir temperature of T_{res} = 53.0°C. The major component of the RBA was a see-through windowed high-pressure cell (P/N 2329-800, Ruska Fluid Products, Chandler Engineering, USA). The maximum operating pressure and temperature of this pressure cell are equal to 68.0 MPa and 148.0°C, respectively. A thin glass tube was filled with the light crude oil and mounted vertically inside the high-pressure cell. Its central section was 5.4 cm long and in a rectangular shape of 0.1 cm × 0.5 cm, which was used to observe the rising CO_2 bubble through the light crude oil column and capture its digital image at any time. There was a circular section of 2.0 cm long at each end of the thin glass tube. A stainless steel syringe needle was installed through the bottom port of the high-pressure cell to reach the bottom circular glass section. This needle was used to form and release the CO_2 bubble into the bottom water phase. It is worthwhile to note that the CO_2-bubble size is largely determined by the needle size for a given crude oil–CO_2 system at a pre-specified test pressure and temperature. A light source (240–341, Dyna–Lume, USA) was used to provide uniform and sufficient illumination of the CO_2 bubble. A digital camera (EOS t2i, Cannon, Canada) was used to observe the rising CO_2 bubble at any time and acquire its sequential digital images at a pre-specified time interval. The see-through windowed high-pressure cell was positioned horizontally between the light source and the digital camera. In addition, a programmable syringe pump, a positive-displacement pump, and three high-pressure transfer cylinders were used to introduce the test fluids (i.e., water, oil, and

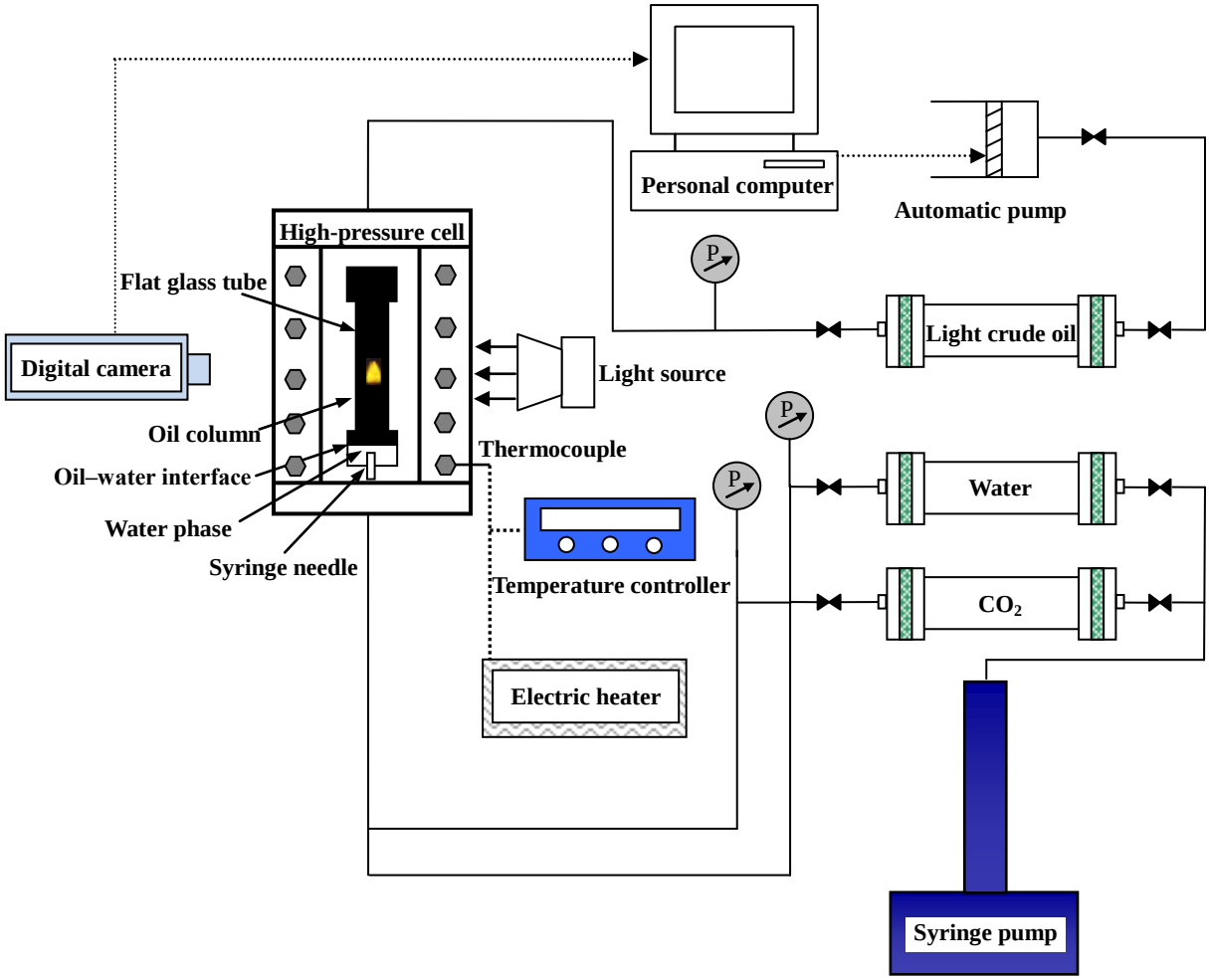

Figure 3.3 Schematic diagram of the rising-bubble apparatus (RBA).

carbon dioxide), control the test pressure, and form the CO_2 bubble each time. The RBA also included an electric heater (HZ-315C, Super Electric Co., Canada) and a temperature controller (Standard-89000-00, Cole–Parmer, Canada) for maintaining the entire apparatus at the pre-specified constant reservoir temperature during each RBA test.

To conduct each CO_2-bubble test with the RBA, the see-through windowed high-pressure cell and the thin glass tube were thoroughly cleaned. Then the entire RBA was pressurized with de-ionized water to a pre-specified test pressure and heated to and maintained at T_{res} = 53.0°C. The light crude oil was injected slowly into the thin glass tube from its top to displace the de-ionized water downwards until the light crude oil–de-ionized water interface was slightly above the bottom syringe needle, which was submerged in the de-ionized water phase. After the RBA reached an equilibrium state, i.e., the light crude oil in the glass tube and the de-ionized water inside the pressure cell were at the same test pressure, a CO_2 bubble was formed at the needle tip and enlarged until it was detached and released into the water phase due to the upward buoyancy force. The CO_2 bubble rose through the water phase, penetrated the light crude oil–water interface, and finally entered the light crude oil column in the central flat section of the thin glass tube. Its rising process was observed and recorded by using the digital camera.

In general, it took 1–4 seconds for a CO_2 bubble to rise through the light crude oil column in the central flat glass tube. In each RBA test, the rising movements of the CO_2 bubble were used to model the miscibility development through the vapourizing process when the gas phase was either pure CO_2 or impure CO_2 with some CH_4. After several CO_2 bubbles were injected to rise through the light crude oil column, the de-ionized water was injected from the bottom of the thin glass tube to displace and remove the CO_2-

diluted light crude oil. Then the fresh light crude oil was introduced slowly from the top by repeating the above-mentioned experimental procedure. The central flat glass tube was L = 5.4 cm and the time interval was set to be Δt = 0.25 seconds for the automatic sequential digital bubble image acquisitions. Six different test pressures for each light crude oil–pure or impure CO_2 system were properly chosen in each series of six CO_2-bubble tests for the MMP determination. Overall, it took about 2–3 hours to complete the six RBA tests for determining the MMP of each light crude oil–CO_2 system at T_{res} = 53.0°C. However, 1–2 days was needed to prepare the test fluids, set up and clean the RBA, conduct a series of six CO_2-bubble tests at six different test pressures, and finally depressurize the entire RBA.

3.7 Dynamic Interfacial Tension (IFT) Measurements

Figure 3.4 shows a schematic diagram of the experimental setup used for measuring the dynamic interfacial tensions (IFTs) between the light crude oil and CO_2 by applying the axisymmetric drop shape analysis (ADSA) technique for the pendant drop case [Cheng *et al.*, 1990]. The major component of this experimental set-up was a see-through windowed high-pressure IFT cell (IFT-10, Temco, USA), whose maximum operating pressure and temperature are equal to P_{max} = 68.0 MPa and T_{max} = 177.0°C. A stainless steel syringe needle was installed at the top of the IFT cell and used to form a pendant oil drop. The light crude oil and CO_2 were stored in two transfer cylinders and heated to T_{res} = 53.0°C. Afterwards, pure CO_2 was injected into the high-pressure IFT cell by using a programmable syringe pump until a pre-specified test pressure was reached. Then the original light crude oil was introduced from its transfer cylinder to the syringe needle by

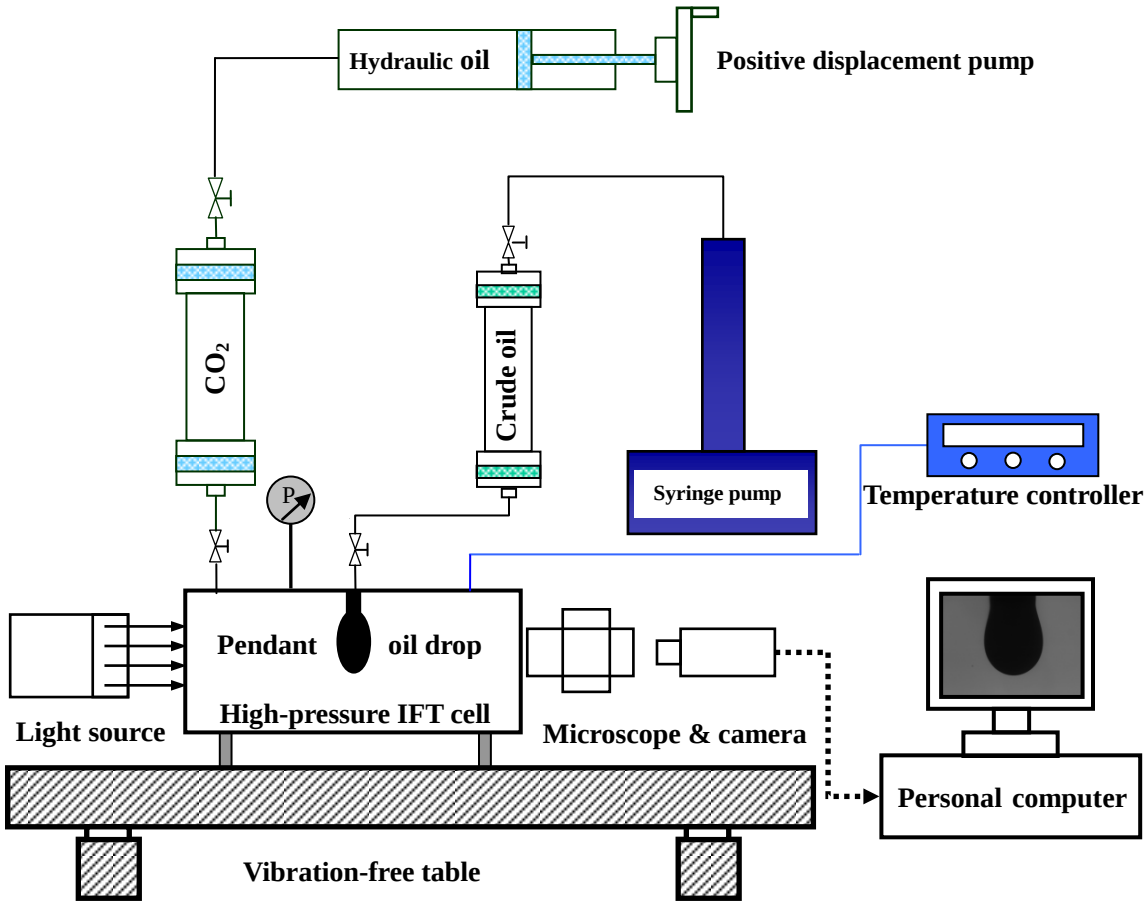

Figure 3.4 Schematic diagram of the experimental setup for measuring the dynamic interfacial tensions (IFTs) of different light crude oil–CO_2 systems under different experimental conditions by applying the axisymmetric drop shape analysis (ADSA) technique for the pendant drop case.

using another programmable syringe pump. A light source and a glass diffuser were used to provide uniform illumination for the pendant oil drop. A microscope camera was used to observe and capture the sequential digital images of the dynamic pendant oil drop surrounded by CO_2 inside the IFT cell at different times. The high-pressure IFT cell was positioned horizontally between the light source and the microscope camera. The entire system was placed on a vibration-free table (RS4000, Newport, USA). The digital image of the dynamic pendant oil drop surrounded by CO_2 at any time was acquired in a tagged image file format (TIFF) by using a digital frame grabber (Ultra II, Coreco Imaging, Canada) and stored in a DELL personal computer.

It is worthwhile to note that in this study, the ratio of the initial gas phase volume (V_{gas}) to the initial oil phase volume (V_{oil}) inside the high-pressure IFT cell was defined as the initial gas–oil ratio (GOR) in volume. The total volume of the IFT cell was measured to be V_{cell} = 49.5 cm^3. For example, the highest initial GOR was found to be 4000:1 in volume when there was no oil pre-injected into the IFT cell prior to each series of the dynamic IFT tests and if the average pendant oil drop size was assumed to be V_{drop} = 12.375 mm^3. On the other hand, the lowest initial GOR of 1:1 in volume was obtained when the light crude oil with the volume of $V_{oil} = 0.5V_{cell}$ was pre-injected into the IFT cell and its upper half was occupied by the gas phase (i.e., pure CO_2) prior to each series of the dynamic IFT tests.

After the pre-injected light crude oil and CO_2 phases inside the IFT cell reached a test pressure at the initial GORs other than 4000:1 in volume and T_{res} = 53.0°C, a pendant oil drop was introduced and formed at the tip of a stainless steel syringe needle. Its sequential digital images at different times were acquired and stored automatically. The

time interval for the sequential digital image acquisition was set to be smaller at the beginning and larger at a later time when the equilibrium IFT was almost achieved. The ADSA technique for the pendant drop case was applied to analyze the digital oil drop image and measure the dynamic IFT between the pendant oil drop and the CO_2 phase. The average IFT value of the three repeated IFT measurements at the same test conditions is reported in this study. The experimental error for such an average equilibrium IFT was found to be ±0.05 mJ/m^2 at each test pressure and T_{res} = 53.0°C, whose experimental errors were equal to ±0.01 MPa and ±0.1°C, respectively. Moreover, it should be noted that the experimental error for the determined MMP is estimated to be ±0.1 MPa. The ADSA program requires the local gravitational acceleration and density difference between the pendant oil drop and the surrounding CO_2 phase as the input data. In this study, the densities of the dead and live light crude oils at different IFT test conditions were measured by using a densitometer (DMA512P, Anton Paar, USA). The CO_2 density under the same IFT test conditions was predicted by using the CMG WinProp module. Five series of the dynamic IFT tests were conducted for the dead light crude oil–CO_2 system at five different initial GORs of 1:1, 3:1, 10:1, 200:1, 4000:1 in volume and T_{res} = 53.0°C and one more series of the dynamic IFT tests were carried out for the live light crude oil–CO_2 system at the initial GOR of 4000:1 in volume, whose experimental conditions are summarized in Table 3.8.

Table 3.8 Experimental conditions of six series of the dynamic interfacial tension (IFT) tests for the dead and live light crude oil–CO_2 systems at five different initial gas–oil ratios (GORs) in volume and the actual reservoir temperature of T_{res} = 53.0°C.

Test no.	Crude oil	GOR (V_{gas}:V_{oil})	Test pressures (MPa)
1	dead	1:1	4.1–10.0
2	dead	3:1	5.7–10.0
3	dead	10:1	4.0–9.6
4	dead	200:1	3.7–10.5
5	dead	4000:1	3.5–12.0
6	live	4000:1	1.8–11.4

CHAPTER 4 SLIM-TUBE TEST RESULTS AND DISCUSSION

Figure 4.1 shows the measured oil recovery factor (ORF) vs. pore volume (PV) of injected CO_2 in each of five slim-tube tests at five different injection pressures and a constant reservoir temperature of T_{res} = 53.0°C. As expected, the ORF increases with the PV of injected CO_2 at each injection pressure and finally reaches its maximum value after at most 1.2 PV of CO_2 is injected. Thus each slim-tube test was terminated at 1.2 PV of injected CO_2 in this study. More specifically, the measured ORFs at lower injection pressures of $P_{inj} \leq 12.0$ MPa are higher than those at higher injection pressures of $P_{inj} \geq 14.0$ MPa in the initial CO_2 injection periods. This is because at the same CO_2 volume injection rate, a larger portion of injected CO_2 displaces the live light crude oil through the slim tube and a smaller portion of injected CO_2 is dissolved into the live light crude oil due to a lower CO_2 solubility at a lower injection pressure [Cao and Gu, 2013]. Quick initial ORF increases occur prior to 0.3, 0.4, and 0.6 PV of injected CO_2, which correspond to P_{inj} = 7.0, 10.0, and 12.0 MPa. At $P_{inj} \geq 14.0$ MPa, the ORF is low at the beginning but increases continuously till almost 1.2 PV of injected CO_2. Therefore, it is inferred from Figure 4.1 that the live light crude oil and the injected CO_2 may be immiscible at $P_{inj} \leq 12.0$ MPa, near-miscible at P_{inj} = 14.0 MPa, and miscible at P_{inj} = 16.0 MPa. Such measured ORFs at 1.2 PV of injected CO_2 vs. injection pressures are listed in Table 4.1 and plotted to determine the minimum miscibility pressure (MMP) from the five slim-tube tests. In this study, two different MMP determination criteria, i.e., the ORF and break-over pressure (BOP) criteria, are applied, analyzed, and compared [Zhang and Gu, 2015].

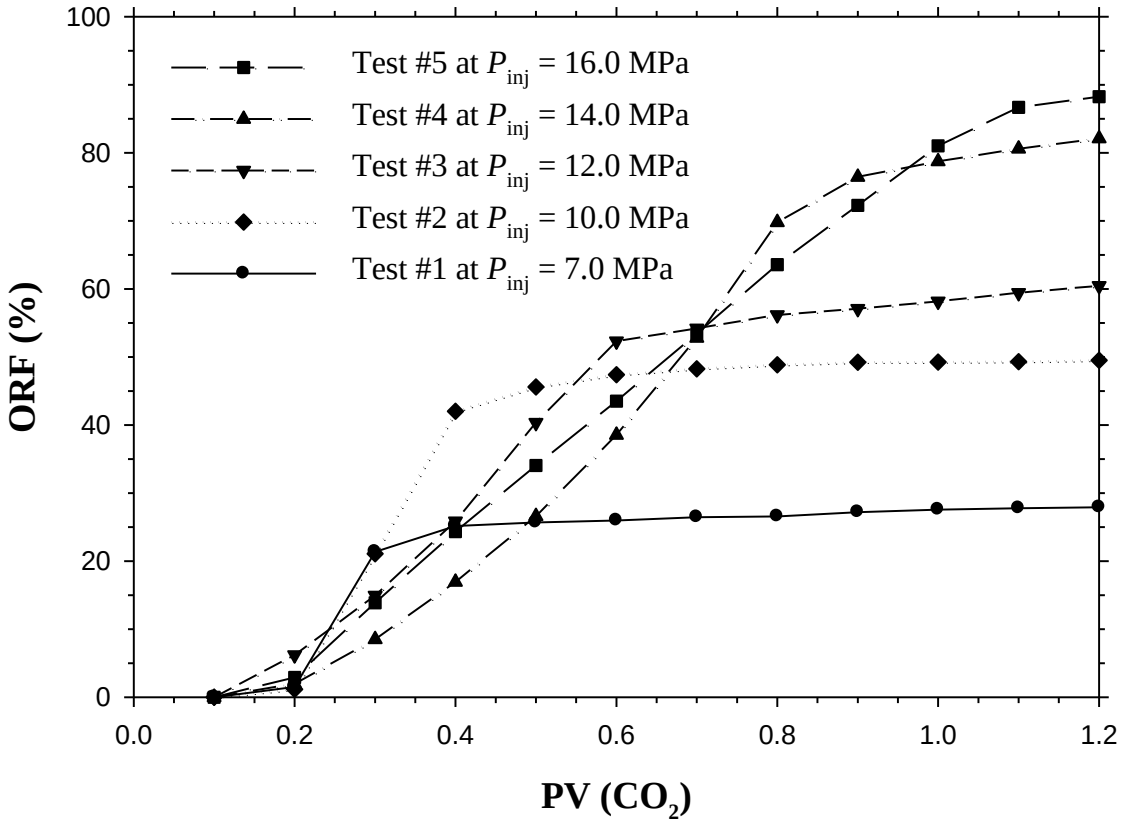

Figure 4.1 Measured oil recovery factor (ORF) vs. volume of injected CO_2 in terms of the pore volume (PV) in each slim-tube test at T_{res} = 53.0 ℃.

Table 4.1 Measured oil recovery factors (ORFs) of five slim-tube tests with the live light crude oil at 1.2 PV of injected pure CO_2 and the actual reservoir temperature of T_{res} = 53.0°C.

Test no.	S_{oi} (%)	P_{inj} (MPa)	ORF (%)
1	98.9	7.0	27.89
2	96.7	10.0	49.51
3	97.5	12.0	60.43
4	98.9	14.0	82.11
5	98.1	16.0	88.23

Notes: S_{oi}: Initial oil saturation

P_{inj}: CO_2 injection pressure

ORF: Oil recovery factor at 1.2 PV of injected CO_2 in terms of the original oil-in-place (OOIP)

4.1 Oil Recovery Factor (ORF) Criterion

Figures 4.2a and b show the linear and quadratic extrapolation methods for using the ORF criterion to determine the MMPs from the five slim-tube tests. By means of the linear or quadratic regression of the first four immiscible and near-miscible slim-tube test data, the MMP is equal to the abscissa value (i.e., the injection pressure) that corresponds to one of the three ordinate values (i.e., the threshold ORFs) of 88, 90, and 95%. It is worthwhile to point out that the first and lowest threshold ORF of 88% is chosen as it is closest to the ORF of 88.23% in the fifth slim-tube test at P_{inj} = 16.0 MPa. The corresponding MMPs are found to be 15.2, 15.4, and 16.1 MPa in Figure 4.2a, where the linear extrapolation method is applied. They are equal to 14.6, 14.8, and 15.3 MPa in Figure 4.2b, where the quadratic extrapolation method is used. Hence, the MMP is better given in a small pressure range than specified as a definitive pressure value if a high threshold ORF cannot be chosen uniquely. Moreover, the MMP determined from the linear extrapolation method is consistently higher than that from the quadratic extrapolation method if the same high threshold ORF is chosen. As expected, the correlation coefficient (R^2 = 0.984) for the former method is smaller than that (R^2 = 0.992) for the latter method.

Figure 4.3 depicts the linear intersection method for using the ORF criterion to determine the two MMPs from the five slim-tube tests with two intersection options chosen in this work. The first intersection option is to find the intersection point of the linear regression of the first four points and the linear regression of the last two points. In this case, the fourth point is used twice as the common point. The second intersection option is to find the intersection point of the linear regression of the first four points and

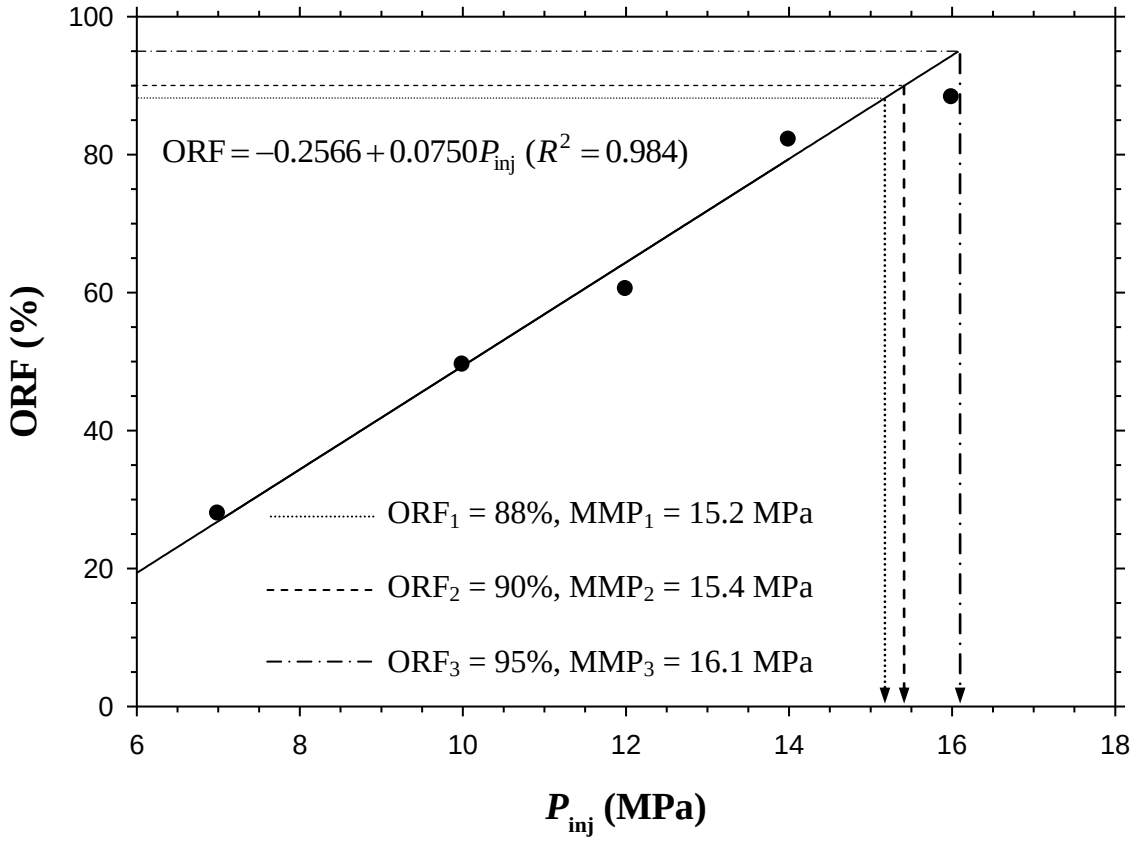

Figure 4.2(a) Determined minimum miscibility pressures (MMPs) of 15.2, 15.4, and 16.1 MPa from the ORF criterion, which correspond to three different threshold ORFs of 88, 90, and 95% by using the linear extrapolation of the first four immiscible and near-miscible slim-tube test data at T_{res} = 53.0°C.

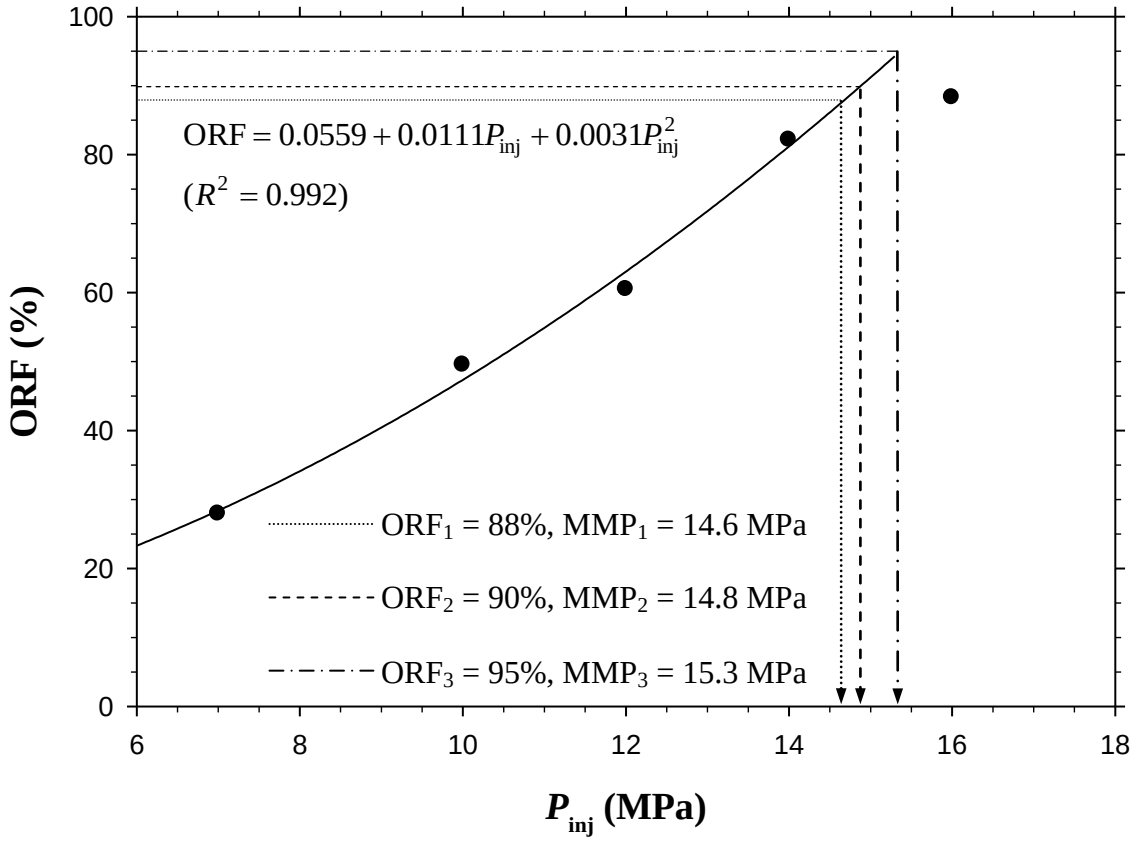

Figure 4.2(b) Determined minimum miscibility pressures (MMPs) of 14.6, 14.8, and 15.3 MPa from the ORF criterion, which correspond to three different threshold ORFs of 88, 90, and 95% by using the quadratic extrapolation of the first four immiscible and near-miscible slim-tube test data at T_{res} = 53.0°C.

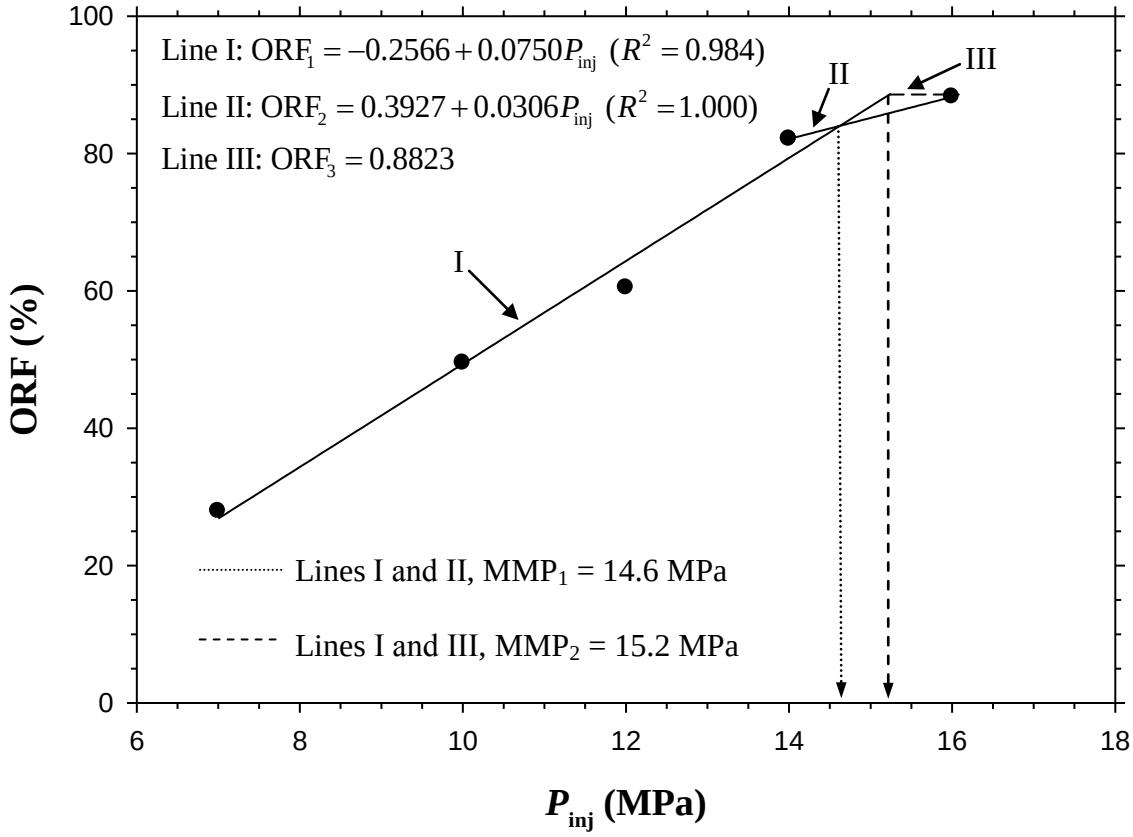

Figure 4.3 Determined minimum miscibility pressures (MMPs) of 14.6 and 15.2 MPa from the ORF criterion, which correspond to two intersection options by using the linear intersection of the five slim-tube test data at T_{res} = 53.0°C.

the fifth point. In principle, the linear intersection method determines the MMP by finding the sudden slope change point in the measured ORF vs. injection pressure curve. This curve is roughly divided into two distinct pressure ranges, i.e., the immiscible and miscible ranges. Based on the five measured ORF vs. injection pressure data of the five slim-tube tests conducted in this study, three straight lines (i.e., Lines I, II, and III) are obtained to represent three linear regression results of the first four, last two, and fifth ORF vs. injection pressure data. The two respective intersection options determine the intersection point of Lines I and II and the intersection point of Lines I and III, as plotted in Figure 4.3. The corresponding two abscissa values of the linear intersection points are equal to two different MMPs. As a result, they are determined to be 14.6 and 15.2 MPa from the linear intersection method for using the ORF criterion with the two intersection options.

4.2 Break-Over Pressure (BOP) Criterion

The MMPs determined by using the above-mentioned two intersection options of the linear intersection method with the ORF criterion may not be accurate enough if the slope change or break-over point is not sharp enough in the measured ORF vs. injection pressure curve [Elsharkawy *et al.*, 1996]. In this case, the BOP criterion is often used to determine the MMP. In terms of this criterion, the MMP is chosen as the injection pressure at which the incremental ORF per incremental injection pressure increase reaches an arbitrarily chosen low threshold slope. Figure 4.4 shows the cubic regression curve of the five measured ORF vs. injection pressure data:

$$\mathrm{ORF} = 0.8311 - 0.2379P_{\mathrm{inj}} + 0.0288P_{\mathrm{inj}}^2 - 0.0009P_{\mathrm{inj}}^3 \quad (R^2 = 0.989) \tag{4.1}$$

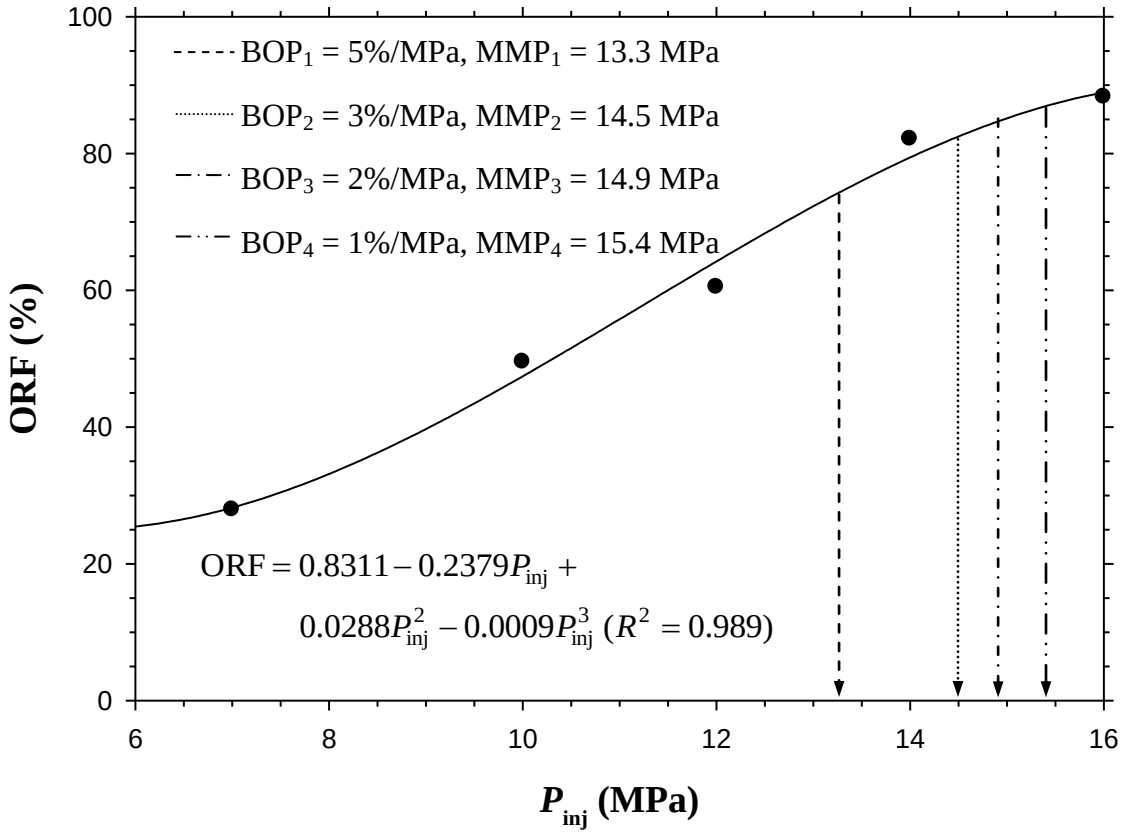

Figure 4.4 Four determined minimum miscibility pressures (MMPs) of 13.3, 14.5, 14.9, and 15.4 MPa from the BOP criterion, which correspond to four different threshold slopes of 5, 3, 2, and 1%/MPa by using the cubic regression of the five slim-tube test data at T_{res} = 53.0°C.

The differentiation of the above cubic function yields:

$$\mathrm{ORF}' = -0.2379 + 0.0576P_{\mathrm{inj}} - 0.0027P_{\mathrm{inj}}^2 \tag{4.2}$$

Equation (4.2) can be used to determine the slope of the cubic regression curve at any point, which represents the incremental ORF per incremental injection pressure increase at any injection pressure. Thus a different MMP is determined from the BOP criterion by using the cubic regression of the five slim-tube test data if a different derivative of the ORF with respect to the injection pressure is chosen. In this study, four different MMPs of 13.3, 14.5, 14.9, and 15.4 MPa are obtained from Equation (4.2), which correspond to four different low threshold slopes or incremental ORFs per incremental injection pressure increase of 5, 3, 2, and 1%/MPa, respectively.

4.3 Comparison of the ORF and BOP Criteria

In this work, the ORF and BOP criteria are used to determine the MMPs from the five slim-tube tests and detailed results are summarized and compared in Table 4.2. More specifically, the linear and quadratic extrapolation methods with three different high threshold ORFs as well as the linear intersection method with two different intersection options are used in the ORF criterion. The cubic regression method with four different low threshold slopes is adopted in the BOP criterion. It is found that different MMP ranges with respect to different threshold values or intersection options are obtained from the same measured ORF vs. injection pressure data if different MMP determination criteria and/or regression methods are employed. Therefore, the MMP is better given in a small pressure range than specified as a unique pressure value in terms of either MMP determination criterion. It is also anticipated that a small common MMP range may be found for a given light crude oil–CO_2 system.

Table 4.2 Determined minimum miscibility pressures (MMPs) and MMP ranges of the live light crude oil–CO_2 system from five slim-tube tests in terms of the oil recovery factor (ORF) and break-over pressure (BOP) criteria at the actual reservoir temperature of T_{res} = 53.0°C.

MMP criterion	Regression method	Threshold value	MMP (MPa)	MMP range (MPa)	Common MMP range (MPa)
ORF	Linear extrapolation[a]	88%	15.2	15.2–16.1	15.2–15.4
		90%	15.4		
		95%	16.1		
	Quadratic extrapolation[b]	88%	14.6	14.6–15.3	
		90%	14.8		
		95%	15.3		
	Linear intersection	Option #1[c]	14.6	14.6–15.2	
		Option #2[d]	15.2		
BOP	Cubic regression	5%/MPa	13.3	13.3–15.4	
		3%/MPa	14.5		
		2%/MPa	14.9		
		1%/MPa	15.4		

Notes:
a: linear regression of the first four points only, which represent four immiscible and near-miscible slim-tube test data
b: quadratic regression of the first four points only, which represent four immiscible and near-miscible slim-tube test data
c: linear regression of the first four points and linear regression of the last two points, where the fourth point is used as the common point
d: linear regression of the first four points and usage of the last or fifth point

Table 4.2 indicates that as expected, the MMP determined from the ORF criterion is higher if a higher threshold ORF from 88, 90, to 95% is chosen. The determined MMPs by using the linear extrapolation method are higher than those by using the quadratic extrapolation method. In addition, the MMPs are equal to 14.6 and 15.2 MPa in terms of the ORF criterion by using the linear intersection method with the two intersection options. These two MMPs agree well with the MMPs determined by using the quadratic extrapolation method. On the other hand, the BOP criterion is based on the cubic regression of the five measured ORF vs. injection pressure data. The cubic regression method used in the BOP criterion is generally considered to best depict the data trend, in comparison with the linear and quadratic extrapolation methods used in the ORF criterion. It is also found that nevertheless, the MMP determined from the BOP criterion is especially sensitive to the low threshold slope (e.g., 5, 3, 2, and 1%/MPa) to be chosen.

Figure 4.5 shows the MMP ranges determined from the ORF criterion by using the linear and quadratic extrapolation methods with three different high threshold ORFs. The MMP ranges of 15.2–16.1 and 14.6–15.3 MPa determined by using these two extrapolation methods from the five slim-tube tests are considered to be more accurate in this study. This finding is consistent with a conclusion made in the literature [Wu and Batycky, 1990], where the MMP determined from the ORF criterion by using the linear intersection method with either intersection option was considered to be less accurate. In addition, the MMPs determined from the BOP criterion by using the cubic regression method are in a much lower pressure range. The determined MMPs are more accurate if lower threshold slopes of 2 to 1%/MPa are used in the BOP criterion. In terms of both the ORF and BOP criteria with different MMP determination methods and threshold values

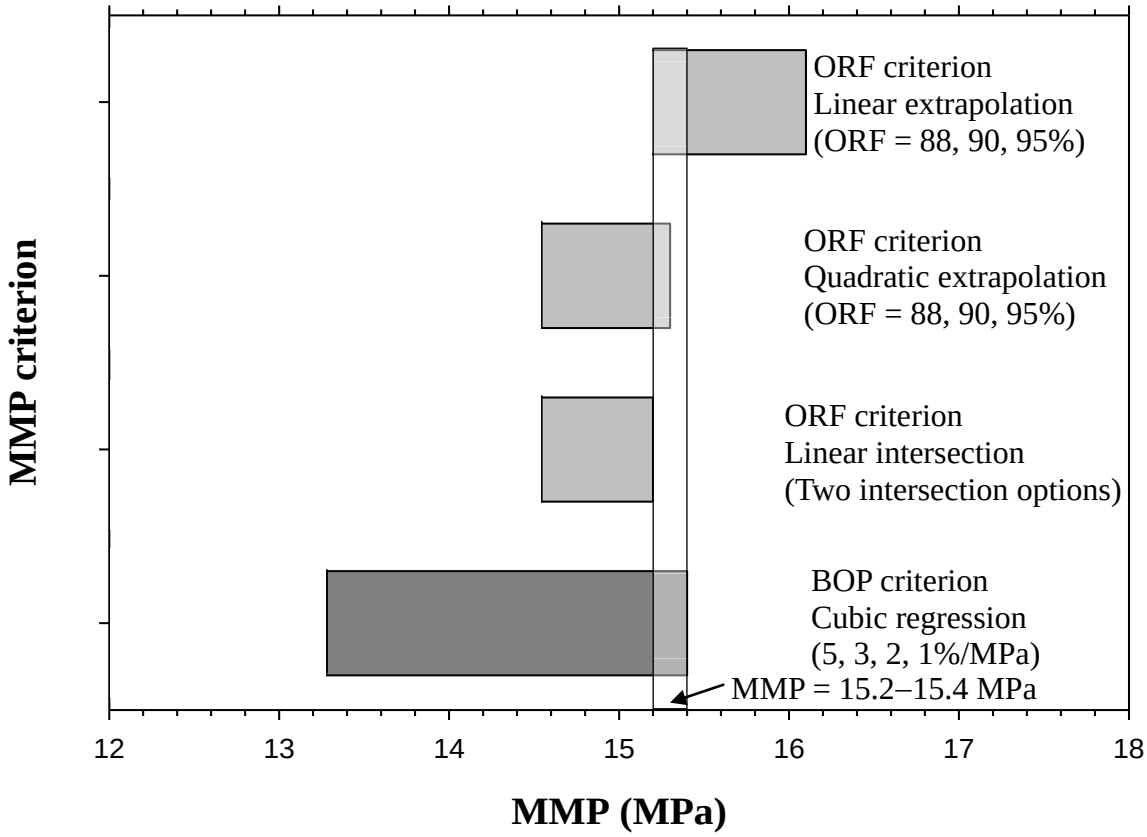

Figure 4.5 The MMP ranges and the common MMP range (MMP = 15.2–15.4 MPa) determined from the ORF and BOP criteria for the five slim-tube tests at T_{res} = 53.0°C.

or intersection options, a small common MMP range of 15.2–15.4 MPa is found for the live light crude oil–CO_2 system used in the five slim-tube tests. This small common MMP range is given in Table 4.2 and marked in Figure 4.5.

CHAPTER 5 COREFLOOD TEST RESULTS AND DISCUSSION

Figure 5.1 shows the measured oil recovery factor (ORF) vs. pore volume (PV) of injected CO_2 for the five coreflood tests with the dead light crude oil–CO_2 system at five different injection pressures. The ORF increases with the PV of injected CO_2 at each injection pressure and finally reaches its maximum value after at most 1.3 PV of CO_2 is injected. In this study, each CO_2 coreflood test was terminated at 2.0 PV of injected CO_2 when no more oil was produced. A quick increase of the initial ORF occurs at P_{inj} = 7.2 MPa. At P_{inj} = 9.2 MPa, the slowest increase of the initial ORF is found and attributed to an increased solubility of supercritical CO_2 in the dead light crude oil [Cao and Gu, 2013]. When the injection pressure is at or above 10.4 MPa, a substantial increase of the ORF is obtained at the end of each coreflood test. Hence, it is speculated from Figure 5.1 that the dead light crude oil–CO_2 system may be immiscible at $P_{inj} \leq 9.2$ MPa, near-miscible at P_{inj} = 10.4 or 12.1 MPa, and miscible at P_{inj} = 14.0 MPa. The measured final ORFs at 2.0 PV of injected CO_2 vs. injection pressures for the five coreflood tests are summarized and given in Table 5.1.

5.1 Oil Recovery Factor (ORF) Criterion

Figures 5.2a and b show the linear and quadratic extrapolation methods to determine the minimum miscibility pressures (MMPs) from the five coreflood tests in terms of the ORF criterion. Three MMPs of 12.3, 12.9, and 14.0 MPa are determined by using the linear extrapolation method in Figure 5.2a, which correspond to three high threshold ORFs of 87, 90, and 95%, respectively. It should be noted that the first and lowest threshold ORF of 87% is chosen as it is closest to the ORF of 87.03% in the fifth

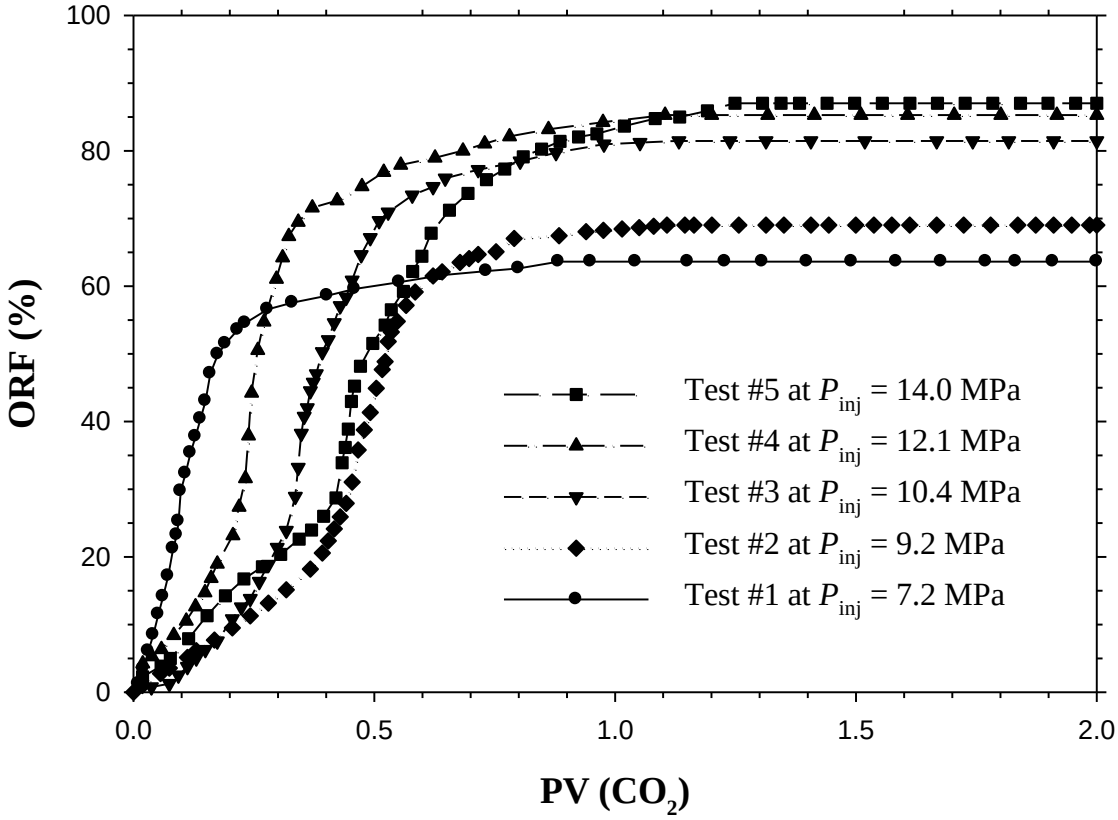

Figure 5.1 Measured oil recovery factor (ORF) vs. volume of injected CO_2 in terms of pore volume (PV) in each coreflood test at T_{res} = 53.0°C.

Table 5.1 Measured oil recovery factors (ORFs) of five coreflood tests with the dead light crude oil at 2.0 PV of injected pure CO_2 and the actual reservoir temperature of T_{res} = 53.0°C.

Test no.	P_{inj} (MPa)	ORF (%)
1	7.2	63.62
2	9.2	69.03
3	10.4	81.45
4	12.1	85.26
5	14.0	87.03

Notes: P_{inj}: CO_2 injection pressure

ORF: Oil recovery factor at 2.0 PV of injected CO_2 in terms of the original oil-in-place (OOIP)

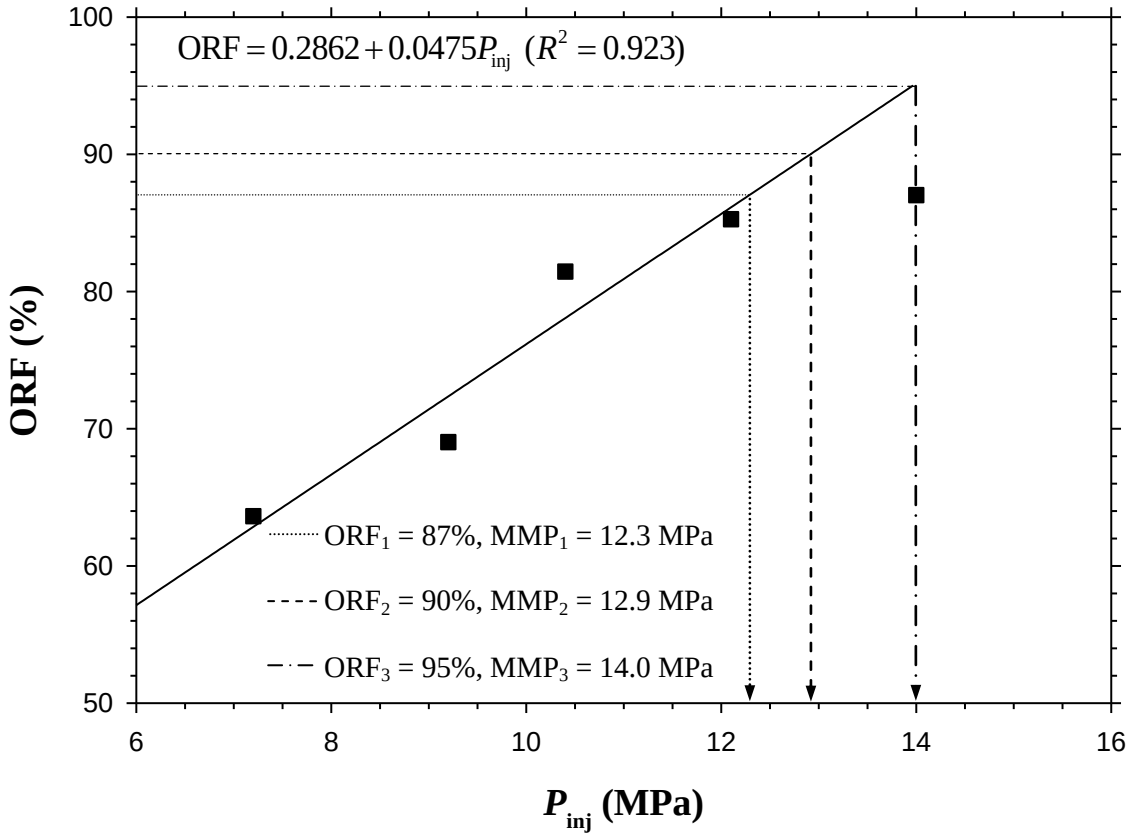

Figure 5.2(a) Determined minimum miscibility pressures (MMPs) of 12.3, 12.9, and 14.0 MPa from the ORF criterion, which correspond to three different threshold ORFs of 87, 90, and 95% by using the linear extrapolation of the first four immiscible and near-miscible coreflood test data at T_{res} = 53.0°C.

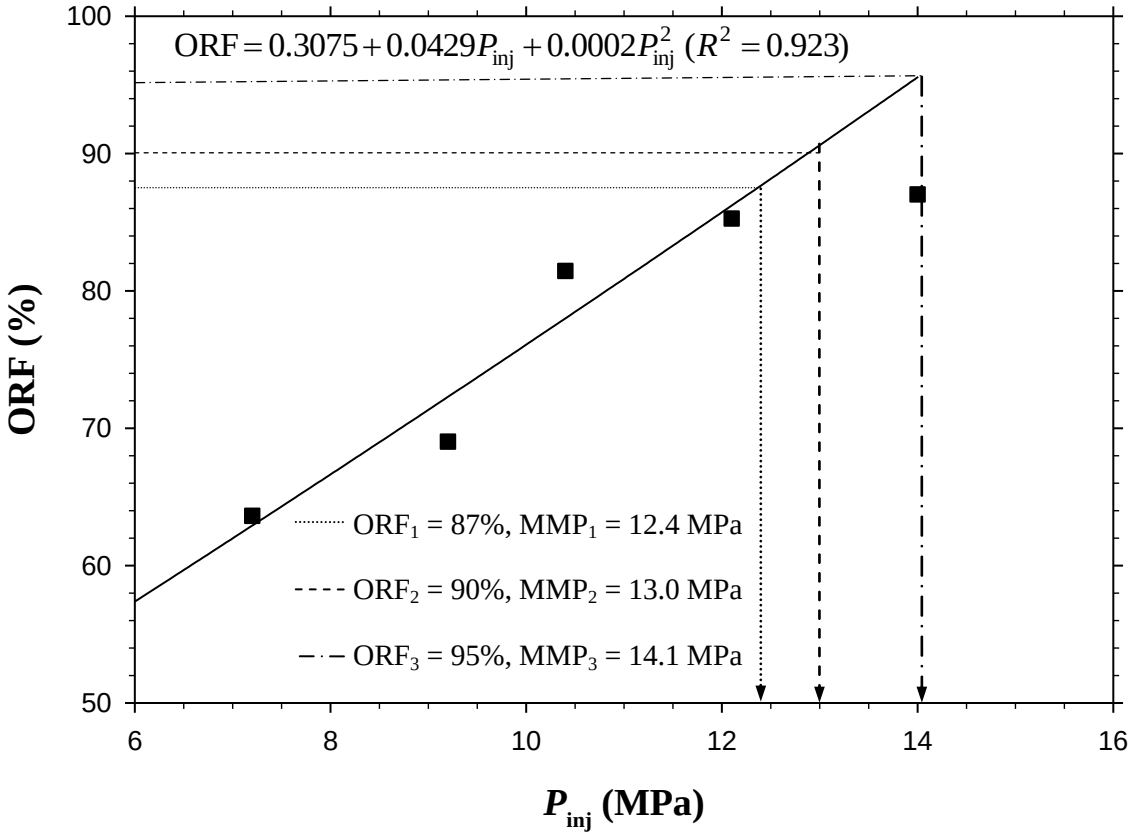

Figure 5.2(b) Determined minimum miscibility pressures (MMPs) of 12.4, 13.0, and 14.1 MPa from the ORF criterion, which correspond to three different threshold ORFs of 87, 90, and 95% by using the quadratic extrapolation of the first four immiscible and near-miscible coreflood test data at T_{res} = 53.0°C.

coreflood test at P_{inj} = 14.0 MPa. Similarly, three determined MMPs are equal to 12.4, 13.0, and 14.1 MPa by using the quadratic extrapolation method in Figure 5.2b, which correspond to the three same threshold ORFs. Each MMP obtained from the latter method is 0.1 MPa higher than that obtained from the former method if the same threshold ORF is used in the ORF criterion. On the other hand, Figure 5.3 shows the linear intersection method for determining the MMP in terms of the ORF criterion from the five coreflood tests. Here, the same two intersection options as those for the five slim-tube tests are adopted to determine two MMPs, respectively. Based on the five measured ORF vs. injection pressure data, two approximate injection pressure ranges are determined, i.e., P_{inj} = 7.2–12.1 MPa for the immiscible and near-miscible cases and P_{inj} = 14.0 MPa for the miscible case. As plotted in Figure 5.3, three straight lines (i.e., Lines I, II, and III) stand for three respective linear regression lines of the first four, last two, and fifth ORF vs. injection pressure data. The first MMP for the first intersection option is determined to be 11.9 MPa at the linear intersection point of Lines I and II. The second MMP of 12.3 MPa for the second intersection option corresponds to the linear intersection point of Lines I and III.

5.2 Break-Over Pressure (BOP) Criterion

The break-over pressure (BOP) criterion is also used to determine the MMPs from the five coreflood tests. Figure 5.4 shows the cubic regression curve of the five measured ORF vs. injection pressure data:

$$\mathrm{ORF} = 2.2385 - 0.5681P_{inj} + 0.0631P_{inj}^2 - 0.0021P_{inj}^3 \quad (R^2 = 0.962) \tag{5.1}$$

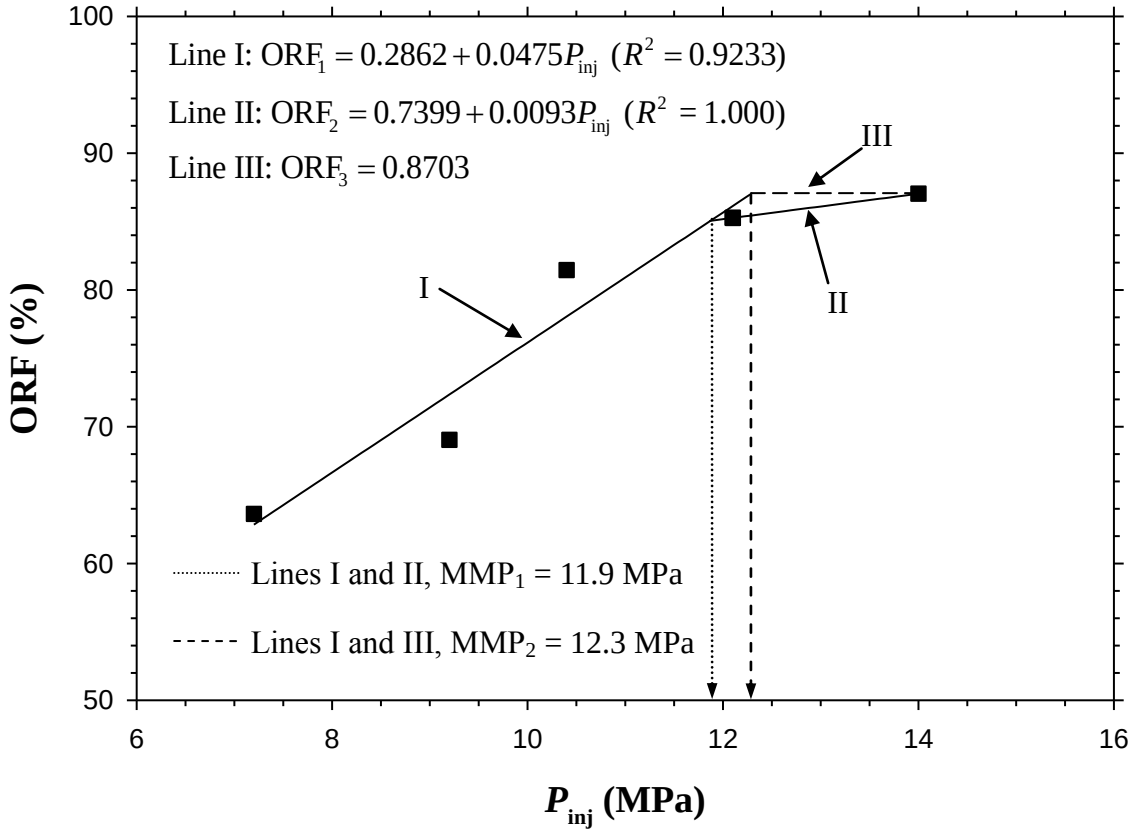

Figure 5.3 Determined minimum miscibility pressures (MMPs) of 11.9 and 12.3 MPa from the ORF criterion, which correspond to two intersection options by using the linear intersection of the five coreflood test data at T_{res} = 53.0°C.

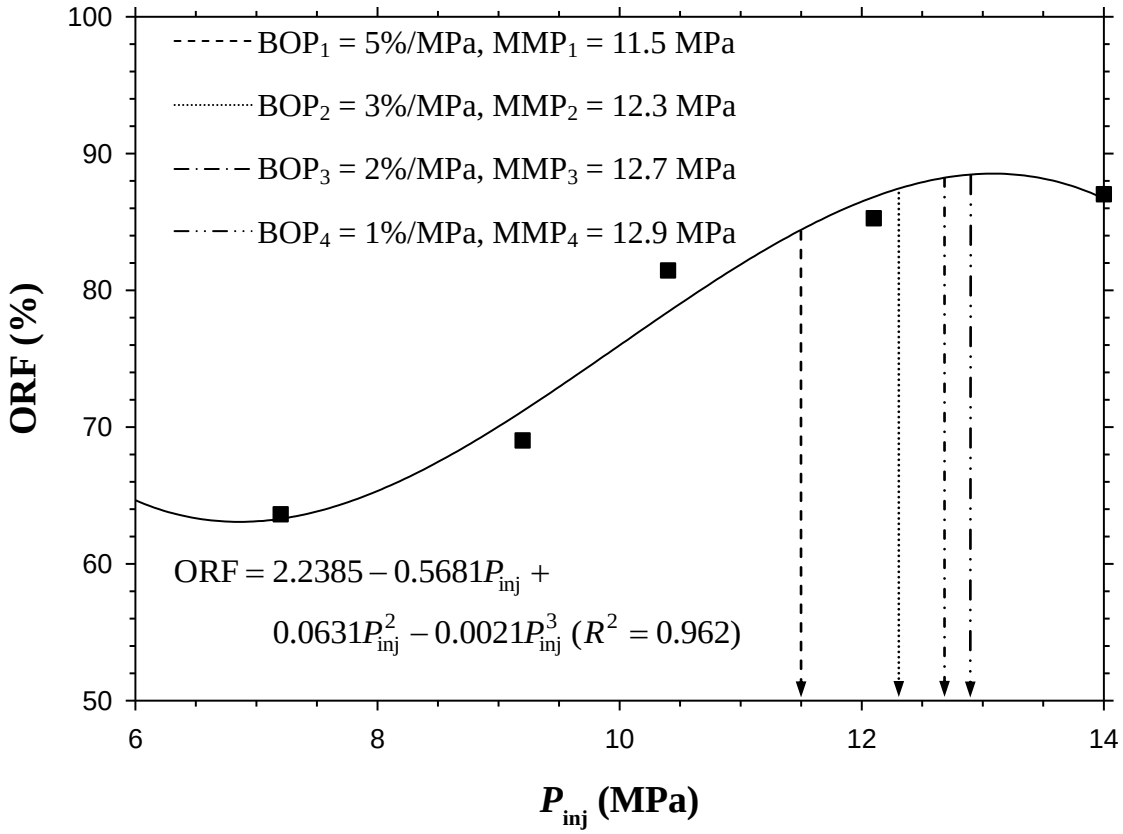

Figure 5.4 Four determined minimum miscibility pressures (MMPs) of 11.5, 12.3, 12.7, and 12.9 MPa from the BOP criterion, which correspond to four different threshold slopes of 5, 3, 2, and 1%/MPa by using the cubic regression of the five coreflood test data at T_{res} = 53.0°C.

The differentiation of the above cubic ORF function with respect to the injection pressure P_{inj} gives:

$$ORF' = -0.5681 + 0.1262P_{inj} - 0.0063P_{inj}^2 \quad (5.2)$$

In a similar manner to the BOP criterion used to determine the MMPs from the five slim-tube tests, four MMPs are found to be 11.5, 12.3, 12.7, and 12.9 MPa from the five coreflood tests if four different low threshold slopes or incremental ORFs per incremental injection pressure increase of 5, 3, 2, and 1%/MPa are used in Equation (5.2), respectively. It should be noted that there is an abnormal decrease in the beginning or ending section of the cubic regression curve, which is attributed to the inherent shortcoming of the cubic regression.

5.3 Comparison of the ORF and BOP Criteria

Table 5.2 summarizes four different MMP ranges, which are determined from the five coreflood tests by using four different methods with different threshold values or intersection options in terms of the ORF and BOP criteria, respectively. It is worthwhile to reiterate that the MMP is better represented by a small pressure range than specified as a unique pressure value. Figure 5.5 shows the common MMP range of 12.4–12.9 MPa in terms of the ORF and BOP criteria. However, the MMP range determined by using the linear intersection method with two intersection options is in a much lower pressure range, in comparison with those determined by using the linear and quadratic extrapolation methods with different high threshold ORFs. The linear intersection method is sensitive to the distribution of the five measured ORF vs. injection pressure data. Furthermore, the determined MMPs are more accurate if relatively lower threshold slopes of 3–1%/MPa rather than a higher threshold slope of 5%/MPa are used in the BOP criterion.

Table 5.2 Determined minimum miscibility pressures (MMPs) and MMP ranges of the dead light crude oil–CO_2 system from five coreflood tests in terms of the oil recovery factor (ORF) and break-over pressure (BOP) criteria at the actual reservoir temperature of T_{res} = 53.0°C.

MMP criterion	Regression method	Threshold value	MMP (MPa)	MMP range (MPa)	Common MMP range (MPa)
ORF	Linear extrapolation[a]	87%	12.3	12.3–14.0	12.4–12.9
		90%	12.9		
		95%	14.0		
	Quadratic extrapolation[b]	87%	12.4	12.4–14.1	
		90%	13.0		
		95%	14.1		
	Linear intersection	Option #1[c]	11.9	11.9–12.3	
		Option #2[d]	12.3		
BOP	Cubic regression	5%/MPa	11.5	11.5–12.9	
		3%/MPa	12.3		
		2%/MPa	12.7		
		1%/MPa	12.9		

Notes:
a: linear regression of the first four points only, which represent four immiscible and near-miscible coreflood test data
b: quadratic regression of the first four points only, which represent four immiscible and near-miscible coreflood test data
c: linear regression of the first four points and linear regression of the last two points, where the fourth point is used twice as the common point
d: linear regression of the first four points and usage of the last or fifth point

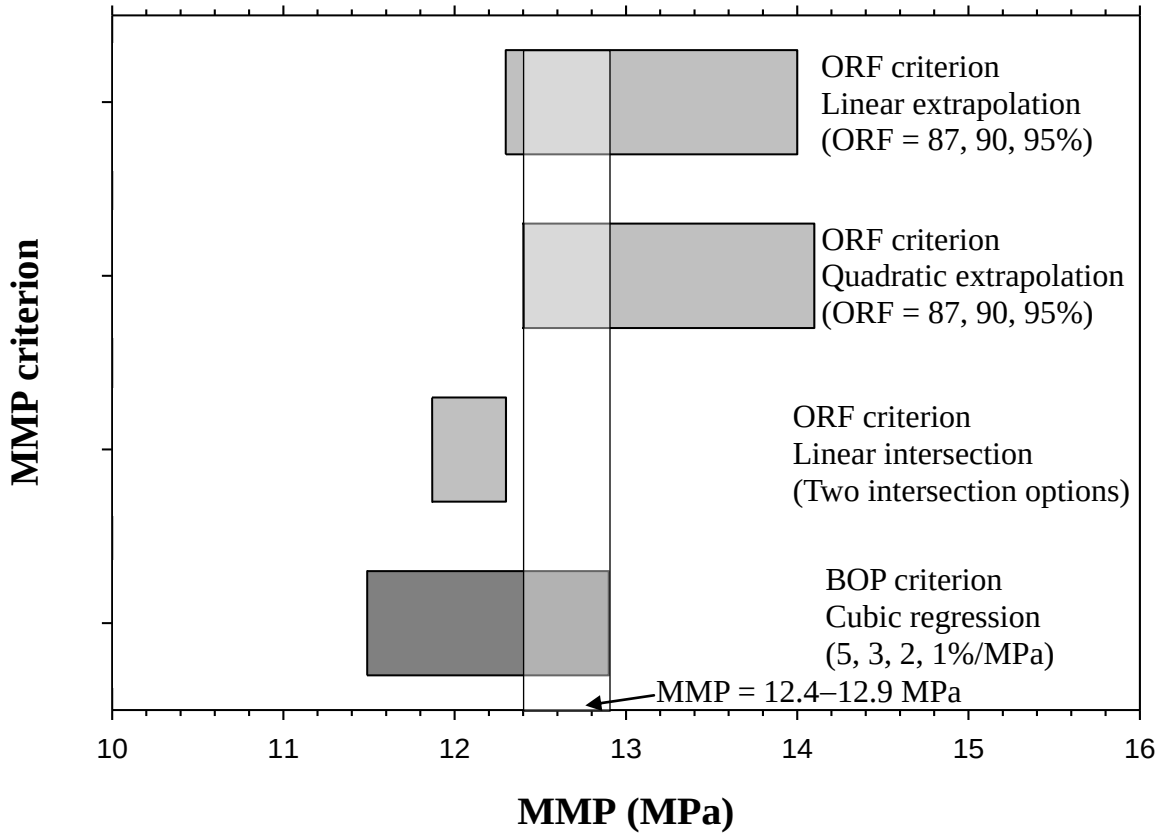

Figure 5.5 The MMP ranges and the common MMP range (MMP = 12.4–12.9 MPa) determined from the ORF and BOP criteria for the five coreflood tests at T_{res} = 53.0°C.

In summary, the linear and quadratic extrapolation methods in terms of the ORF criterion are more accurate for determining the MMP from the slim-tube or coreflood tests. On the other hand, caution should be taken when the linear intersection method in terms of the ORF criterion is used to determine the MMP from the slim-tube or coreflood tests as it is sensitive to the distribution of the measured ORF vs. injection pressure data. In this study, the first four immiscible and near-miscible slim-tube or coreflood test data are chosen and included in the first injection pressure range in order to apply the linear intersection method and determine the MMP more accurately. Moreover, it is worthwhile to note that the live light crude oil–CO_2 system was used in the five slim-tube tests, whereas the dead light crude oil–CO_2 system was used in the five coreflood tests in this work. Accordingly, the detailed experimental results in Table 4.2 and Figure 4.5 as well as Table 5.2 and Figure 5.5 indicate that the determined MMP range of 15.2–15.4 MPa for the live light crude oil–CO_2 system is significantly higher than the determined MMP range of 12.4–12.9 MPa for the dead light crude oil–CO_2 system.

CHAPTER 6 TEST RESULTS AND DISCUSSION OF RISING-BUBBLE APPARATUS (RBA)

6.1 Qualitative Criteria

6.1.1 Light crude oil–pure CO_2 system

In this study, the first series of six CO_2-bubble tests with the rising-bubble apparatus (RBA) were conducted for the light crude oil–pure CO_2 system at T_{res} = 53.0°C [Zhang and Gu, 2016a]. Figures 6.1a–f show the sequential digital images of the rising pure CO_2 bubbles through the light crude oil column at six different test pressures, P = 8.5, 9.5, 10.5, 12.0, 13.0, and 13.2 MPa, respectively. It is observed that the rising pure CO_2-bubble shape, size, colour, and rising height vary as the bubble rises through the light crude oil column in each test. Overall, they strongly depend on the test pressure. In the first lower test pressure range of P = 8.5, 9.5, and 10.5 MPa, as shown in Figures 6.1a–c, the pure CO_2 bubbles are similar to each other in terms of the bubble shape, size, colour, and rising height. More specifically, the bubble has a spherical (P = 8.5 MPa) or conic (P = 9.5 and 10.5 MPa) cap due to a relatively higher interfacial tension (IFT), while its bottom remains flat due to a much lower IFT. The bubble shrinks slightly and is transparent during its rising process. The pure CO_2 bubble can reach the top of the light crude oil column inside the central flat glass tube of L = 5.4 cm. At P = 12.0, 13.0, and 13.2 MPa, as shown in Figures 6.1d–f, initially, the bubble has an ellipsoidal cap at the top and one mixing tail at the bottom. Then the bubble becomes elongated and fuzzy. It tends to disappear gradually and cannot reach the top of the light crude oil column. Near the end, the pure CO_2 bubble breaks into two parts. The upper part moves upwards much faster than the lower part in the second higher test pressure range.

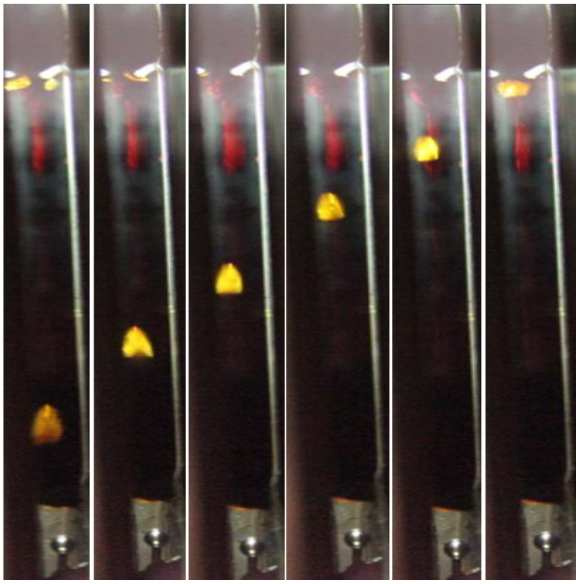

(a) 8.5 MPa

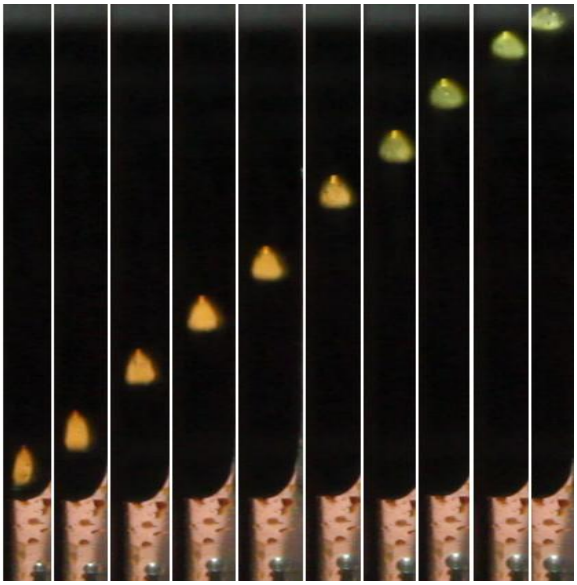

(b) 9.5 MPa

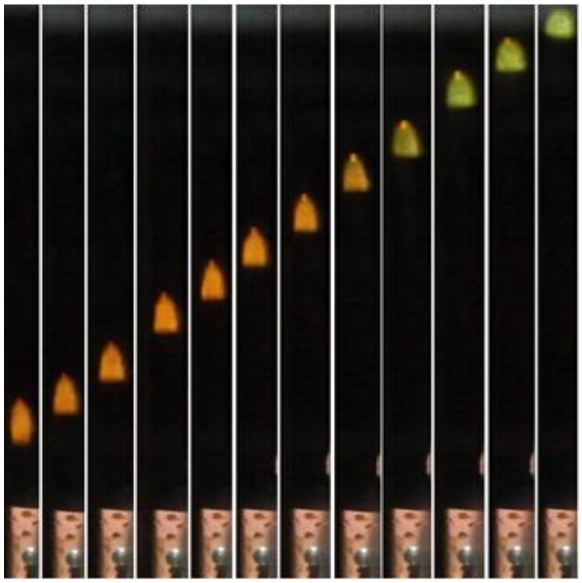

(c) 10.5 MPa

Figure 6.1(a–c) Sequential digital images of rising pure CO_2 bubbles through the light crude oil column inside a central flat glass tube of L = 5.4 cm with the time interval of Δt = 0.25 s at T_{res} = 53.0°C and three lower test pressures of **(a)** 8.5 MPa; **(b)** 9.5 MPa; and **(c)** 10.5 MPa.

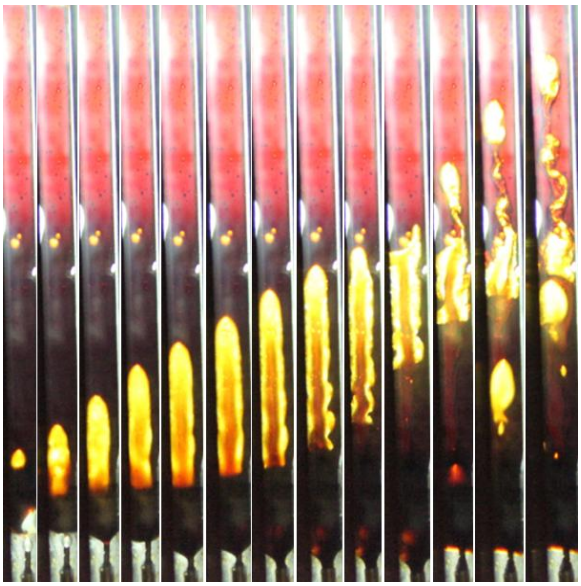

(d) 12.0 MPa

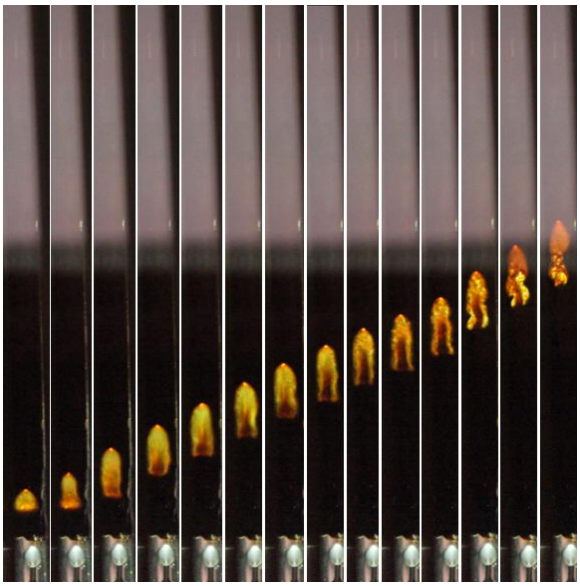

(e) 13.0 MPa

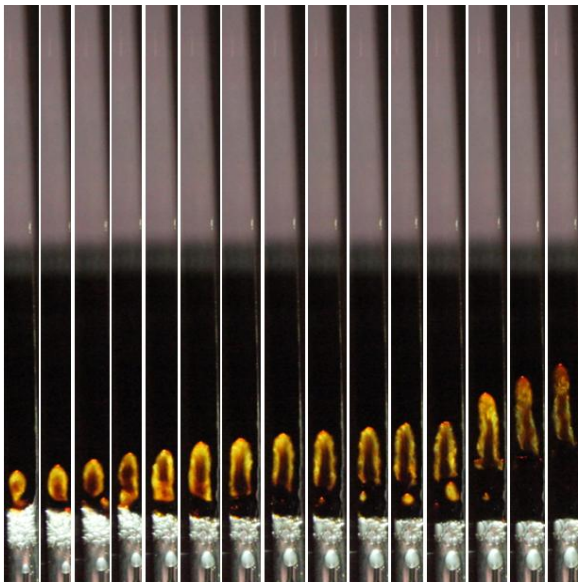

(f) 13.2 MPa

Figure 6.1(d–f) Sequential digital images of rising pure CO_2 bubbles through the light crude oil column inside a central flat glass tube of L = 5.4 cm with the time interval of Δt = 0.25 s at T_{res} = 53.0°C and three higher test pressures of **(d)** 12.0 MPa; **(e)** 13.0 MPa; and **(f)** 13.2 MPa.

In this work, four existing qualitative technical criteria, which are based on the overall bubble appearance, are applied to estimate the minimum miscibility pressure (MMP) of the light crude oil–pure CO_2 system at T_{res} = 53.0°C. Table 6.1 summarizes the overall bubble appearances for the light crude oil–pure CO_2 system at six different test pressures in terms of the bubble shape, size, colour, and rising height. It is inferred from these four qualitative criteria that the light crude oil and pure CO_2 may be immiscible at $P \leq 10.5$ MPa and miscible at $P \geq 12.0$ MPa. In addition, it is found that the bubble breaks into two parts near the end of each test at $P \geq 12.0$ MPa, which is referred to as a new bubble break-up (BBU) qualitative technical criterion for estimating the MMP and also included in Table 6.1. The BBU is a result of the strong mutual interactions between the light crude oil and the pure CO_2 bubble at a high test pressure. The upper part of the broken bubble consists of relatively pure CO_2 and thus has a much higher IFT with the oil phase, whereas its lower part is composed of pure CO_2 and some extracted hydrocarbons (HCs) and thus has a much lower IFT with the oil phase. The upper part is quickly separated from the lower part due to the IFT imbalance so that the bubble breaks up near the end of each test at $P \geq 12.0$ MPa. The estimated MMP range of 10.5–12.0 MPa by using the BBU criterion is found to be the same as the MMP range estimated by using the bubble-shape, size, colour, and rising height criteria. Hence, the BBU is proposed as the fifth qualitative technical criterion for estimating the MMP in this study.

It is worthwhile to point out that the technical interpretation of the miscibility development and the MMP estimation from the above-mentioned five qualitative criteria can be inappropriate, inaccurate, and even subjective in some cases. Moreover, the overall bubble appearance can also be considerably affected by some experimental

Table 6.1 Qualitative criteria based on the overall bubble appearance for estimating the minimum miscibility pressure (MMP) of the light crude oil–pure CO_2 system at the actual reservoir temperature of T_{res} = 53.0°C from the rising-bubble apparatus (RBA) tests.

Pressure (MPa)	Bubble shape (top + bottom)	Bubble size	Bubble colour	Bubble height	Bubble break-up (BBU)	Relative to the MMP	MMP (MPa)
8.5	spherical + flat	shrink	transparent	to the top	no	below	10.5–12.0
9.5	conic + flat	shrink	transparent	to the top	no	below	
10.5	**conic + flat**	**shrink**	**transparent**	**to the top**	**no**	**near**	
12.0	**ellipsoidal + tail**	**elongate → break up**	**fuzzy**	**near the top**	**yes**	**above**	
13.0	ellipsoidal + tail	elongate → break up	fuzzy	midway	yes	above	
13.2	ellipsoidal + tail	elongate → break up	fuzzy	small	yes	above	
References	[Christiansen and kim, 1986; Christiansen and Haines, 1987]	[Sibbald *et al*., 1991; Rao and Lee, 2003]	[Elsharkawy *et al*., 1996]	[Poettmann *et al*., 1992]	This study		

Notes: The first highlighted row in the bold face indicates the lower limit of the estimated MMP range;
The second highlighted row in the bold face indicates the upper limit of the estimated MMP range.

factors. For example, the optical focus of the digital camera and the light intensity of the light source may affect the bubble shape, size, and colour. The bubble size also strongly depends on the needle size and test pressure, whereas the maximum bubble-rising height depends on the total height of the thin glass tube used to hold the light crude oil column in the RBA tests. Furthermore, the estimated MMP range relies on the proper selection and specific interval of the test pressures to some extent. For instance, the estimated MMP range of the light crude oil–pure CO_2 system would be smaller if 2–3 more tests were conducted in the pressure range of 10.5–12.0 MPa.

6.1.2 Light crude oil–impure CO_2 system

The second series of six CO_2-bubble tests with the RBA were performed for the light crude oil–impure CO_2 system at T_{res} = 53.0°C. The impure CO_2 sample was composed of 74.87 mol.% CO_2 + 25.13 mol.% CH_4. Figures 6.2a–f show the sequential digital images of the rising impure CO_2 bubbles through the light crude oil column at six different test pressures, i.e., 21.0, 22.0, 23.0, 24.0, 25.0, and 26.0 MPa, respectively. It is observed that at $P \leq 23.0$ MPa, the impure CO_2 bubbles have conic caps and their sizes are reduced slightly with time. They are transparent at P = 21.0 and 22.0 MPa but become fuzzy at P = 23.0 MPa. Moreover, they can reach the top of the light crude oil column at P = 21.0–23.0 MPa. Figures 6.2a–c indicate that the light crude oil and the impure CO_2 may be immiscible at $P \leq 22.0$ MPa and near-miscible at P = 23.0 MPa. As depicted in Figures 6.2d–f, each impure CO_2 bubble has an ellipsoidal cap and a mixing tail most times. It is found that the impure CO_2 bubble breaks into two parts near the end of each test at $P \geq 24.0$ MPa. The bubble is slightly elongated until it breaks up. It becomes fuzzy and rises slowly through the light crude oil column prior to its break-up. Therefore, the

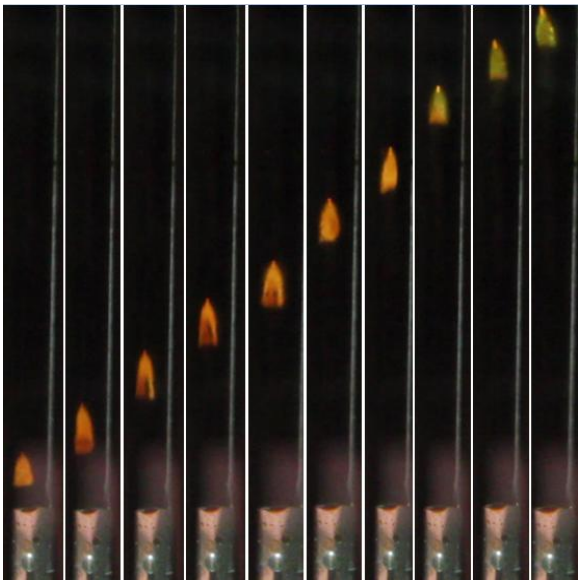

(a) 21.0 MPa

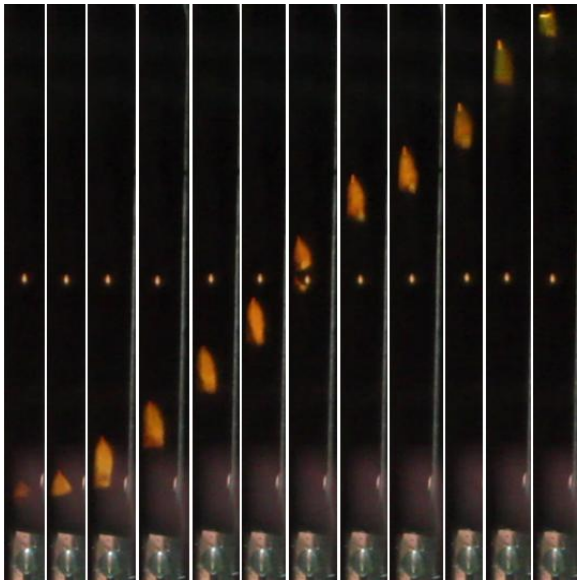

(b) 22.0 MPa

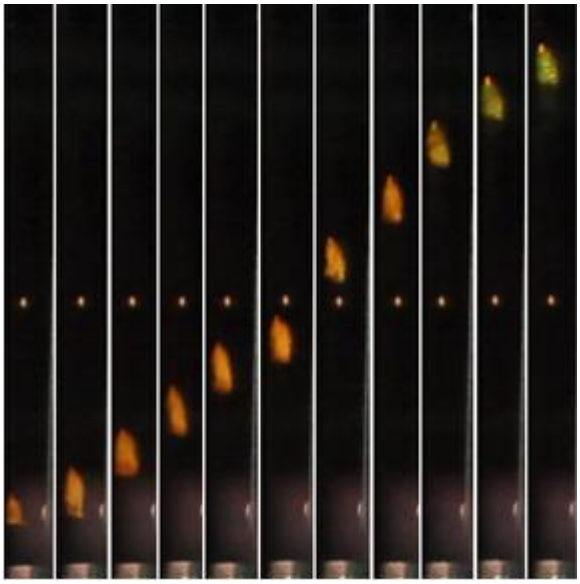

(c) 23.0 MPa

Figure 6.2(a–c) Sequential digital images of rising impure CO_2 (74.87 mol.% CO_2 + 25.13 mol.% CH_4) bubbles through the light crude oil column inside a central flat glass tube of L = 5.4 cm with the time interval of Δt = 0.25 s at T_{res} = 53.0°C and three lower test pressures of **(a)** 21.0 MPa; **(b)** 22.0 MPa; and **(c)** 23.0 MPa.

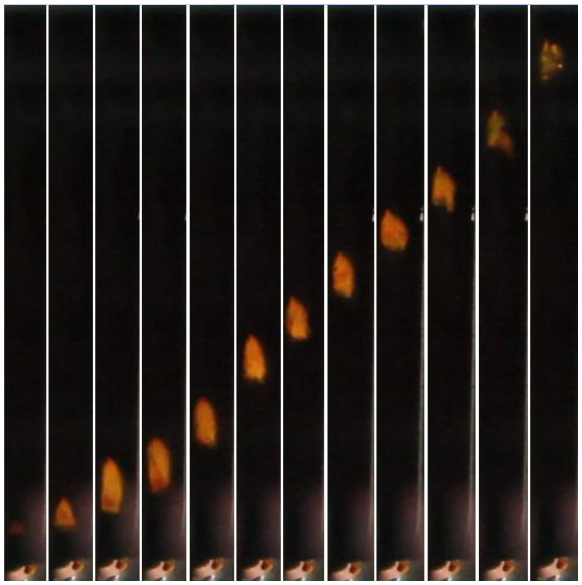

(d) 24.0 MPa

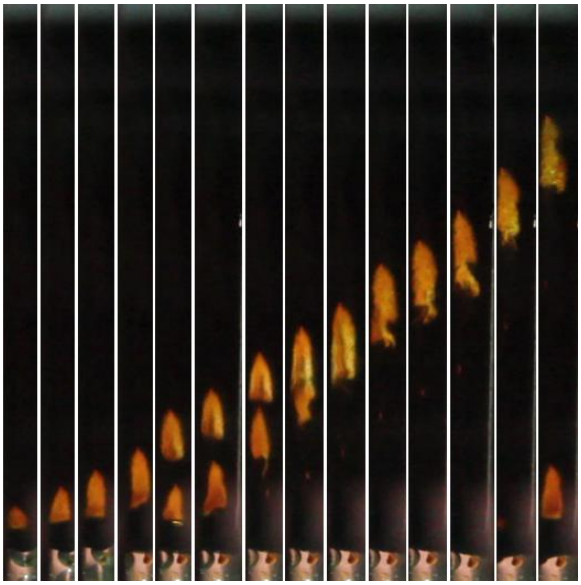

(e) 25.0 MPa

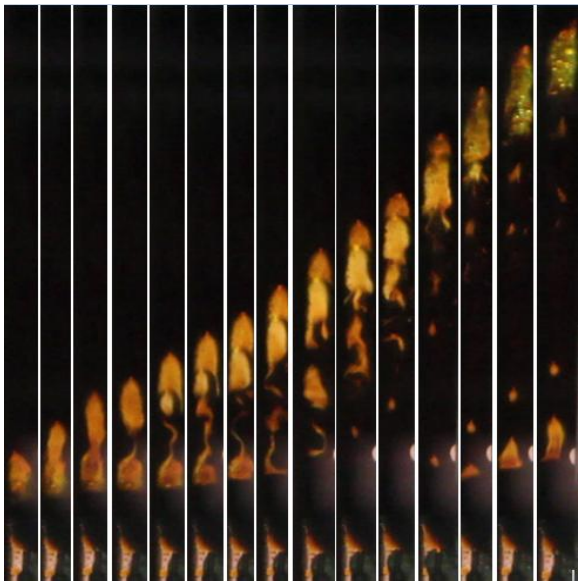

(f) 26.0 MPa

Figure 6.2(d–f) Sequential digital images of rising impure CO_2 (74.87 mol.% CO_2 + 25.13 mol.% CH_4) bubbles through the light crude oil column inside a central flat glass tube of L = 5.4 cm with the time interval of Δt = 0.25 s at T_{res} = 53.0°C and three higher test pressures of **(d)** 24.0 MPa; **(e)** 25.0 MPa; and **(f)** 26.0 MPa.

multi-contact miscibility (MCM) may be achieved at the MMP range of 23.0–24.0 MPa by using the four existing and new BBU qualitative criteria. At an even higher test pressure (e.g., 26.0 MPa), the impure CO_2 bubble in Figure 6.2f breaks up more quickly after it contacts the light crude oil. The upper part (mostly impure CO_2) rises faster, while the lower part (mostly impure CO_2 plus extracted HCs) becomes a long mixing wake and moves upwards much more slowly. Table 6.2 lists the four existing qualitative criteria in terms of the bubble appearance (i.e., the bubble shape, size, colour, and rising height) and compares them with the novel BBU qualitative criterion for estimating the MMP of the light crude oil–impure CO_2 system at T_{res} = 53.0°C.

It is worthwhile to emphasize that the estimated respective MMPs by using the BBU qualitative criterion for the light crude oil–pure CO_2 system and the light crude oil–impure CO_2 system are found to be consistent with those estimated by using the four existing qualitative criteria. Moreover, the BBU can be much more easily observed and recorded in the RBA tests. The BBU is an excellent qualitative criterion because it is not only relatively independent of the experimental factors, such as the glass tube height and bubble size, but also relatively sensitive to the experimental conditions, such as the test pressure and gas composition. Thus the novel BBU qualitative criterion is more objective and easier to be applied for estimating the MMP than the four existing qualitative criteria, which are based on the overall bubble appearance.

6.2 BRH and BRV Quantitative Criteria

6.2.1 Light crude oil–pure CO_2 system

Figure 6.3a shows the measured bubble-rising height (BRH) vs. time data with the

Table 6.2 Qualitative criteria based on the overall bubble appearance for estimating the minimum miscibility pressure (MMP) of the light crude oil–impure CO_2 (74.87 mol.% CO_2 + 25.13 mol.% CH_4) system at the actual reservoir temperature of T_{res} = 53.0°C from the rising-bubble apparatus (RBA) tests.

Pressure (MPa)	Bubble shape (top + bottom)	Bubble size	Bubble colour	Bubble height	Bubble break-up (BBU)	Relative to the MMP	MMP (MPa)
21.0	conic + flat	shrink	transparent	to the top	no	below	23.0–24.0
22.0	conic + flat	shrink	transparent	to the top	no	below	
23.0	**conic + flat**	**shrink**	**fuzzy**	**to the top**	**no**	**near**	
24.0	**ellipsoidal + tail**	**elongate → break up**	**fuzzy**	**near the top**	**yes**	**above**	
25.0	ellipsoidal + tail	elongate → break up	fuzzy	near the top	yes	above	
26.0	ellipsoidal + wake	elongate → break up	fuzzy	midway	yes	far above	
References	[Christiansen and kim, 1986; Christiansen and Haines, 1987]	[Sibbald *et al*., 1991; Rao and Lee, 2003]	[Elsharkawy *et al*., 1996]	[Poettmann *et al*., 1992]	This study		

Notes: The first highlighted row in the bold face indicates the lower limit of the estimated MMP range;
The second highlighted row in the bold face indicates the upper limit of the estimated MMP range.

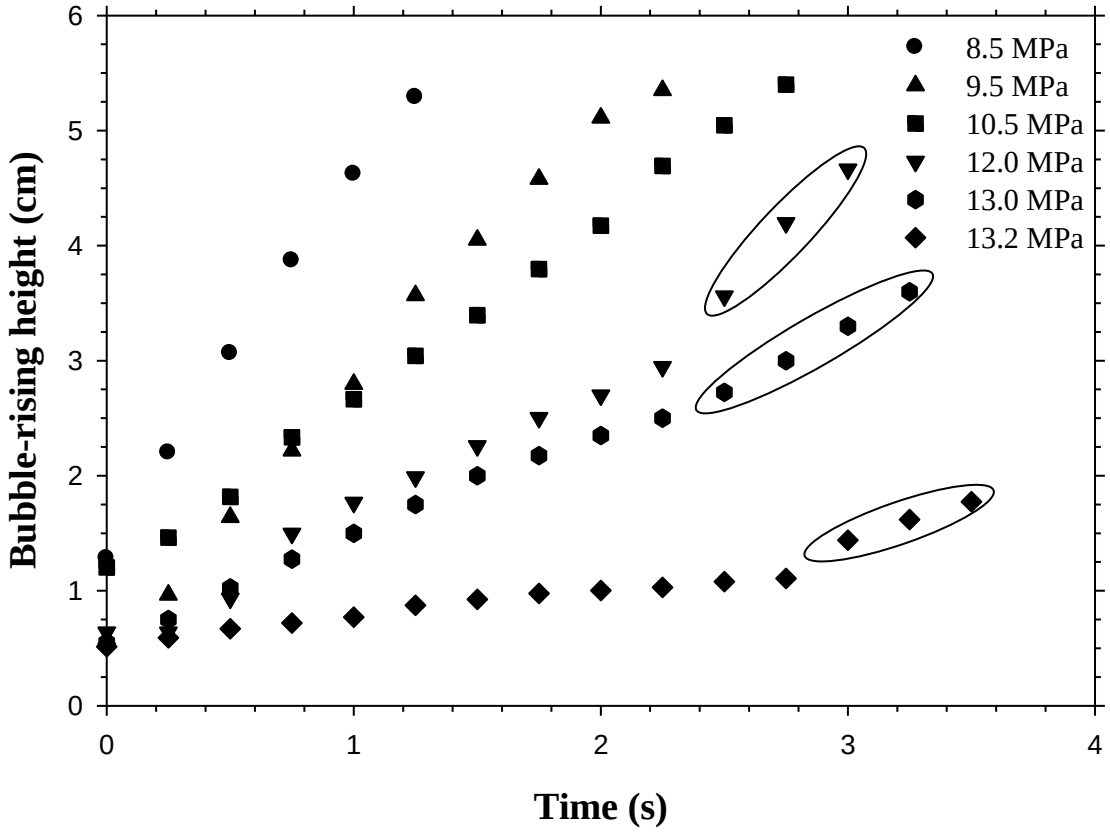

Figure 6.3(a) Measured bubble-rising height (BRH) vs. time data with the RBA for the light crude oil–pure CO_2 system at six different test pressures and T_{res} = 53.0°C, where the circled data points are for the upper part after pure CO_2 bubble breaks into two parts near the end.

RBA at six different test pressures and T_{res} = 53.0°C for the light crude oil–pure CO_2 system. As expected, the measured BRH is increased with time at each test pressure and reaches its maximum value at the end of each test. More specifically, at $P \leq 10.5$ MPa, the measured BRH is increased with time linearly till the end. This fact means that pure CO_2 bubble rises at a constant velocity at each test pressure in this lower pressure range. At $P \geq 12.0$ MPa, however, the measured BRH is increased with time in two distinct periods. The BRH is increased linearly and more slowly with time in the first long period prior to the BBU, whereas it is increased linearly but more quickly with time in the second short period post the BBU. The upper part of the bubble moves upwards much faster than the lower part after the BBU occurs. At the end, however, the maximum BRHs at $P \geq 12.0$ MPa are still substantially smaller than those at $P \leq 10.5$ MPa. This is because the mutual interactions between the light crude oil and pure CO_2 become stronger in the higher pressure range. At a higher pressure, CO_2 is more capable of extracting HCs from the oil phase so that it is easier for the BBU to occur and for the MCM to develop. Figure 6.3a suggests that the light crude oil and pure CO_2 may be immiscible at $P \leq 10.5$ MPa but miscible at $P \geq 12.0$ MPa.

Figure 6.3b shows the measured maximum BRH vs. test pressure data. In this case, the linear intersection method is applied to use the BRH criterion and determine the MMP by finding the sudden slope change point in the measured maximum BRH vs. test pressure curve. Two straight lines are obtained to represent two linear regression equations of the first three (Line I for $P \leq 10.5$ MPa) and last three (Line II for $P \geq 12.0$ MPa) BRHs, respectively. The intersection point of Lines I and II is found, whose abscissa value is considered to be the MMP. As a result, the MMP is determined to be

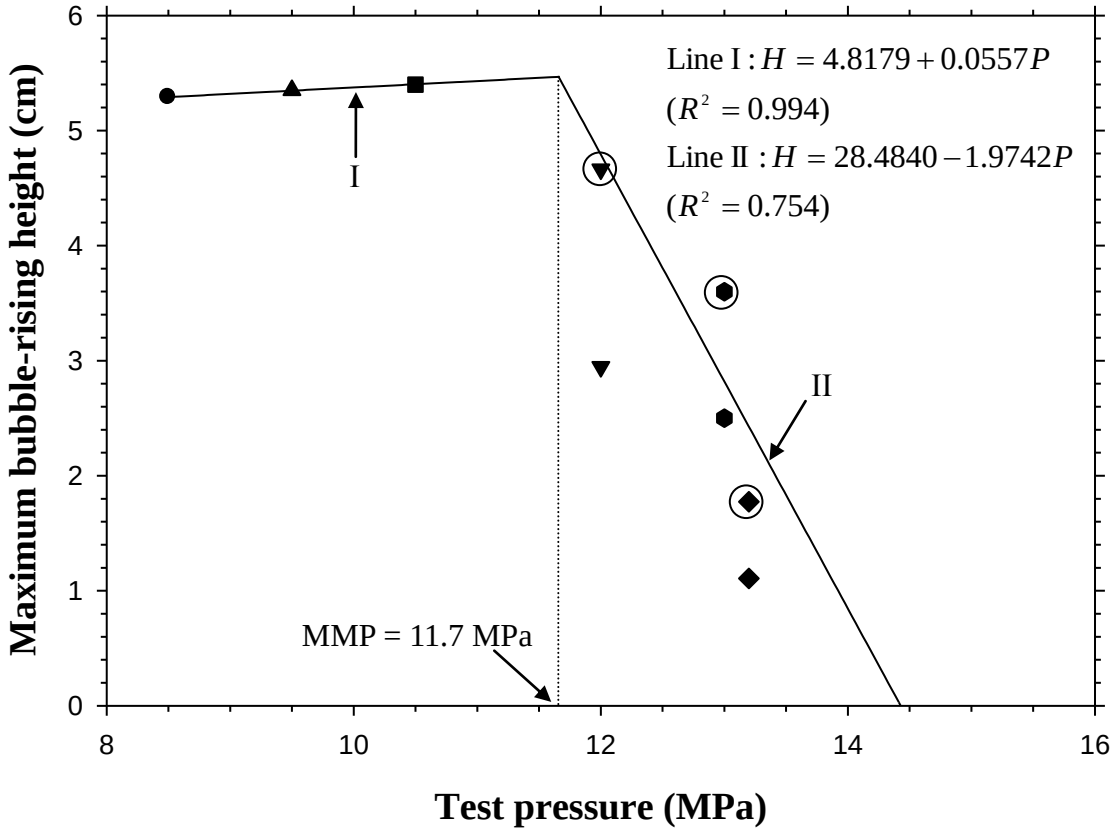

Figure 6.3(b) Determined minimum miscibility pressure (MMP) from the bubble-rising height (BRH) criterion with the RBA for the light crude oil–pure CO_2 system at T_{res} = 53.0°C, where the circled data points are for the upper part after pure CO_2 bubble breaks into two parts near the end.

11.7 MPa for the light crude oil–pure CO_2 system at T_{res} = 53.0°C by using the new BRH quantitative criterion with the RBA. Precisely speaking, the measured maximum BRH is slightly increased with the test pressure in the immiscible or near-miscible case. This is attributed to weak mutual interactions between the light crude oil and CO_2 bubble in the low pressure range. There is a larger amount of CO_2 inside the CO_2 bubble at a higher test pressure so that it lasts longer. However, the measured maximum BRH is drastically decreased as the test pressure is increased in the miscible case. There are strong mutual interactions between the light crude oil and CO_2 bubble in the high pressure range. The CO_2 bubble disappears quickly in this case.

On the other hand, the bubble-rising velocity (BRV) for the light crude oil–pure CO_2 system in each test is calculated by applying the linear regression of the measured BRH vs. time data in Figure 6.3a and differentiating the resultant equation with respect to time. Figure 6.4a shows the BRV vs. time data at six different test pressures and T_{res} = 53.0°C. Obviously, the BRV is reduced as the test pressure is increased. At $P \leq 10.5$ MPa, the BRV remains high and constant from the beginning to the end of each test. At $P \geq 12.0$ MPa, the BRV remains low and constant in the first long period prior to the BBU, whereas it is suddenly increased but remains constant in the second short period post the BBU. The velocity of the upper bubble part is higher and is marked by a circle in Figure 6.4a. Furthermore, Figure 6.4b shows the average BRV vs. test pressure data. It is found that the average BRV is linearly reduced with the increased test pressure at $P \leq 10.5$ MPa. The corresponding abscissa value is obtained to be 12.4 MPa by extrapolating Line I to zero BRV. Thus the MMP of the light crude oil–pure CO_2 system at T_{res} = 53.0°C is determined to be 12.4 MPa by using the new BRV quantitative criterion with the RBA. It

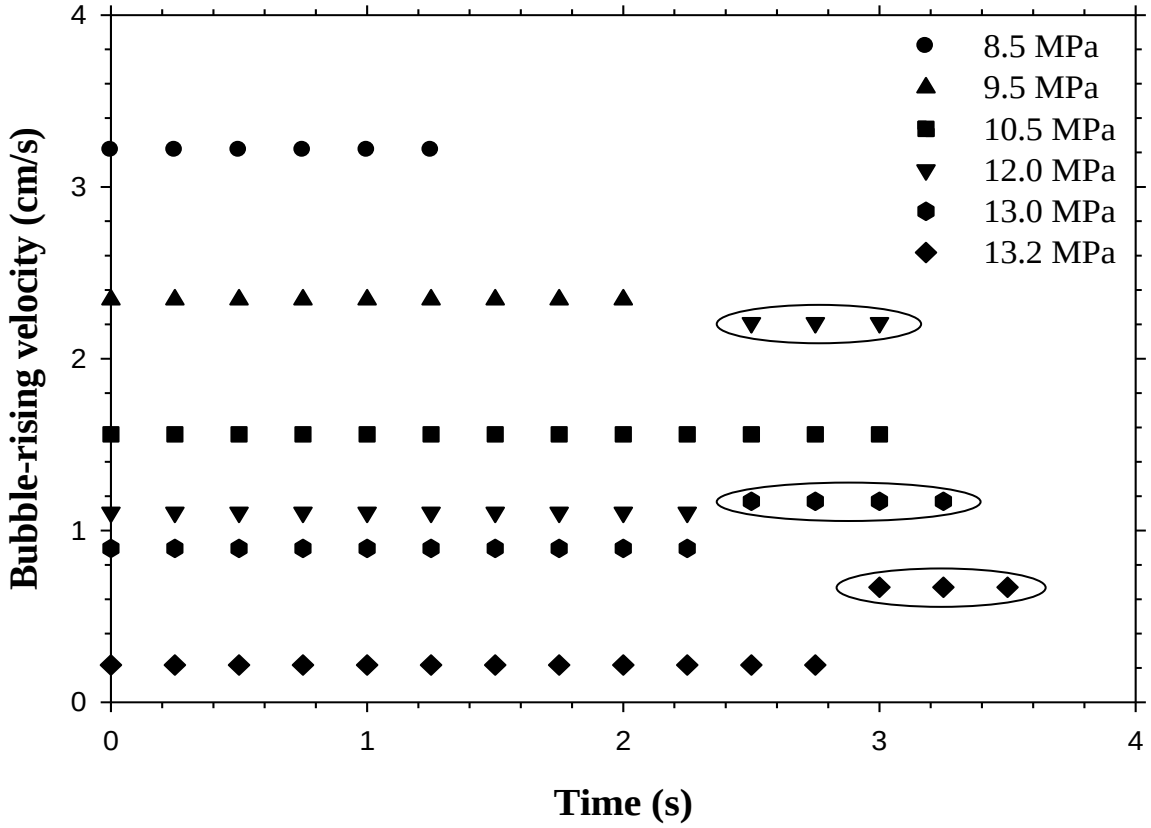

Figure 6.4(a) Measured bubble-rising velocity (BRV) vs. time data with the RBA for the light crude oil–pure CO_2 system at six different test pressures and T_{res} = 53.0°C, where the circled data points are for the upper part after pure CO_2 bubble breaks into two parts near the end.

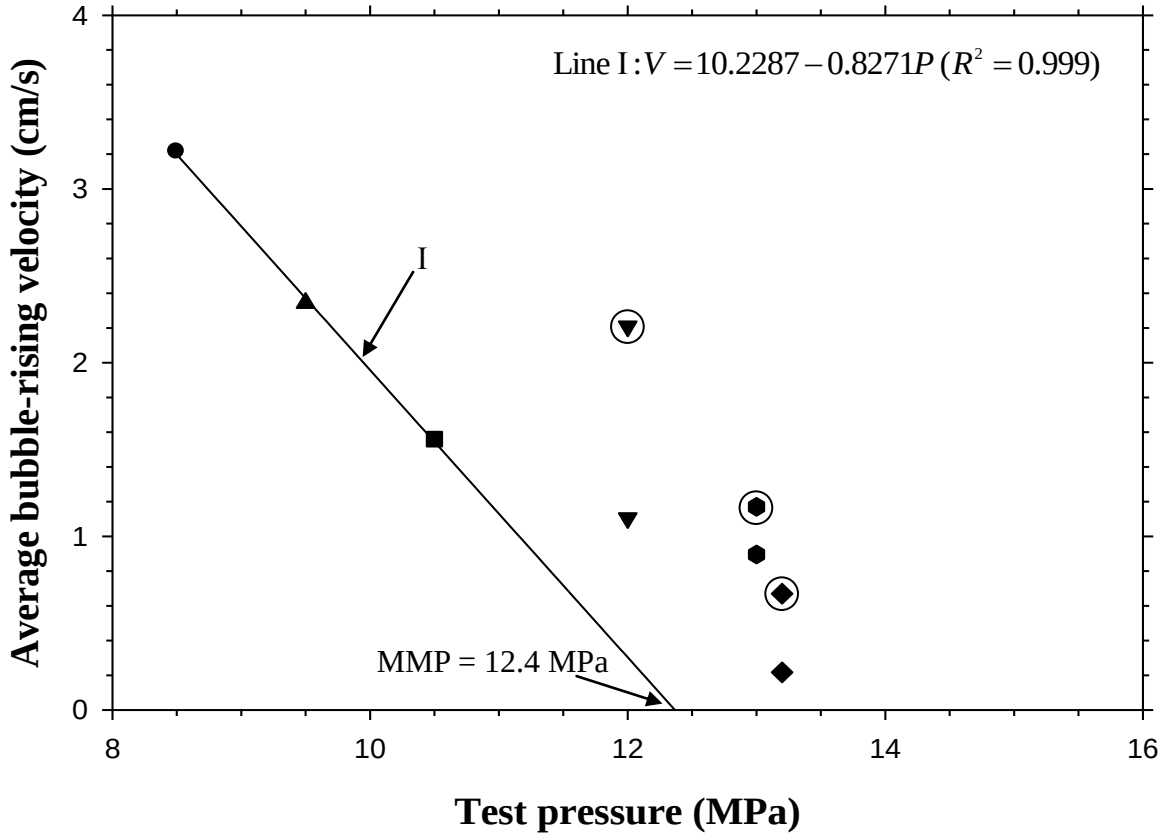

Figure 6.4(b) Determined minimum miscibility pressure (MMP) from the bubble-rising velocity (BRV) criterion with the RBA for the light crude oil–pure CO_2 system at T_{res} = 53.0°C, where the circled data points are for the upper part after pure CO_2 bubble breaks into two parts near the end.

should be noted that at $P \geq 12.0$ MPa, nevertheless, there are two average BRVs for the upper and lower parts of a broken bubble post the BBU, respectively.

Table 6.3 summarizes the determined MMPs of the light crude oil–pure CO_2 system at T_{res} = 53.0°C from the RBA tests, coreflood tests, and VIT technique. It is found that the determined respective MMPs of 11.7 and 12.4 MPa by using the new BRH and BRV quantitative criteria agree fairly well with the estimated MMP range of 10.5–12.0 MPa by using the above-mentioned four existing and new BBU qualitative criteria. The MMPs determined from the RBA tests are slightly lower than 12.4–12.9 MPa determined from the coreflood tests by using the oil recovery factor (ORF) and break-over pressure (BOP) criteria [Zhang and Gu, 2015]. However, they are relatively higher than 10.6 MPa determined from the VIT technique by using the zero-IFT criterion [Gu *et al*., 2013]. These two trends are different from those reported in the literature [Thomas *et al*., 1994; Rao and Lee, 2003]. Further studies are needed in order to understand the differences of the determined MMPs from the RBA tests, coreflood tests, and VIT technique.

6.2.2 Light crude oil–impure CO_2 system

Figure 6.5a shows the measured BRH vs. time data with the RBA at six different test pressures and T_{res} = 53.0°C for the light crude oil–impure CO_2 (74.87 mol.% CO_2 + 25.13 mol.% CH_4) system. Overall, the measured BRH is increased with time and reaches its maximum value at the end of each test. More specifically, at $P \leq 23.0$ MPa, the measured BRH is increased with time almost linearly till the end. At $P \geq 24.0$ MPa, there are two distinct periods of the measured BRH vs. time data, one before and the other after the BBU. Hence, it is speculated from Figure 6.5a that the light crude oil–impure CO_2 system may be immiscible at $P \leq 22.0$ MPa, near-miscible at $P = 23.0$ MPa, and miscible at $P \geq$

Table 6.3 Quantitative criteria for determining the minimum miscibility pressures (MMPs) of the light crude oil–pure CO_2 system at the actual reservoir temperature of T_{res} = 53.0°C from the rising-bubble apparatus (RBA) tests, coreflood tests, and vanishing interfacial tension (VIT) technique.

Method	RBA tests		Coreflood tests	VIT
MMP criterion	Bubble-rising height (BRH)	Bubble-rising velocity (BRV)	Oil recovery factor (ORF) and break-over pressure (BOP)	Zero-IFT
MMP (MPa)	11.7	12.4	12.4–12.9	10.6
Reference	This study		[Zhang and Gu, 2015]	[Gu *et al*., 2013]

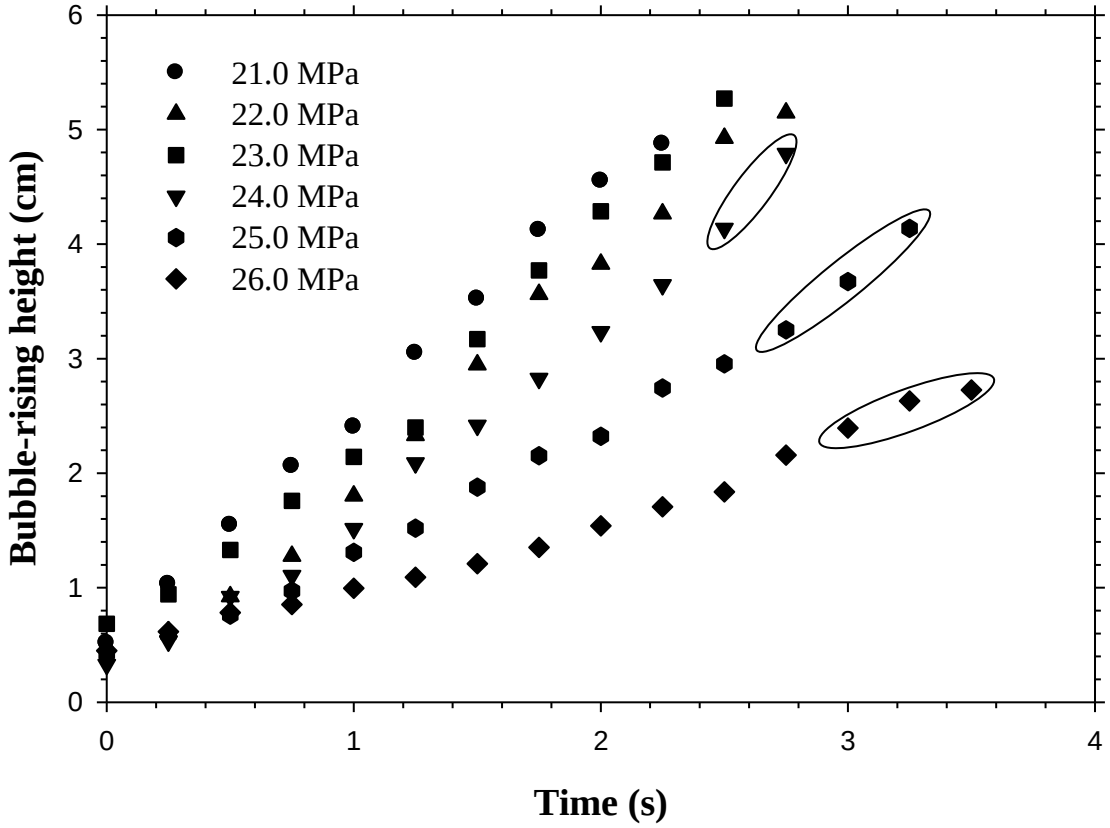

Figure 6.5(a) Measured bubble-rising height (BRH) vs. time data with the RBA for the light crude oil–impure CO_2 (74.87 mol.% CO_2 + 25.13 mol.% CH_4) system at six different test pressures and T_{res} = 53.0°C, where the circled data points are for the upper part after impure CO_2 bubble breaks into two parts near the end.

24.0 MPa. Furthermore, the measured maximum BRH vs. test pressure data are plotted in Figure 6.5b in order to determine the MMP quantitatively by using the BRH criterion with the RBA. The measured maximum BRH vs. test pressure data under the near-miscible condition is included in the immiscible range, which is consistent with the practice in the previous study [Zhang and Gu, 2015]. Thus the first three maximum BRH vs. test pressure data are linearly regressed in the first immiscible range (Line I for $P \leq$ 23.0 MPa). In addition, the last three maximum BRH vs. test pressure data are linearly regressed in the second miscible range (Line II for $P \geq$ 24.0 MPa). The linear intersection method is used again to find the intersection point of two straight lines (i.e., Lines I and II), whose abscissa value is considered to be the MMP. In this way, the MMP is determined to be 23.5 MPa for the light crude oil–impure CO_2 system at T_{res} = 53.0°C by using the new BRH quantitative criterion with the RBA. It is worthwhile to note that the overall range of the maximum BRH for the light crude oil–impure CO_2 system in Figure 6.5b is slightly smaller than that for the light crude oil–pure CO_2 system in Figure 6.3b. This means that the BRH is sensitive to the CO_2 bubble composition. Hence, the BRH is an excellent quantitative criterion for determining the MMPs of different crude oil–CO_2 systems.

The new BRV quantitative criterion is also used to determine the MMP of the light crude oil–impure CO_2 system at T_{res} = 53.0°C. Figure 6.6a shows the BRV vs. time data with the RBA at six different test pressures. The circled data points are for the upper part after the impure CO_2 bubble breaks into two parts at an increased test pressure. Similar to the data for the light crude oil–pure CO_2 system, here, the BRV is also lowered as the test pressure is increased. The average BRV vs. test pressure data are plotted in Figure 6.6b.

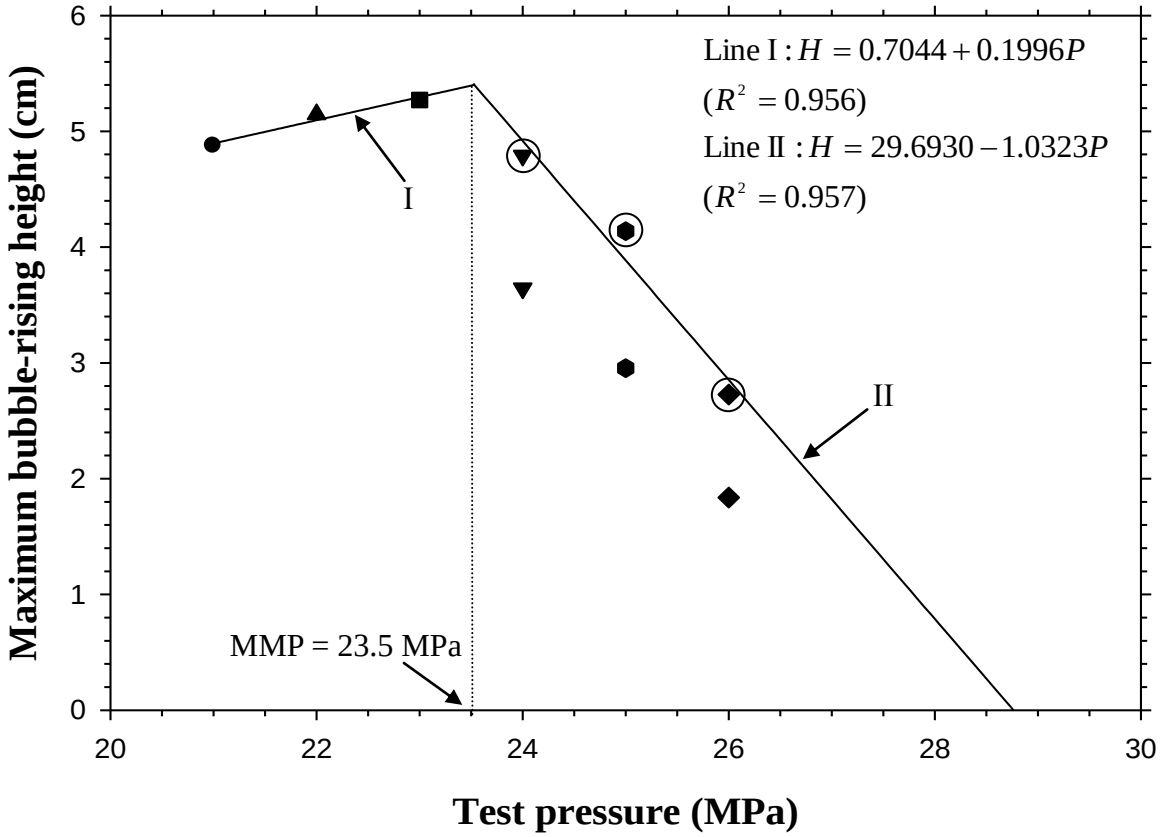

Figure 6.5(b) Determined minimum miscibility pressure (MMP) from the bubble-rising height (BRH) criterion with the RBA for the light crude oil–impure CO_2 (74.87 mol.% CO_2 + 25.13 mol.% CH_4) system at T_{res} = 53.0°C, where the circled data points are for the upper part after impure CO_2 bubble breaks into two parts near the end.

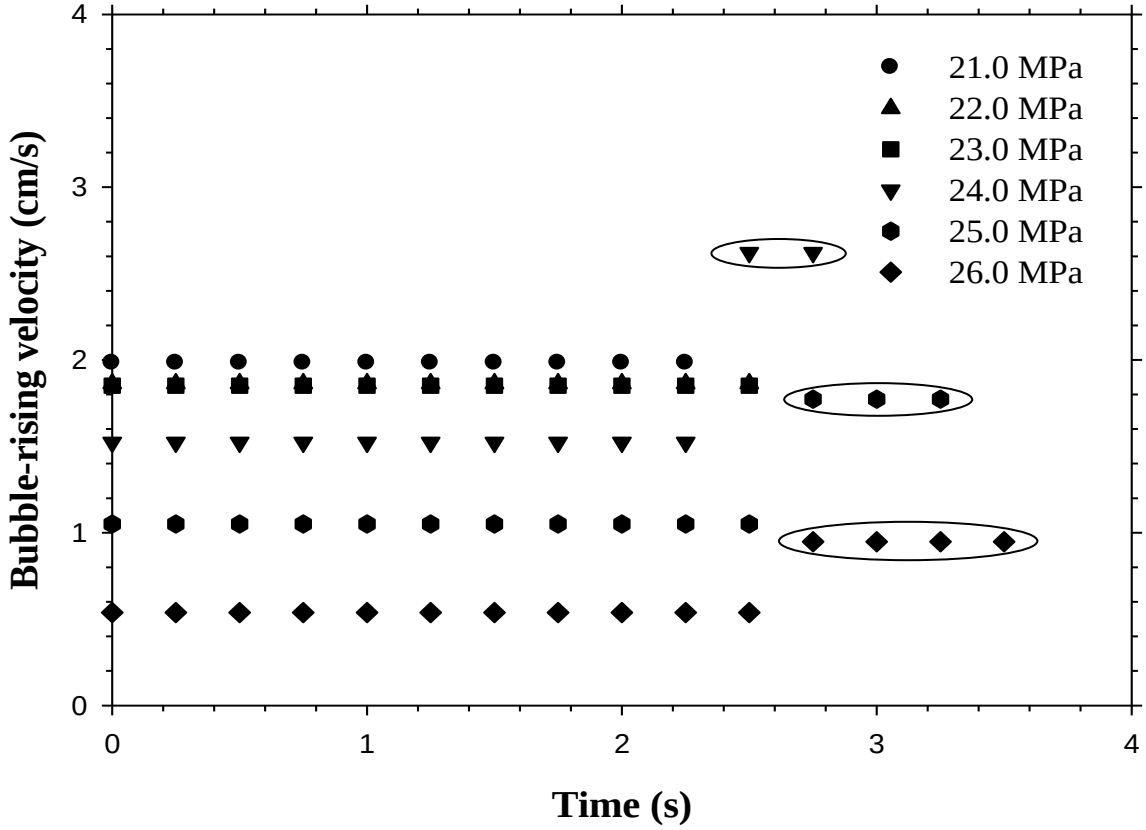

Figure 6.6(a) Measured bubble-rising velocity (BRV) vs. time data with the RBA for the light crude oil–impure CO_2 (74.87 mol.% CO_2 + 25.13 mol.% CH_4) system at six different test pressures and T_{res} = 53.0°C, where the circled data points are for the upper part after impure CO_2 bubble breaks into two parts near the end.

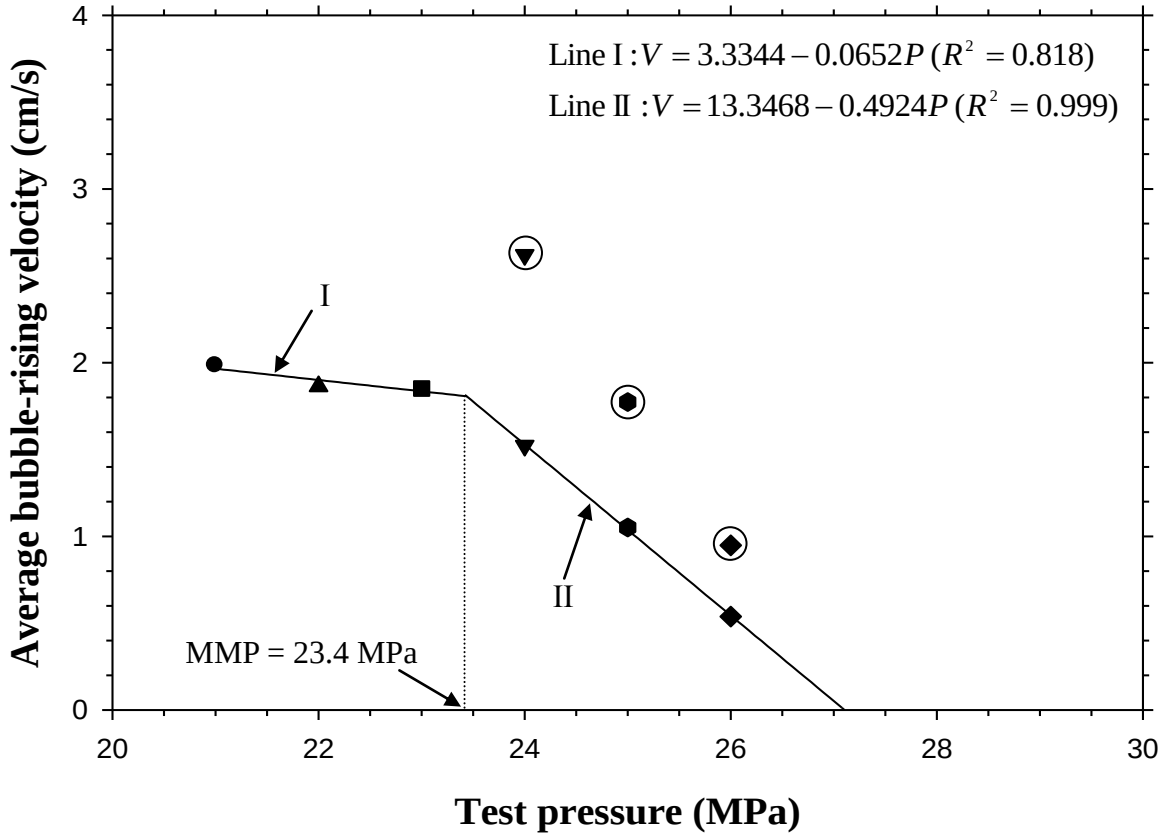

Figure 6.6(b) Determined minimum miscibility pressure (MMP) from the bubble-rising velocity (BRV) criterion with the RBA for the light crude oil–impure CO_2 (74.87 mol.% CO_2 + 25.13 mol.% CH_4) system at T_{res} = 53.0°C, where the circled data points are for the upper part after impure CO_2 bubble breaks into two parts near the end.

The linear intersection method is used to determine the MMP of the light crude oil–impure CO_2 system by means of the BRV criterion, which is different from the linear extrapolation method used to determine the MMP of the light crude oil–pure CO_2 system. This is because CH_4 has a much lower solubility in the light crude oil and a much weaker HCs-extraction ability. Thus the addition of CH_4 considerably weakens the mutual interactions and severely inhibits the miscibility development between the light crude oil and CO_2–CH_4 bubble, especially at low test pressures. In Figure 6.6b, the average BRV of the impure CO_2 bubble remains high and is close to each other in the immiscible or near-miscible range. Two straight lines are obtained to represent two linear regression results in the first immiscible (Line I for $P \leq 23.0$) and second miscible (Line II for $P \geq 24.0$) ranges, respectively. Accordingly, the MMP is determined to be 23.4 MPa at the linear intersection point of Lines I and II. At $P \geq 24.0$ MPa, the velocity of the upper part after the BBU is marked by a circle, which is too high to be used in the MMP determination.

In this study, both the BRH and BRV criteria are used to determine the MMPs of the light crude oil–impure CO_2 system and the detailed results are summarized and compared in Table 6.4. The MMP range of the light crude oil–impure CO_2 system is found to be 23.4–23.5 MPa by using these two new quantitative technical criteria with the RBA. This MMP range agrees well with the estimated MMP range of 23.0–24.0 MPa by using the four existing and BBU qualitative criteria with the RBA. However, it is considerably higher than the previously determined MMP of 21.4 MPa from the VIT technique for the same light crude oil–impure CO_2 system [Gu *et al*., 2013].

In summary, the new BRH and BRV quantitative criteria, plus the novel BBU

Table 6.4 Quantitative criteria for determining the minimum miscibility pressures (MMPs) of the light crude oil–impure CO_2 (74.87 mol.% CO_2 + 25.13 mol.% CH_4) system at the actual reservoir temperature of T_{res} = 53.0°C from the rising-bubble apparatus (RBA) tests and vanishing interfacial tension (VIT) technique.

Method	RBA tests		VIT
MMP criterion	Bubble-rising height (BRH)	Bubble-rising velocity (BRV)	Zero-IFT
MMP (MPa)	23.5	23.4	21.4
Reference	This study		[Gu *et al*., 2013]

qualitative criterion, are proven to be accurate and objective for the MMP determinations. The determined MMP of 23.4–23.5 MPa for the light crude oil–impure CO_2 system is significantly higher than 11.7–12.4 MPa for the light crude oil–pure CO_2 system. Furthermore, Figures 6.3a and b and Figures 6.5a and b show that the measured BRH data and maximum BRH data for the two light crude oil–pure and impure CO_2 systems have similar trends. The BRH criterion can be applied similarly for these two systems and thus it is insensitive to pure or impure CO_2 used in the RBA tests. It is also worthwhile to emphasize that the measured maximum BRH strongly depends on the height of the flat glass tube installed in the RBA, which may consequently compromise the accuracy of the determined MMPs. On the contrary, Figures 6.4a and b and Figures 6.6a and b depict that the measured BRV data and average BRV data for the two light crude oil–pure and impure CO_2 systems have quite different trends. Hence, the BRV criterion has to be applied differently by using the linear extrapolation method for the former system and the linear intersection method for the latter system, respectively. Overall, the BRV criterion is more sensitive to pure or impure CO_2 used in the RBA tests. Therefore, the BRV criterion with the RBA is expected to be more objective, sensitive, and accurate for the MMP determination, though it is mathematically derived from the BRH criterion with the RBA.

CHAPTER 7 TEST RESULTS AND DISCUSSION OF VANISHING INTERFACIAL TENSION (VIT) TECHNIQUE

In this study, the measured initial and equilibrium interfacial tensions (IFTs) and determined minimum miscibility pressures (MMPs) between the dead light crude oil and CO_2 in Tests #1–5 at five initial gas–oil ratios (GORs) of 1:1, 3:1, 10:1, 200:1, 4000:1 in volume and the actual reservoir temperature of T_{res} = 53.0°C are plotted in Figures 7.1a–e, respectively [Zhang and Gu, 2016b]. Moreover, the measured equilibrium IFT vs. test pressure data and determined MMPs for the live light crude oil–CO_2 system in Test #6 are compared with those for the dead light crude oil–CO_2 system in Test #5 at the same initial GOR of 4000:1 in volume and shown in Figure 7.2. It should be noted that these six figures include and depict the measured initial/equilibrium IFT vs. test pressure data to the lowest IFTs at the highest test pressures in Tests #1–6, which were used in the linear regressions and extrapolations for the MMP determinations. It is found from Figures 7.1a–e that the measured initial IFTs and determined MMPs for the dead light crude oil–CO_2 system at five different initial GORs are always slightly higher than the measured equilibrium IFTs and determined MMPs. Both the measured initial and equilibrium IFTs are reduced almost linearly with the test pressure in Tests #1–5 due to an increased CO_2 solubility in the pendant oil drop at a higher test pressure [Wang *et al*., 2010]. It is also found from Figure 7.2 that the measured equilibrium IFTs for the live light crude oil–CO_2 system are always lower than those for the dead light crude oil–CO_2 system at the same initial GOR of 4000:1 in volume. However, the live light crude oil–CO_2 system has a slightly higher MMP in Test #6 than that for the dead light crude

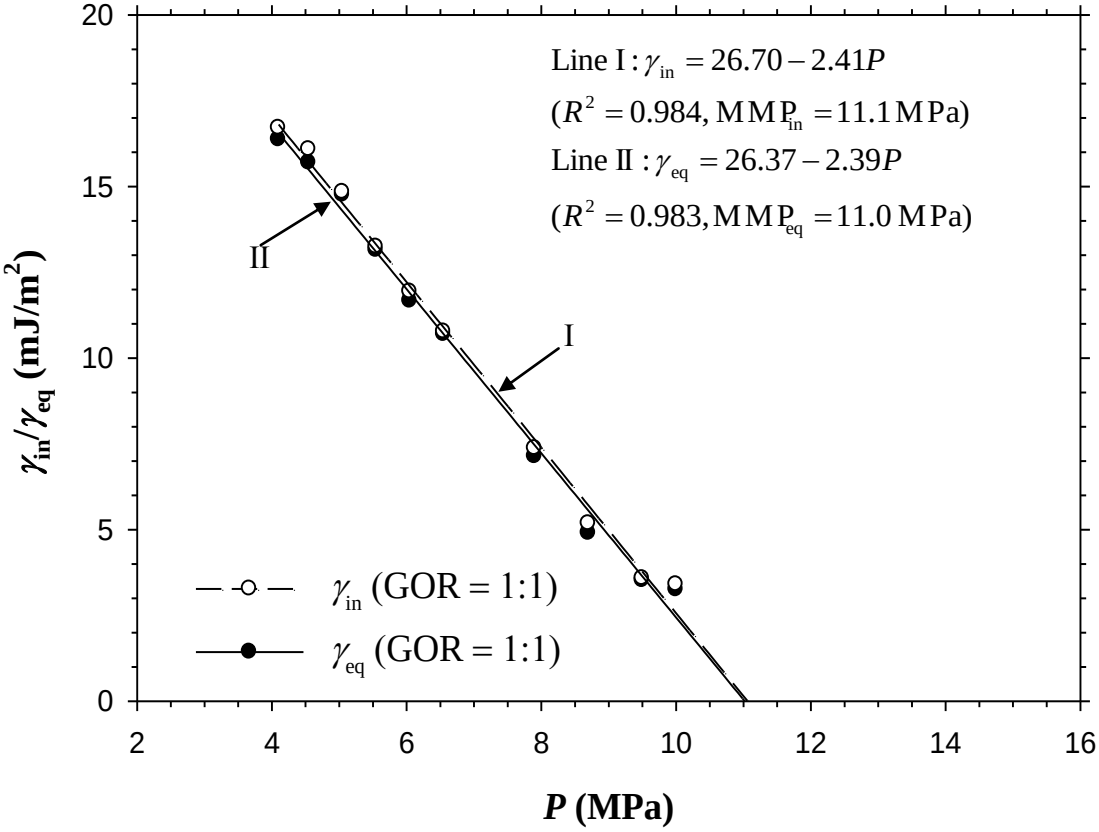

Figure 7.1(a) Measured initial and equilibrium interfacial tensions (IFTs) and determined minimum miscibility pressures (MMPs) in Test #1 (the dead light crude oil–CO_2 system, initial GOR of 1:1 in volume, T_{res} = 53.0°C).

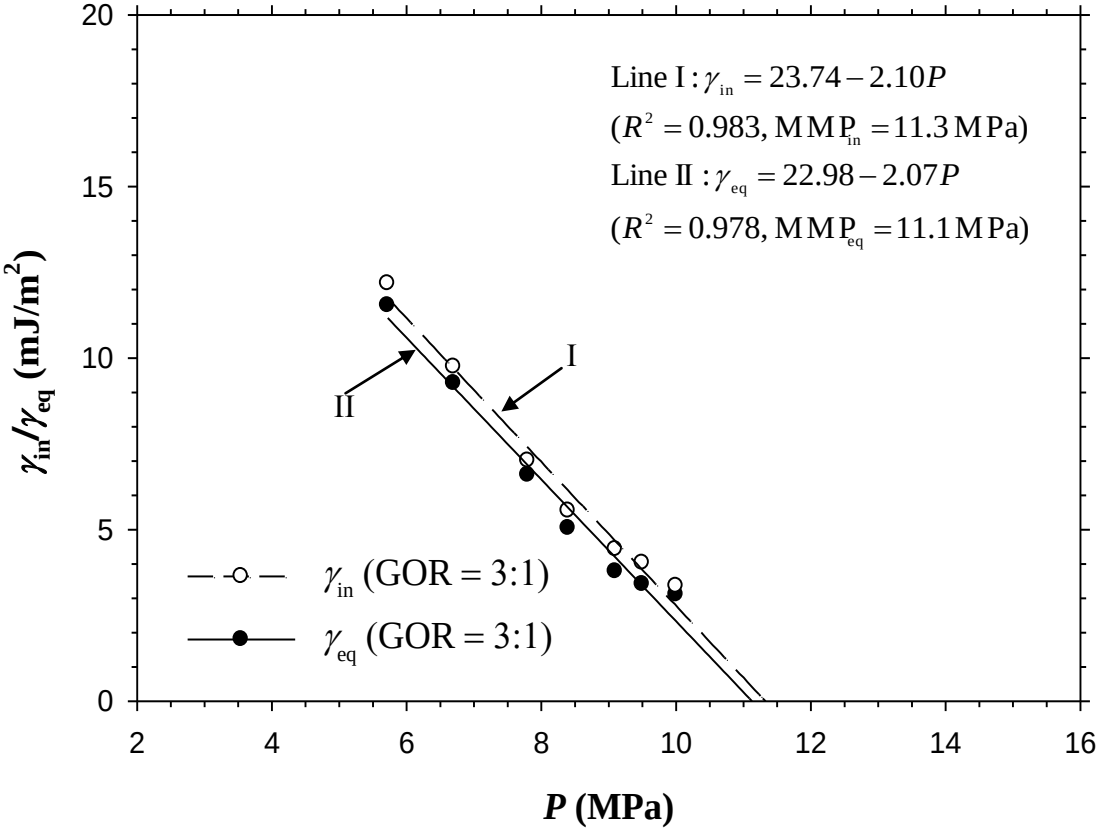

Figure 7.1(b) Measured initial and equilibrium interfacial tensions (IFTs) and determined minimum miscibility pressures (MMPs) in Test #2 (the dead light crude oil–CO_2 system, initial GOR of 3:1 in volume, T_{res} = 53.0°C).

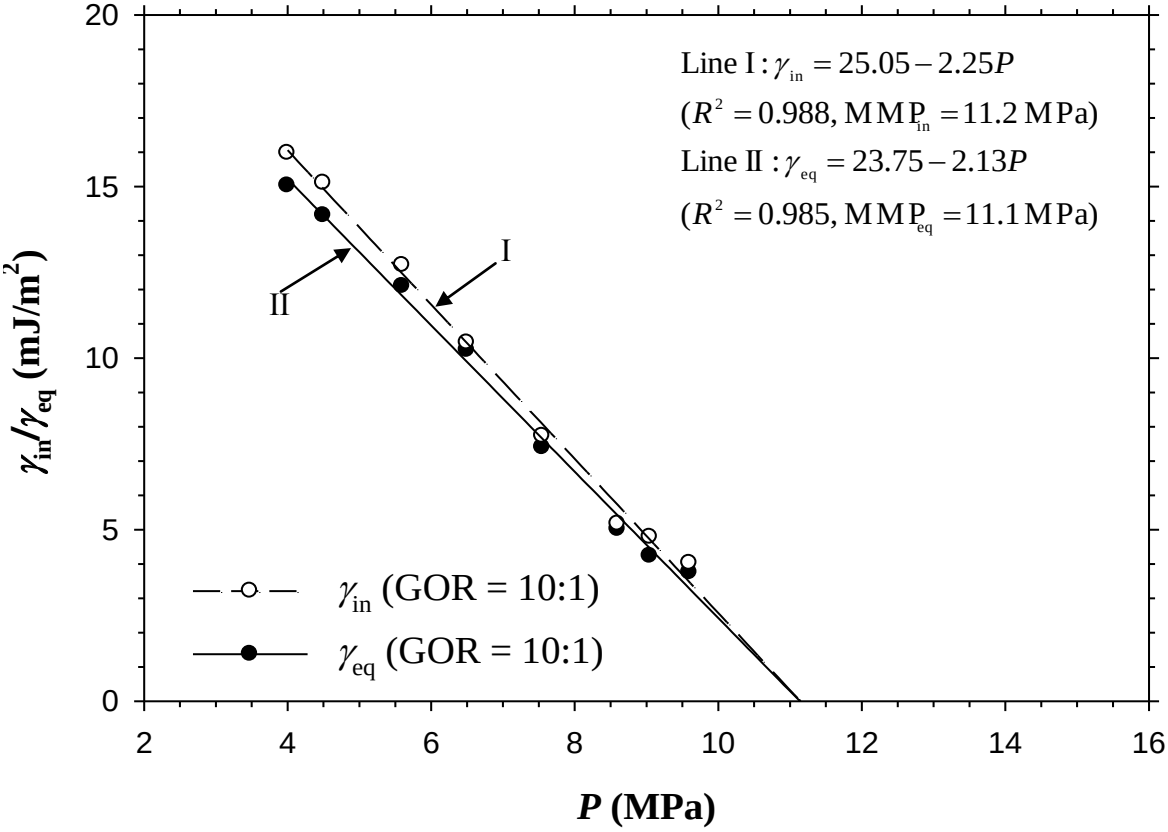

Figure 7.1(c) Measured initial and equilibrium interfacial tensions (IFTs) and determined minimum miscibility pressures (MMPs) in Test #3 (the dead light crude oil–CO_2 system, initial GOR of 10:1 in volume, T_{res} = 53.0°C).

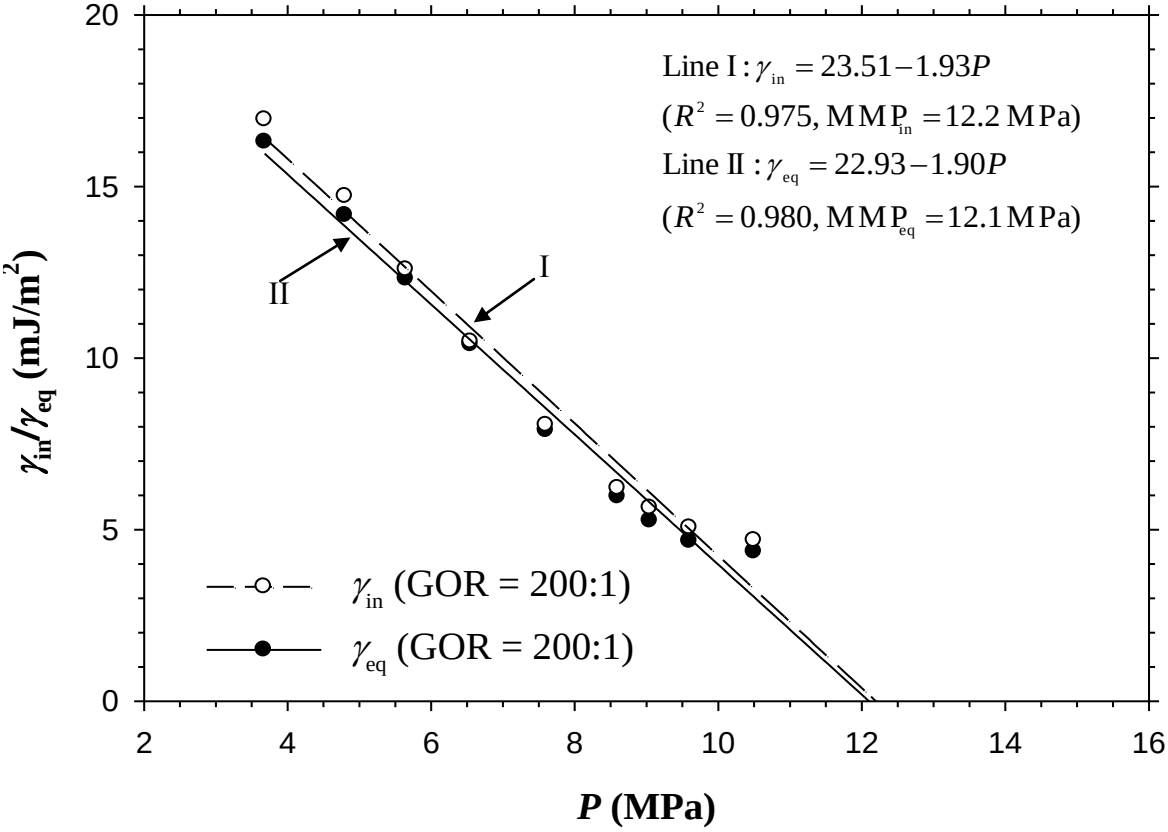

Figure 7.1(d) Measured initial and equilibrium interfacial tensions (IFTs) and determined minimum miscibility pressures (MMPs) in Test #4 (the dead light crude oil–CO_2 system, initial GOR of 200:1 in volume, T_{res} = 53.0°C).

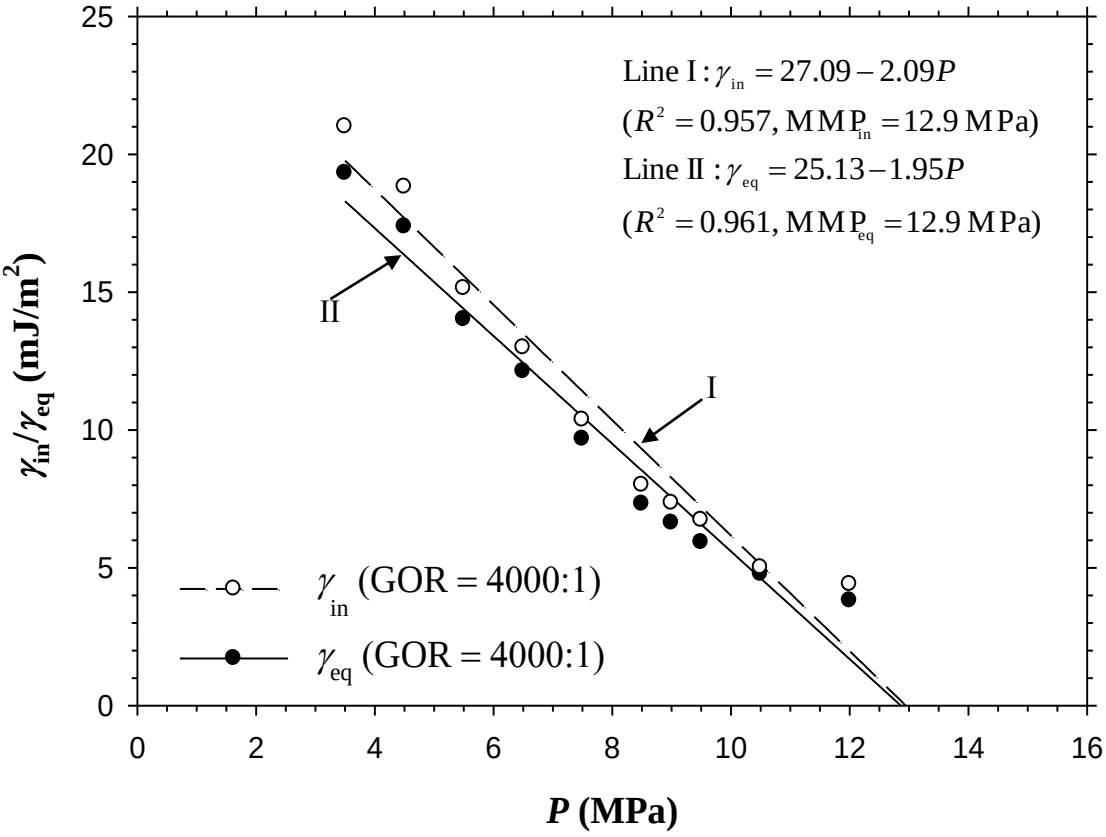

Figure 7.1(e) Measured initial and equilibrium interfacial tensions (IFTs) and determined minimum miscibility pressures (MMPs) in Test #5 (the dead light crude oil–CO_2 system, initial GOR of 4000:1 in volume, T_{res} = 53.0°C).

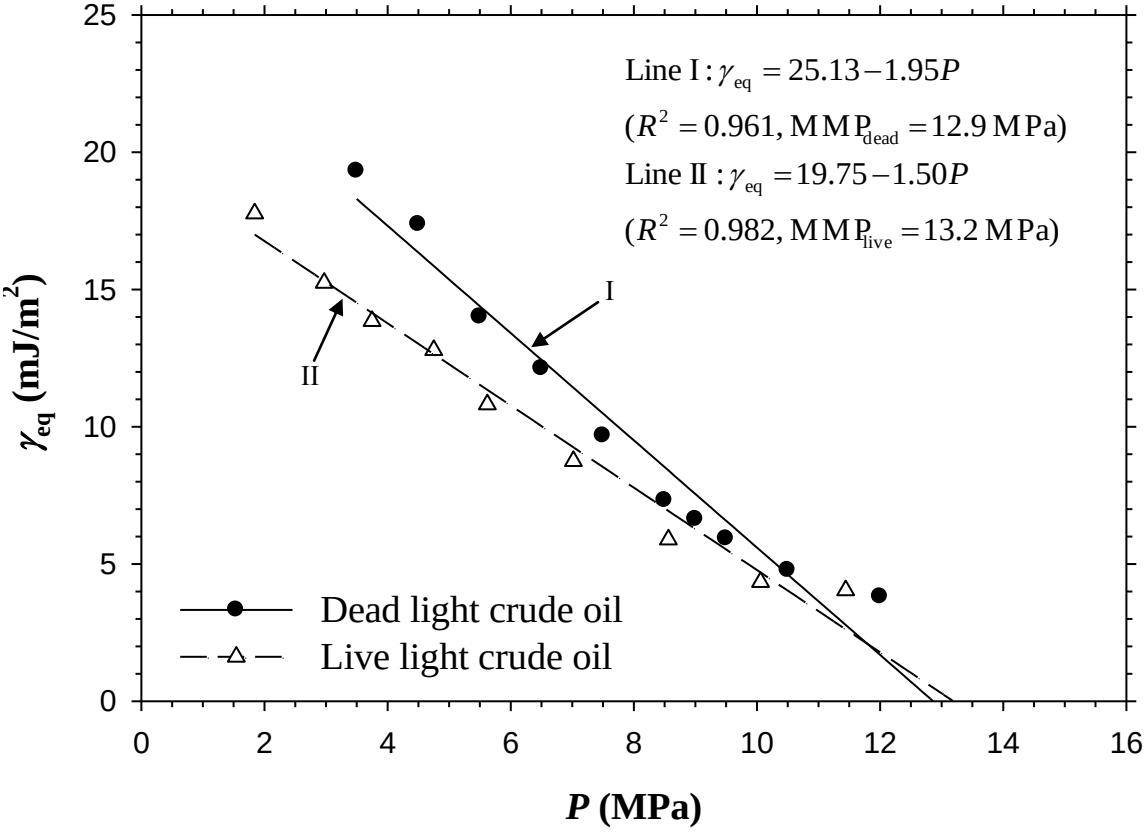

Figure 7.2 Measured equilibrium interfacial tensions (IFTs) and determined minimum miscibility pressures (MMPs) in Test #6 (the live light crude oil–CO_2 system, initial GOR of 4000:1 in volume, T_{res} = 53.0°C), in comparison with those in Test #5 (the dead light crude oil–CO_2 system, initial GOR of 4000:1 in volume, T_{res} = 53.0°C).

oil–CO_2 system in Test #5. As expected, pre-dissolved CH_4-dominated HCs in the live light crude oil help to increase the MMP of the former system [Gu *et al*., 2013].

7.1 Linear Correlation Coefficient (LCC) Criterion

In terms of the vanishing interfacial tension (VIT) technique, the MMP is determined by linearly regressing and extrapolating the measured equilibrium IFT vs. test pressure data to zero IFT. Mathematically, the linearity of such a linear regression is largely represented by the so-called linear correlation coefficient (LCC) or R^2. The LCC of each linear regression of data points from the highest equilibrium IFT measured at the lowest pressure to any equilibrium IFT measured at an arbitrarily chosen test pressure in each test is obtained by using SigmaPlot software (Version 11.0). Such calculated LCCs are listed in Tables 7.1–6 for Tests #1–6, respectively. As an example, here, the LCCs in Table 7.5 for Test #5 (the dead light crude oil–CO_2 system, initial GOR of 4000:1 in volume, T_{res} = 53.0°C) are analyzed and discussed in detail. It is found from Table 7.5 that in general, the LCC is slightly reduced as the test pressure is increased. The calculated LCCs are always larger than 0.990 until the linear regression is performed up to P = 12.0 MPa. Here, R_c^2 = 0.990 is considered to be a critical LCC. At P = 12.0 MPa, the LCC is suddenly reduced to R^2 = 0.961, which is significantly smaller than R_c^2 for the first time. Therefore, the corresponding equilibrium IFT of 3.80 mJ/m^2 at P = 12.0 MPa becomes the lowest equilibrium IFT to be used in the linear regression and extrapolation for the MMP determination in Test #5. The intersection point of the linear extrapolation and the abscissa is considered to be the MMP. As a result, the MMP of the dead light crude oil–CO_2 system at the initial GOR of 4000:1 in volume and T_{res} = 53.0°C

Table 7.1 Measured ten equilibrium interfacial tensions (IFTs) at ten different test pressures in Test #1 (the dead light crude oil–CO_2 system, initial GOR of 1:1 in volume, T_{res} = 53.0°C) and determined minimum miscibility pressures (MMPs) from the vanishing interfacial tension (VIT) technique.

P (MPa)	4.1	4.6	5.1	5.6	6.1	6.6	7.9	8.7	9.5	**10.0**[d]
γ_{eq} (mJ/m^2)	16.36	15.69	14.75	13.14	11.66	10.69	7.13	4.90	3.51	**3.25**
R^{2} [a]	–	1.000	0.996	0.989	0.991	0.992	0.994	0.997	0.997	**0.983**
δ [b] (nm)	–	1.498	1.881	3.221	2.958	1.945	2.636	2.789	1.727	**0.529**
VIT-MMP [c] (MPa)	–	15.0	13.7	11.6	10.9	10.9	10.8	10.7	10.8	**11.0**

Notes:

a: Linear correlation coefficient of each linear regression of the measured equilibrium IFT vs. test pressure date till the chosen test pressure

b: Interfacial thickness obtained from finite difference approximation of the negative derivative of the measured equilibrium IFTs with respect to the test pressure till the chosen test pressure

c: Determined MMP of the dead light crude oil–CO_2 system from the VIT technique by linearly extrapolating the measured equilibrium IFT vs. test pressure data till the chosen test pressure to zero IFT

d: The highlighted column in the bold face represents the lowest equilibrium IFT measured at the highest test pressure to be used in the linear regression and extrapolation for the MMP determination

Table 7.2 Measured seven equilibrium interfacial tensions (IFTs) at seven different test pressures in Test #2 (the dead light crude oil–CO_2 system, initial GOR of 3:1 in volume, T_{res} = 53.0°C) and determined minimum miscibility pressures (MMPs) from the vanishing interfacial tension (VIT) technique.

P (MPa)	5.7	6.7	7.8	8.4	9.1	9.5	**10.0**[d]
γ_{eq} (mJ/m^2)	11.53	9.26	6.58	5.04	3.77	3.40	**3.10**
R^2 [a]	–	1.000	0.999	0.999	0.998	0.992	**0.978**
δ [b] (nm)	–	2.312	2.435	2.575	1.809	1.021	**0.608**
VIT-MMP [c] (MPa)	–	10.7	10.6	10.5	10.6	10.8	**11.1**

Notes:

a: Linear correlation coefficient of each linear regression of the measured equilibrium IFT vs. test pressure date till the chosen test pressure

b: Interfacial thickness obtained from finite difference approximation of the negative derivative of the measured equilibrium IFTs with respect to the test pressure till the chosen test pressure

c: Determined MMP of the dead light crude oil–CO_2 system from the VIT technique by linearly extrapolating the measured equilibrium IFT vs. test pressure data till the chosen test pressure to zero IFT

d: The highlighted column in the bold face represents the lowest equilibrium IFT measured at the highest test pressure to be used in the linear regression and extrapolation for the MMP determination

Table 7.3 Measured eight equilibrium interfacial tensions (IFTs) at eight different test pressures in Test #3 (the dead light crude oil–CO_2 system, initial GOR of 10:1 in volume, T_{res} = 53.0°C) and determined minimum miscibility pressures (MMPs) from the vanishing interfacial tension (VIT) technique.

P (MPa)	4.0	4.5	5.6	6.5	7.6	8.6	9.1	**9.6**[d]
γ_{eq} (mJ/m^2)	15.02	14.15	12.09	10.22	7.39	5.01	4.22	**3.74**
R^{2} [a]	–	1.000	0.999	0.999	0.992	0.995	0.997	**0.989**
δ [b] (nm)	–	1.732	1.875	2.073	2.700	2.269	1.740	**0.872**
VIT-MMP [c] (MPa)	–	12.7	12.2	11.9	11.2	11.0	11.0	**11.1**

Notes:

a: Linear correlation coefficient of each linear regression of the measured equilibrium IFT vs. test pressure date till the chosen test pressure

b: Interfacial thickness obtained from finite difference approximation of the negative derivative of the measured equilibrium IFTs with respect to the test pressure till the chosen test pressure

c: Determined MMP of the dead light crude oil–CO_2 system from the VIT technique by linearly extrapolating the measured equilibrium IFT vs. test pressure data till the chosen test pressure to zero IFT

d: The highlighted column in the bold face represents the lowest equilibrium IFT measured at the highest test pressure to be used in the linear regression and extrapolation for the MMP determination

Table 7.4 Measured nine equilibrium interfacial tensions (IFTs) at nine different test pressures in Test #4 (the dead light crude oil–CO_2 system, initial GOR of 200:1 in volume, T_{res} = 53.0°C) and determined minimum miscibility pressures (MMPs) from the vanishing interfacial tension (VIT) technique.

P (MPa)	3.7	4.8	5.7	6.6	7.6	8.6	9.1	9.6	**10.5**[d]
γ_{eq} (mJ/m^2)	16.29	14.16	12.30	10.39	7.89	5.96	5.26	4.66	**4.35**
R^{2} [a]	–	1.000	0.999	0.999	0.998	0.999	0.999	0.996	**0.980**
δ [b] (nm)	–	1.906	2.181	2.123	2.387	1.930	1.558	1.085	**0.341**
VIT-MMP [c] (MPa)	–	12.2	11.8	11.6	11.3	11.4	11.5	11.6	**12.1**

Notes:

a: Linear correlation coefficient of each linear regression of the measured equilibrium IFT vs. test pressure date till the chosen test pressure

b: Interfacial thickness obtained from finite difference approximation of the negative derivative of the measured equilibrium IFTs with respect to the test pressure till the chosen test pressure

c: Determined MMP of the dead light crude oil–CO_2 system from the VIT technique by linearly extrapolating the measured equilibrium IFT vs. test pressure data till the chosen test pressure to zero IFT

d: The highlighted column in the bold face represents the lowest equilibrium IFT measured at the highest test pressure to be used in the linear regression and extrapolation for the MMP determination

Table 7.5 Measured twelve equilibrium interfacial tensions (IFTs) at twelve different test pressures in Test #5 (the dead light crude oil–CO_2 system, initial GOR of 4000:1 in volume, T_{res} = 53.0°C) and determined minimum miscibility pressures (MMPs) from the vanishing interfacial tension (VIT) technique and coreflood tests for the dead light crude oil–CO_2 system at the actual reservoir temperature of T_{res} = 53.0°C.

P (MPa)	3.5	4.5	5.5	6.5	7.5	8.5	9.0	9.5	10.5	**12.0**[e]	13.5	15.0
γ_{eq} (mJ/m^2)	19.31	17.37	14.00	12.12	9.67	7.31	6.62	5.91	4.77	**3.80**	3.78	3.30
R^2 [a]	–	1.000	0.995	0.997	0.993	0.996	0.995	0.994	0.996	**0.961**	0.913	0.871
δ [b] (nm)	–	1.939	3.365	1.883	2.453	2.355	1.380	1.416	1.148	**0.644**	0.014	0.320
VIT-MMP [c] (MPa)	–	13.5	10.9	11.3	11.4	11.5	11.7	11.8	12.2	**12.9**	13.9	19.1
Coreflood tests-MMP [d] (MPa)	12.4 – 12.9 [Zhang and Gu, 2015]											

Notes:
- a: Linear correlation coefficient of each linear regression of the measured equilibrium IFT vs. test pressure date till the chosen test pressure
- b: Interfacial thickness obtained from finite difference approximation of the negative derivative of the measured equilibrium IFTs with respect to the test pressure till the chosen test pressure
- c: Determined MMP of the dead light crude oil–CO_2 system from the VIT technique by linearly extrapolating the measured equilibrium IFT vs. test pressure data till the chosen test pressure to zero IFT
- d: Determined MMP of the dead light crude oil–CO_2 system from the coreflood tests
- e: The highlighted column in the bold face represents the lowest equilibrium IFT measured at the highest test pressure to be used in the linear regression and extrapolation for the MMP determination

Table 7.6 Measured twelve equilibrium interfacial tensions (IFTs) at twelve different test pressures in Test #6 (the live light crude oil–CO_2 system, initial GOR of 4000:1 in volume, T_{res} = 53.0°C) and determined minimum miscibility pressures (MMPs) from the vanishing interfacial tension (VIT) technique and slim-tube tests for the live light crude oil–CO_2 system at the actual reservoir temperature of T_{res} = 53.0°C.

P (MPa)	1.8	3.0	3.8	4.8	5.6	7.0	8.6	10.1	**11.4**[e]	15.0	16.6	18.1
γ_{eq} (mJ/m^2)	17.77	15.24	13.79	12.87	10.81	8.75	5.89	4.34	**4.04**	3.28	2.56	1.75
R^2 [a]	–	1.000	0.996	0.997	0.993	0.990	0.995	0.994	**0.982**	0.923	0.889	0.886
δ [b] (nm)	–	2.239	1.782	1.060	2.276	1.471	1.857	1.033	**0.217**	0.211	0.472	0.539
VIT-MMP [c] (MPa)	–	9.8	10.4	12.1	11.9	12.1	12.0	12.5	**13.2**	15.1	16.7	17.7
Slim-tube tests-MMP [d] (MPa)	15.2 – 15.4 [Zhang and Gu, 2015]											

Notes:
- a: Linear correlation coefficient of each linear regression of the measured equilibrium IFT vs. test pressure date till the chosen test pressure
- b: Interfacial thickness obtained from finite difference approximation of the negative derivative of the measured equilibrium IFTs with respect to the test pressure till the chosen test pressure
- c: Determined MMP of the live light crude oil–CO_2 system from the VIT technique by linearly extrapolating the measured equilibrium IFT vs. test pressure data till the chosen test pressure to zero IFT
- d: Determined MMP of the live light crude oil–CO_2 system from the slim-tube tests
- e: The highlighted column in the bold face represents the lowest equilibrium IFT measured at the highest test pressure to be used in the linear regression and extrapolation for the MMP determination

is determined to be 12.9 MPa from the VIT technique, which agrees well with 12.4–12.9 MPa from the coreflood tests [Zhang and Gu, 2015]. Hence, $R_c^2 = 0.990$ is proposed to be the critical value of the new quantitative LCC criterion for determining the MMP from the VIT technique. The MMP can be accurately determined from the measured equilibrium IFT vs. test pressure data once the LCC is smaller than $R_c^2 = 0.990$ for the first time.

As another important example, the measured equilibrium IFT vs. test pressure data and the calculated LCCs for Test #6 (the live light crude oil–CO_2 system, initial GOR of 4000:1 in volume, T_{res} = 53.0°C) are given in Table 7.6. In this case, the obtained LCCs are always larger than 0.990 until the linear regression is performed up to P = 11.4 MPa. It is for the first time that $R^2 = 0.982$ at this test pressure becomes smaller than $R_c^2 = 0.990$. Hence, the corresponding equilibrium IFT of 4.04 mJ/m^2 at P = 11.4 MPa becomes the lowest equilibrium IFT to be included in the linear regression and extrapolation for the MMP determination in Test #6. The corresponding MMP of the live light crude oil at the initial GOR of 4000:1 in volume and T_{res} = 53.0°C is determined to be 13.2 MPa from the VIT technique, which is much lower than 15.2–15.4 MPa from the slim-tube tests [Zhang and Gu, 2015]. It should be noted that in Test #6 with an extremely high initial GOR of 4000:1, no any oil phase was pre-injected into the IFT cell and saturated with CO_2 phase to reach an equilibrium state before the live light crude oil was introduced to form a pendant oil drop. In this special case, the live oil composition was solely represented by an extremely small pendant oil drop, which had a minimal but noticeable effect on the determined MMP, in comparison with the MMP of 12.9 MPa for

the dead light crude oil–CO_2 system. This is why such determined MMP of the live light crude oil–CO_2 system from the VIT technique is about 2 MPa lower than that from the slim-tube tests, in which the same live light crude oil was used to saturate the entire sand-packed slim tube.

7.2 Critical Interfacial Thickness (CIT) Criterion

In surface thermodynamics, the interfacial thickness (δ) is defined as the negative partial derivative of the measured interfacial tension (γ) with respect to the test pressure (P) at the constant temperature [Morrow, 1991], i.e., $\delta = -(\frac{\partial \gamma}{\partial P})_T$, though it can be estimated by using a variety of methods [Lekner and Henderson, 1978]. In this study, the interfacial thickness is obtained by using the forward finite difference approximation (FDA) of the negative partial derivative of the measured equilibrium IFT (γ_{eq}) vs. test pressure data, i.e., $\delta \approx -(\frac{\Delta \gamma_{eq}}{\Delta P})_T$. Such obtained interfacial thicknesses are listed in Tables 7.1–6 for Tests #1–6, respectively. For instance, the measured equilibrium IFT of the dead light crude oil–CO_2 system in Test #5 (the dead light crude oil–CO_2 system, initial GOR of 4000:1 in volume, T_{res} = 53.0°C) is reduced from 19.31 to 17.37 mJ/m^2 when the test pressure is increased from 3.5 to 4.5 MPa. Thus the interfacial thickness is determined to be $\delta = 1.939\,\text{nm}$ at P = 4.5 MPa. Such determined interfacial thicknesses at P = 4.5–15.0 MPa for Test #5 are listed and compared in Table 7.5. It is found that the interfacial thickness fluctuates considerably but is always larger than $\delta_c = 1.0\,\text{nm}$ until P = 12.0 MPa. Here, $\delta_c = 1.0\,\text{nm}$ is considered to be a critical interfacial thickness (CIT). At this pressure, the interfacial thickness is suddenly reduced to $\delta = 0.644\,\text{nm}$, which is

significantly lower than δ_c for the first time. As a result, the linear regression and extrapolation of the measured equilibrium IFT vs. test pressure data up to P = 12.0 MPa gives the same MMP of 12.9 MPa as that determined from the first new LCC criterion. The CIT of $\delta_c = 1.0$ nm is referred to as the second new quantitative criterion for determining the MMP from the VIT technique.

Similarly, the measured equilibrium IFT vs. test pressure data (γ_{eq} = 17.77–1.75 mJ/m^2 at P = 1.8–18.1 MPa) in Test #6 (the live light crude oil, initial GOR of 4000:1 in volume, T_{res} = 53.0°C) are used to calculate the interfacial thicknesses at different test pressures, which are given in Table 7.6. The interfacial thickness of $\delta = 0.217$ nm at P = 11.4 MPa is calculated to be much smaller than the CIT of $\delta_c = 1.0$ nm for the first time. Thus the MMP is determined to be 13.2 MPa for the live light crude oil–CO_2 system by applying the new CIT criterion from the VIT technique, which is the same as the MMP determined by applying the first new LCC criterion from the VIT technique and agrees fairly with 15.2–15.4 MPa from the slim-tube tests [Zhang and Gu, 2015]. Overall, the two new quantitative LCC and CIT technical criteria with R_c^2 = 0.990 and $\delta_c = 1.0$ nm are proposed and applied to determine the MMPs of the dead and live light crude oil–CO_2 systems from the VIT technique. Such determined MMPs are further compared with and verified by that for the former system from the coreflood tests and that for the latter system from the slim-tube tests, respectively.

In this work, $\delta_c = 1.0$ nm is considered to be the critical interfacial thickness (CIT) in developing the CIT criterion for determining the MMPs of the dead and live light crude oil–CO_2 systems from the VIT technique. This critical value needs some technical

discussion. In general, the hydrocarbons (HCs) are the dominated components (95–98 wt.%) of a light crude oil [McCain, 1990]. As a homologous series of the HCs, the alkane molecules (C_nH_{2n+2}) are often assumed to represent the HC molecules of the light crude oils due to their simple chemical structures. Based on the compositional analysis result of the dead light crude oil in Table 3.1 and its measured molecular weight of MW_{oil} = 212.1 g/mol, three typical alkanes of octane (C_8H_{18}), decane ($C_{10}H_{22}$), and octadecane ($C_{18}H_{38}$) are selected to represent the dead light crude oil. The molecular sizes of these three alkanes are calculated to be 1.0, 1.3, and 2.4 nm by using a predictive algorithm of B3LYP/6-31G* [Becke, 1988; Lee *et al*., 1988]. Obviously, the molecular size of each alkane is increased as the carbon number is increased, which is schematically shown in Figure 7.3. On the other hand, it is well known that the molecular size of CO_2 is equal to 0.33 nm [Breck, 1974].

In practice, any heptane plus alkanes are usually lumped altoghther as a plus pseudo-fraction (C_{7+}) and considered to be the intermediate HCs of the light crude oil [Whitson and Brule, 2000]. Hence, the dynamic multi-contact miscibility (MCM) occurs when the light and intermediate HCs of a crude oil and the CO_2 phase at the crude oil–CO_2 interface become miscible. In this case, the interfacial thickness will be approximately equal to the molecular sizes of these light and intermediate HCs (i.e., up to C_8H_{18}) and CO_2, which are close to 1.0 nm, keeping in mind that CO_2 molecular size of 0.33 nm is much smaller by comparison. Thus it is assumed that the dynamic MCM of the dead/live light crude oil–CO_2 system is developed and achieved once the interfacial thickness of the light crude oil–CO_2 mixture is smaller than the molecular size of 1.0 nm for octane (C_8H_{18}) for the first time. The MMP is determined from the measured equilibrium IFT vs.

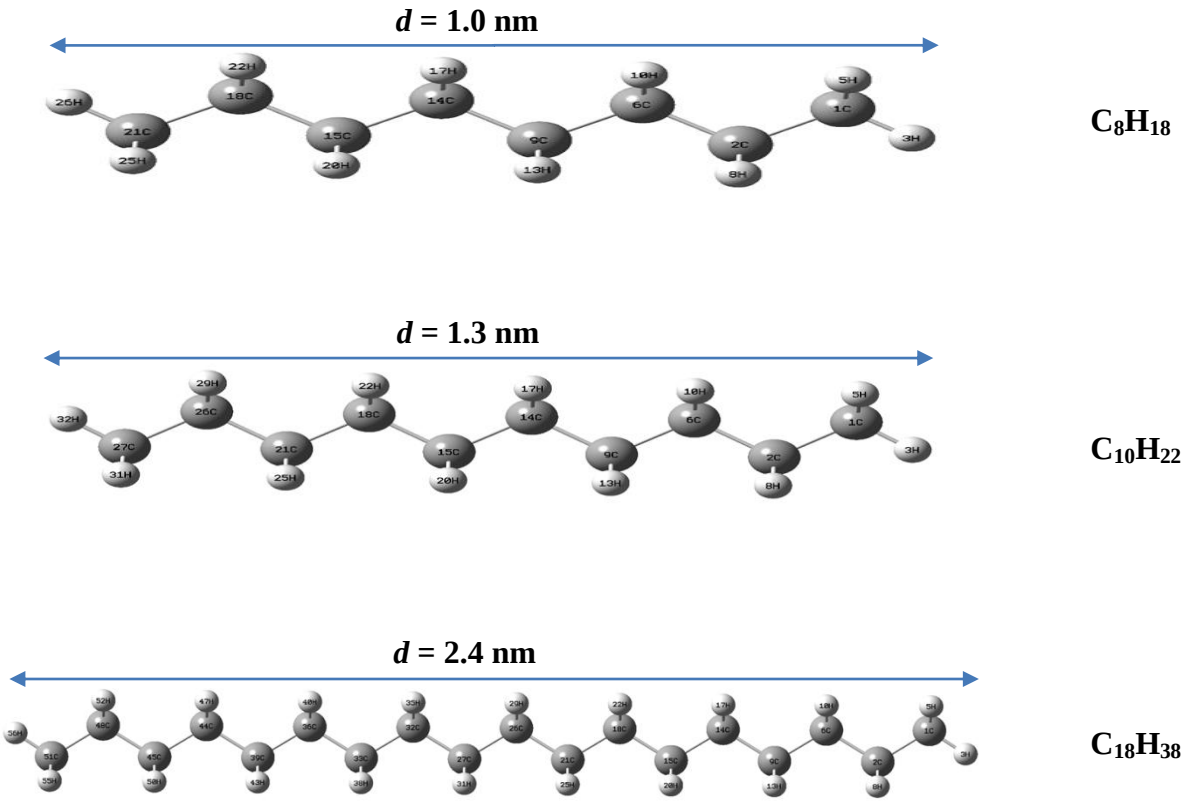

Figure 7.3 Molecular structures of octane (C_8H_{18}), decane ($C_{10}H_{22}$), and octadecane ($C_{18}H_{38}$) and their respective calculated molecular sizes of *d* = 1.0, 1.3, and 2.4 nm by using an predictive algorithm, B3LYP/6-31G∗ [Becke, 1988; Lee *et al.*, 1988].

test pressure data to the lowest IFT measured at the highest pressure, at which the corresponding interfacial thickness becomes smaller than the CIT (i.e., $\delta < \delta_c = 1.0\,\text{nm}$) for the first time. In this way, the CIT becomes the second new quantitative technical criterion for the MMP determinations from the VIT technique.

7.3 Initial vs. Equilibrium Interfacial Tensions (IFTs)

In this study, the initial IFT was measured by capturing the first one or two pendant oil drop images once the pendant oil drop surrounded by CO_2 was formed at the tip of the syringe needle inside the IFT cell. After approximately 30–60 min, the pendant oil drop and the surrounding CO_2 phase reached an equilibrium state, at which the former was completely saturated with the latter so that the equilibrium IFT was achieved. Figures 7.1a–e show the measured initial/equilibrium IFT vs. test pressure data of the dead light crude oil–CO_2 system at five different initial GORs of 1:1, 3:1, 10:1, 200:1, and 4000:1 in volume, respectively. It is found that the initial IFT is marginally higher than or equal to the equilibrium IFT at each test pressure. With the measured initial and equilibrium IFT vs. test pressure data (i.e., γ_{in} and γ_{eq} vs. P data), two respective MMP_{in} and MMP_{eq} are determined from the VIT technique by using the newly-proposed LCC and CIT criteria. These MMPs are included in Figures 7.1a–e and listed in Table 7.7 for comparison. In consideration of the experimental error of ±0.1 MPa for the MMP determination, such determined MMP_{in} and MMP_{eq} from each series of the dynamic IFT tests are almost the same. This is because the pendant oil drops used in the dynamic IFT tests are sufficiently small so that they can be completely saturated with CO_2 almost instantaneously. In this special case, it is accurate enough to use the initial IFT vs. test

Table 7.7 Summary of the determined minimum miscibility pressures (MMPs) of the dead and live light crude oil–CO_2 systems in six series of the dynamic interfacial tension (IFT) tests at five different initial gas–oil ratios (GORs) in volume and the actual reservoir temperature of T_{res} = 53.0°C.

Test no.	γ_{in} [a] (mJ/m^2)	MMP_{in} [b] (MPa)	γ_{eq} [c] (mJ/m^2)	MMP_{eq} [d] (MPa)
1	16.70–3.40	11.1	16.36–3.25	11.0
2	12.17–3.35	11.3	11.53–3.10	11.1
3	15.97–4.02	11.2	15.02–3.74	11.1
4	16.95–4.68	12.2	16.29–4.35	12.1
5	21.00–4.40	12.9	19.31–3.80	12.9
6	–	–	17.77–4.04	13.2

Notes:
a: Measured initial IFTs in the test pressure range
b: Determined MMP by linearly regressing and extrapolating the measured initial IFT vs. test pressure data to zero IFT
c: Measured equilibrium IFTs in the test pressure range
d: Determined MMP by linearly regressing and extrapolating the measured equilibrium IFT vs. test pressure data to zero IFT

pressure data that are measured at the beginning rather than the equilibrium IFT vs. test pressure data that have to be measured at the end to determine the MMP from the VIT technique.

7.4 Oil Composition Effect

In Figure 7.2, the measured equilibrium IFT vs. test pressure data for the live light crude oil–CO_2 system in Test #6 are shown and compared with those for the dead light crude oil–CO_2 system in Test #5 at the same initial GOR of 4000:1 in volume and T_{res} = 53.0°C. Although the measured equilibrium IFTs for the live light crude oil–CO_2 system are found to be always lower than those for the dead light crude oil–CO_2 system, the determined MMP of 13.2 MPa for the former system is slightly higher than 12.9 MPa for the latter system. In the live light crude oil–CO_2 system [Gu *et al*., 2013], pre-dissolution of the CH_4-dominated HC gas (66.50 mol.% CH_4 + 11.41 mol.% C_2H_6 + 11.39 mol.% C_3H_8 + 10.70 mol.% *n*-C_4H_{10}) into the dead light crude oil weakens the mutual interactions and prevents the miscibility development between the live light crude oil and the surrounding CO_2, which causes the MMP to be higher. Overall, the oil composition effect on the determined MMP is found to be minimal but measurable for the live light crude oil–CO_2 system. This is largely because in this study, the oil composition effect was solely represented by extremely small pendant oil drops ($V_{drop} \approx 12.375$ mm^3) in Tests #5 and #6 at the same extremely high initial GOR of 4000:1 in volume.

7.5 Initial Gas–Oil Ratio (GOR) Effect

The measured equilibrium IFT vs. test pressure data for the dead light crude oil–CO_2 system at five different initial GORs of 1:1, 3:1, 10:1, 200:1, 4000:1 in volume and T_{res} =

53.0°C are plotted in Figures 7.1a–e. Both the measured equilibrium IFTs and determined MMP at a lower initial GOR (e.g., 1:1 to 10:1 in volume) are found to be lower than those at a higher initial GOR (e.g., 200:1 and 4000:1 in volume). This is because at a low initial GOR, both the dead light crude oil and CO_2 phases are substantially modified due to the two-way mass-transfer processes, i.e., CO_2 dissolution into the dead light crude oil and light HCs extraction to the CO_2 phase. In this way, they become much similar so that their MCM can be easily reached and their MMP is low. The five MMPs determined at five different initial GORs from Figures 7.1a–e are further plotted and compared in Figure 7.4a to show the initial GOR effect on the determined MMP of the dead light crude oil–CO_2 system. It is found from this figure that the determined MMP remains almost the same (11.0–11.1 MPa) at the lower initial GORs of 1:1 to 10:1 in volume, whereas it is quickly increased to 12.1 or even 12.9 MPa as the initial GOR is increased to 200:1 or 4000:1 in volume. Therefore, the initial GOR effect on the determined MMP from the VIT technique is negligible in a lower initial GOR range of 1:1 to 10:1 in volume but becomes remarkable in a higher initial GOR range of 200:1 to 4000:1 in volume.

It is worthwhile to point out that in the VIT technique, the MMP is determined by linearly regressing and extrapolating the measured equilibrium IFT vs. test pressure data from a series of the dynamic IFT tests to zero IFT. Either the LCC or CIT criterion can be used to determine the lowest equilibrium IFT measured at the highest test pressure, which is to be included in the linear regression and extrapolation for the MMP determination. At a fixed initial GOR in volume, CO_2 concentration is increased but the oil concentration is decreased when the test pressure used in each dynamic IFT test is increased by adding

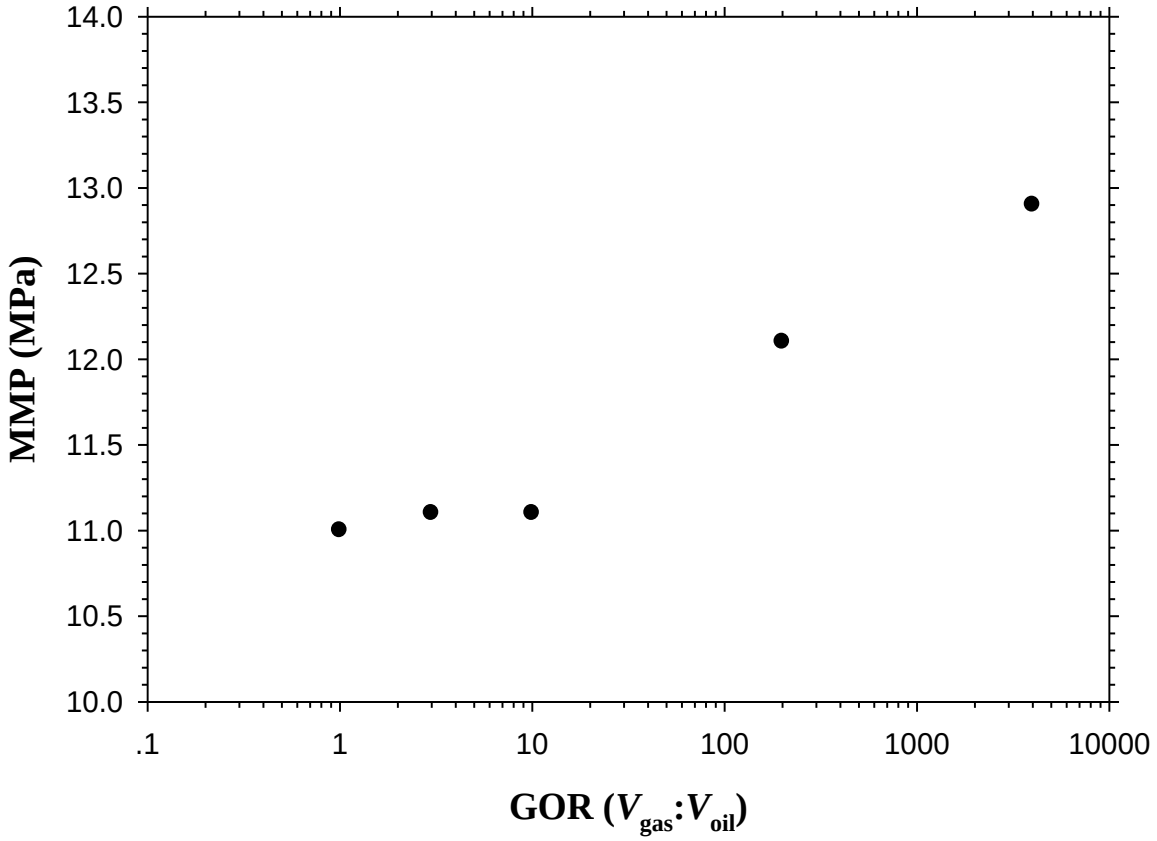

Figure 7.4(a) Measured minimum miscibility pressures (MMPs) of the dead light crude oil–CO_2 system in Tests #1–5 at five different initial gas–oil ratios (GORs) of 1:1, 3:1, 10:1, 200:1, 4000:1 in volume and the actual reservoir temperature of T_{res} = 53.0°C.

more CO_2 into the IFT cell. Hence, the MMP is determined from a series of the dynamic IFT tests at different test pressures so that CO_2 and oil concentrations change with the test pressure. The measured MMPs of the dead light crude oil–CO_2 system in Tests #1–5 with five fixed different GORs in volume or in five different CO_2 concentration ranges are further plotted in Figure 7.4b, where each CO_2 concentration range corresponds to different test pressures at each given initial GOR in volume. It is seen from this figure that at three lower initial GORs (1:1, 3:1, and 10:1 in volume) and correspondingly in a large CO_2 concentration range (31.76–94.69 mol.%), the determined MMP from the VIT technique remains virtually the same. At two higher initial GORs (200:1 and 4000:1 in volume) and correspondingly in an extremely small range of high CO_2 concentrations (98.79–99.99 mol.%), however, the determined MMPs are apparently higher. In the second case, the determined MMP of a crude oil–CO_2 system from the VIT technique strongly depends on the initial overall fluid composition [Ayirala and Rao, 2006b], i.e., the initial compositions of the gas and oil phases as well as the initial gas−oil ratio (GOR).

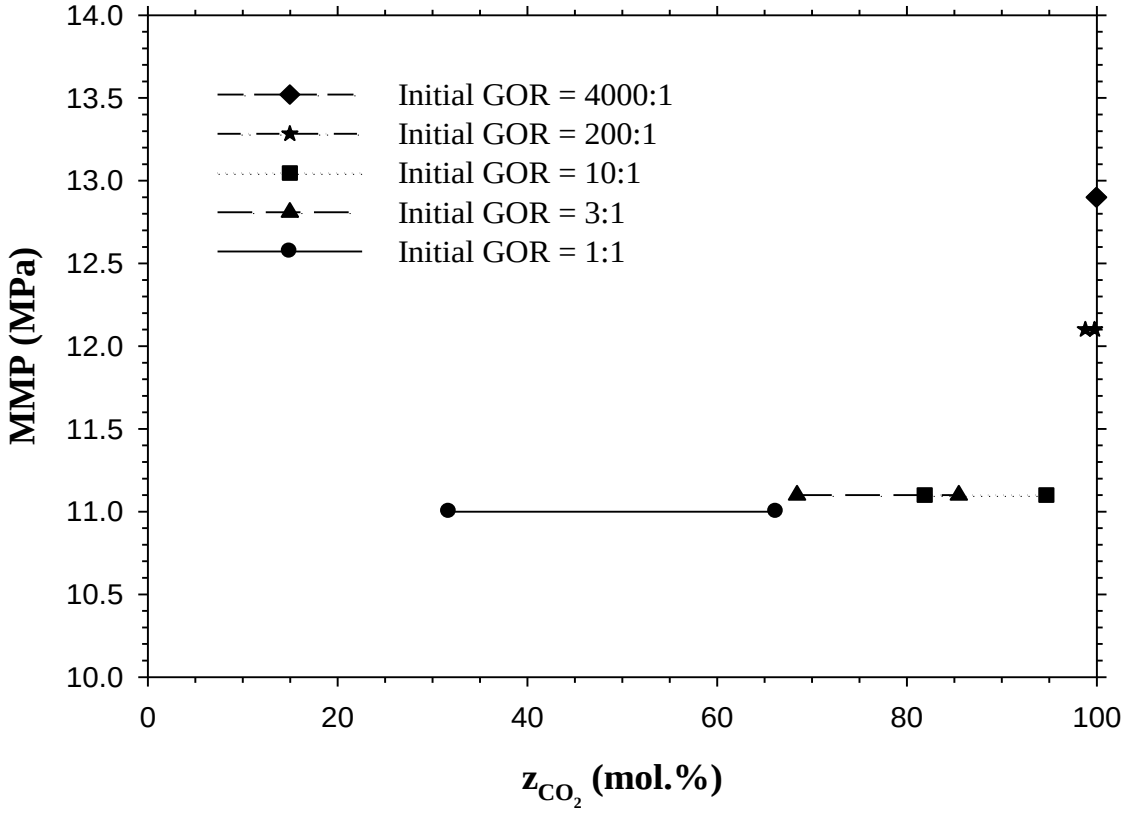

Figure 7.4(b) Measured minimum miscibility pressures (MMPs) of the dead light crude oil–CO_2 system in Tests #1–5 at the actual reservoir temperature of T_{res} = 53.0°C and in five different CO_2 concentration ranges, z_{CO_2} = 31.76–66.21, 68.41–85.46, 81.87–94.69, 98.79–99.77, and 99.93–99.99 mol.%, which correspond to different test pressure ranges at five different initial gas–oil ratios (GORs) of 1:1, 3:1, 10:1, 200:1, 4000:1 in volume, respectively.

CHAPTER 8 CONCLUSIONS AND RECOMMENDATIONS

8.1 Conclusions

In this study, one qualitative and several quantitative technical criteria are developed and applied to determine the minimum miscibility pressures (MMPs) from four experimental methods. The major conclusions that can be drawn from this study are listed as follows:

1. The oil recovery factor (ORF) and break-over pressure (BOP) quantitative criteria are examined and applied to determine the MMPs from the slim-tube and coreflood tests. One novel qualitative criterion, i.e., the bubble break-up (BBU), and four new quantitative criteria, i.e., the bubble-rising height (BRH) and bubble-rising velocity (BRV), the linear correlation coefficient (LCC) and critical interfacial thickness (CIT), are developed and used to determine the MMPs from the rising-bubble apparatus (RBA) tests and vanishing interfacial tension (VIT) technique, respectively.
2. It is found that different MMP ranges with respect to different threshold values or intersection options are obtained by applying different MMP determination criteria and/or regression methods from the slim-tube and coreflood tests, even though the same measured ORF vs. injection pressure data are used. Therefore, it is suggested that the MMP is better given in a small pressure range than specified as a definitive pressure value.
3. In terms of the ORF and BOP criteria, two MMP ranges of 15.2–15.4 MPa and 12.4–12.9 MPa at T_{res} = 53.0°C are determined from the five slim-tube tests for the live light crude oil–CO_2 system and the five coreflood tests for the dead light crude

oil–CO_2 system, respectively. The determined MMP ranges of these two light crude oil–CO_2 systems are significantly different.

4. The novel qualitative BBU criterion is used to interpret the miscibility developments and estimate the MMP ranges of 10.5–12.0 MPa and 23.0–24.0 MPa for the light crude oil–pure and impure CO_2 systems with the RBA, respectively. The BBU qualitative criterion is consistent with but better than the four existing qualitative criteria, i.e., the bubble shape, size, colour, and rising height. It is easy to be observed, relatively independent of the experimental factors and sensitive to the experimental conditions.
5. Two new quantitative criteria, i.e., the BRH and BRV, are applied to determine the MMP ranges of 11.7–12.4 MPa and 23.4–23.5 MPa at T_{res} = 53.0°C with the RBA for the light crude oil–pure and impure CO_2 (74.87 mol.% CO_2 + 25.13 mol.% CH_4) systems, respectively. As expected, the determined MMP range for the former system is significantly lower than that for the latter system.
6. With the measured equilibrium interfacial tension (IFT) vs. test pressure data, the MMP is determined from the VIT technique when the corresponding LCC is smaller than the critical value and/or the interfacial thickness becomes less than the CIT (i.e., $R^2 < R_c^2 = 0.990$ and/or $\delta < \delta_c = 1.0$ nm) for the first time.
7. Two new LCC and CIT technical criteria are used to determine the MMPs of the dead and live light crude oil–CO_2 systems from the VIT technique. Such determined respective MMPs of 12.9 and 13.2 MPa agree well with 12.4–12.9 MPa for the former system from the coreflood tests but poorly with 15.2–15.4 MPa for the latter system from the slim-tube tests.

8. The determined MMPs of the dead light crude oil–CO_2 system from the measured initial and equilibrium IFTs are found to be essentially the same. This is because the pendant oil drops used in the IFT tests are sufficiently small so that they can be completely saturated with CO_2 almost instantaneously.
9. The determined MMP of the live light crude oil–CO_2 system is slightly higher than that of the dead light crude oil–CO_2 system. The oil composition effect on the determined MMP from the VIT technique is measureable but minimal because sufficiently small pendant oil drops and the extremely high initial GOR in volume are used in the dynamic IFT tests.
10. It is found that at lower initial GORs (1:1, 3:1, and 10:1 in volume) or correspondingly in a large CO_2 concentration range (31.76–94.69 mol.%), the determined MMP remains almost the same and the initial GOR effect is negligible. At higher initial GORs (200:1 and 4000:1 in volume) or correspondingly in an extremely small range of high CO_2 concentrations (98.79–99.99 mol.%), however, the determined MMPs are significantly higher and the initial GOR effect becomes remarkable.

8.2 Recommendations

1. Four experimental methods, i.e., the slim-tube tests, coreflood tests, RBA, and VIT technique, can be applied to determine the MMP of a given light crude oil–CO_2 system. The miscibility developments in these four experimental methods and their determined MMPs need to be further studied and better understood.
2. Visualization method (e.g., X-ray scanning) can be applied to visualize the

miscibility developments in the slim-tube and/or coreflood tests. In addition, the produced oils and gases obtained in each slim-tube and/or coreflood tests can be analyzed to study the crude oil and gas composition changes with the miscibility developments and then compare the experimental data of the dead and live light crude oil–CO_2 systems.

3. A smaller test pressure interval can be chosen for conducting the RBA tests in order to make the qualitative criteria more accurate for the MMP determinations. In addition, a mathematical model can be formulated to study the CO_2-bubble size and colour changes with the miscibility development.
4. More series of the dynamic IFT tests for various light crude oil–CO_2 systems can be conducted in order to test the newly-developed LCC and CIT technical criteria for the MMP determinations. On the other hand, molecular simulations or some microscopic chemistry tests of the crude oil–CO_2 interface can be undertaken to further understand the critical interfacial thickness.
5. It is found that at low initial GORs (1:1–10:1 in volume) or in a large CO_2 concentration range (31.76–94.69 mol.%), the initial GOR effect is negligible on the MMP determination. Thus a lower initial GOR in volume is suggested for the future dynamic IFT tests by pre-injecting a certain amount of oil into the bottom of the IFT cell in order to minimize the initial GOR effect on the MMP determination.
6. A comprehensive predictive model needs to be developed for estimating the MMPs of different light crude oil–CO_2 systems. Such estimated MMPs can be compared with and verified by those determined from four different experimental methods, i.e., the slim-tube and coreflood tests, RBA, and VIT technique.

REFERENCES

ABI/INFORM Global. EOR/Heavy Oil Survey: Miscible CO_2 Continues to Eclipse Steam in US EOR Production. Oil & Gas J., 112 (4), 78–79, 2012.

Ali, S. M., Thomas, S. The Promises and Problems of Enhanced Oil Recovery Methods. J. Can. Pet. Technol., 35 (7), 57–63, 1996.

Al-Mjeni, R., John van Wunnik, S. A. P. C., Edwards, J., Felber, B. J., Gurpinar, O., Miller, G. J. H. C., Jackson, C., Kristensen, M. R., Lim, F., Ramamoorthy, R. Has the Time Come for EOR? Oil Review, 22 (4), 16–35, 2010.

Aycaguer, A. C., Lev-On, M., Winer, A. M. Reducing Carbon Dioxide Emissions with Enhanced Oil Recovery Projects: A Life Cycle Assessment Approach. Energy & Fuels, 15 (2), 303–308, 2001.

Ayirala, S. C., Rao, D. N. Comparative Evaluation of a New MMP Determination Technique. Paper SPE 99606, presented at the SPE/DOE symposium on Improved Oil Recovery, Tulsa, OK, April 22–26, 2006a.

Ayirala, S. C., Rao, D. N. A New Mechanistic Parachor Model to Predict Dynamic Interfacial Tension and Miscibility in Multicomponent Hydrocarbon Systems. J. Colloid Interface Sci., 299 (1), 321–331, 2006b.

Ayirala, S. C., Rao, D. N. Comparative Evaluation of a New Gas–Oil Miscibility Determination Technique. J. Can. Pet. Technol., 50 (9–10), 71–81, 2011.

Becke, A. D. Density-Functional Exchange-Energy Approximation with Correct Asymptotic Behaviour. Phys. Rev. A, 38 (6), 3098–3100, 1988.

Breck, D. W. Zeolite Molecular Sieves: Structure, Chemistry, and Use. John Wiley & Sons, Inc., New York, 1974.

Brock, W. R., Bryan, L. A. Summary Results of CO_2 EOR Field Tests, 1972–1987. Paper SPE 18977, presented at the SPE Joint Rocky Mountain Regional/Low-Permeability Reservoirs Symposium and Exhibition, Denver, CO, March 6–8, 1989.

Cao, M. Oil Recovery Mechanisms and Asphaltene Precipitation Phenomenon in CO_2 Flooding Processes. MASc. Thesis, University of Regina, 2012.

Cao, M., Gu, Y. Physicochemical Characterization of Produced Oils and Gases in Immiscible and Miscible CO_2 Flooding Processes. Energy & Fuels, 27 (1), 440–453, 2013.

Cheng, P., Li, D., Boruvka, L., Rotenberg, Y., Neumann, A. W. Automation of Axisymmetric Drop Shape Analysis for Measurements of Interfacial Tensions and Contact Angles. Colloid Surf., 43 (2), 151–167, 1990.

Christensen, J. R., Stenby, E. H., Skauge, A. Review of WAG Field Experience. SPE Res. Eval. & Eng., 4 (2), 97–106, 2001.

Christiansen, R. L., Haines, H. K. Rapid Measurement of Minimum Miscibility Pressure with the Rising-Bubble Apparatus. SPE Res. Eng., 2 (4), 523–527, 1987.

Christiansen, R. L., Kim, H. Apparatus and Method for Determining the Minimum Miscibility Pressure of a Gas in a Liquid. United States Patent No. 4627273, December 9, 1986.

Chung, F. T. H., Jones, R. A., Burchfield, T. E. Recovery of Viscous Oil under High Pressure by CO_2 Displacement: A Laboratory Study. Paper SPE 17588, presented at

the SPE International Meeting on Petroleum Engineering, Tianjin, China, November 1–4, 1988.

Deffrene, P., Marle, C., Pacsirszky, J., Jeantet, M. La Determination des Pressions de Miscibilite. Revue IFP16, n6, 1961.

Dong, M., Huang, S. S., Dyer, S. B., Mourits, F. M. A Comparison of CO_2 Minimum Miscibility Pressure Determinations for Weyburn Crude Oil. J. Pet. Sci. Eng., 31 (1), 13–22, 2001.

Dong, M., Huang, S. S., Srivastava, R. K. Effect of Solution Gas in Oil on CO_2 Minimum Miscibility Pressure. J. Can. Pet. Technol., 39 (11), 53–61, 2000.

Duncan, G. Enhanced Recovery Engineering: Part 1, World Oil. 215 (9), 95–100, 1994.

Ekundayo, J. M., Ghedan, S. G. Minimum Miscibility Pressure Measurement with Slim Tube Apparatus-How Unique is the Value? Paper SPE 165966, presented at the SPE Reservoir Characterization and Simulation Conference and Exhibition, Abu Dhabi, UAE, September 16–18, 2013.

Elsharkawy, A. M., Poettmann, F. H., Christiansen, R. L. Measuring CO_2 Minimum Miscibility Pressures: Slim-Tube or Rising-Bubble Method? Energy & Fuels, 10 (2), 443–449, 1996.

Escrochi, M., Mehranbod, N., Ayatollahi, S. The Gas–Oil Interfacial Behaviour during Gas Injection into an Asphaltenic Oil Recovery. J. Chem. Eng. Data, 58 (9), 2513–2526, 2013.

Fazlali, A., Nikookar, M., Agha–Aminiha, A., Mohammadi, A. H. Prediction of Minimum

Miscibility Pressure in Oil Reservoirs Using A Modified SAFT Equation of State. Fuel, 108 (6), 675–681, 2013.

Fazlali, A., Nikookar, M., Mohammadi, A. H. Computational Procedure for Determination of Minimum Miscibility Pressure of Reservoir Oil. Fuel, 106 (4), 707–711, 2013.

Flock, D. L., Nouar, A. Parametric Analysis on the Determination of the Minimum Miscibility Pressure in Slim Tube Displacements. J. Can. Pet. Technol., 23 (5), 80–88, 1984.

Folden, C. G. Enhanced Recovery of Light and Medium Crude Oil in Canada. J. Can. Pet. Technol., 26 (1), 37–43, 1987.

Gardner, J. W., Orr, Jr. F. M., Patel, P. D. The Effect of Phase Behaviour on CO_2 Flood Displacement Efficiency. J. Pet. Technol., 33 (11), 2067–2081, 1981.

Godec, M. L., Kuuskraa, V. A., Leeuwen, T. V., Melzer, L. S., Wildgust, N. CO_2 Storage in Depleted Oil Fields: The Worldwide Potential for Carbon Dioxide Enhanced Oil Recovery. Energy Procedia, 4 (2), 2162–2169, 2011.

Green, D. W., Willhite, G. P. Enhanced Oil Recovery, Textbook Series, Vol. 6, SPE, Richardson, TX, 1998.

Grigg, R. B. Dynamic Phase Composition, Density, and Viscosity Measurements during CO_2 Displacement of Reservoir Oil. Paper SPE 28974, presented at the SPE International Symposium on Oil Field Chemistry, San Antonio, TX, February 14–17, 1995.

Gu, Y., Hou, P., Luo, W. Effects of Four Important Factors on the Measured Minimum

Miscibility Pressure and First-Contact Miscibility Pressure. J. Chem. Eng. Data, 58 (5), 1361−1370, 2013.

Høier, L., Whitson, C. H. Miscibility Variation in Compositionally Grading Reservoirs. SPE Res. Eval. & Eng., 4 (1), 36−43, 2001.

Holm, L. W., Josendal, V. A. Mechanisms of Oil Displacement by Carbon Dioxide. J. Pet. Technol., 26 (12), 1427–1436, 1974.

Holm, L. W., Josendal, V. A. Effect of Oil Composition on Miscible Type Displacement by Carbon Dioxide. SPE J., 22 (1), 87–98, 1982.

Huang, E. T. S. The Effect of Oil Composition and Asphaltene Content on CO_2 Displacement. Paper SPE 24131, presented at the SPE/DOE Eighth Symposium on Enhanced Oil Recovery, Tulsa, OK, April 22−24, 1992.

Huang, S. S., Dyer, S. B. Miscible Displacement in the Weyburn Reservoir: A Laboratory Study. J. Can. Pet. Technol., 32 (7), 42–52, 1993.

Hutchinson, C. A., Braun, Jr. R. T. Phase Relations of Miscible Displacement in Oil Recovery. AIChE J., 7 (1), 64–72, 1961.

Jaubert, J. N., Arras, L. Properly Defining the Classical Vapourizing and Condensing Mechanisms When a Gas Is Injected into a Crude Oil. Ind. Eng. Chem. Res., 37 (12), 4860–4869, 1998.

Jerauld, G. R. A Case Study in Scaleup for Multicontact Miscible Hydrocarbon Gas Injection. SPE Res. Eval. & Eng., 1 (6), 575–582, 1998.

Jessen, K., Michelsen, M. L., Stenby, E. H. Global Approach for Calculation of Minimum

Miscibility Pressure. Fluid Phase Equilibr., 153 (2), 251–263, 1998.

Jessen, K., Orr, Jr. F. M. On Interfacial-Tension Measurements to Estimate Minimum Miscibility Pressures. SPE Res. Eval. & Eng., 11 (5), 933–939, 2008.

Johns, R. T., Fayers, F. J., Orr, Jr. F. M. Effect of Gas Enrichment and Dispersion on Nearly Miscible Displacements in Condensing/Vapourizing Drives. SPE Advanced Technology Series, 2 (2), 26–34, 1994.

Koottungal, L. 2012 Worldwide EOR Survey. Oil & Gas J., 110 (4), 57–69, 2012.

Kuuskraa, V. A. QC Updates Carbon Dioxide Projects in OGJ's Enhanced Oil Recovery Survey. Oil & Gas J., 110 (7), 72–77, 2012.

Lee, C., Yang, W., Parr, R. G. Development of the Colle–Salvetti Correlation-Energy Formula into a Functional of the Electron Density. Phys. Rev. B, 37 (2), 785–789, 1988.

Lekner, J., Henderson, J. R. Theoretical Determination of the Thickness of a Liquid–Vapour Interface. Physica A: Statistical Mechanics and Its Applications, 94 (3–4), 545–558, 1978.

Li, Z. Optimum Timing for CO_2-EOR after Waterflooding and Soaking Effect on Miscible CO_2 Flooding in a Tight Sandstone Formation. MASc. Thesis, University of Regina, 2014.

Martin, D. F., Taber, J. J. Carbon Dioxide Flooding. J. Pet. Technol., 44 (4), 396–400, 1992.

McCain, W. D. The Properties of Petroleum Fluids. PennWell Books, Tulsa, OK, 1990.

Mihcakan, M., Poettmann, F. H. Minimum Miscibility Pressure, Rising-Bubble

Apparatus, and Phase Behavior. Paper SPE/DOE 27815, presented at the SPE/DOE Improved Oil Recovery symposium, Tulsa, OK, April 17–20, 1994.

Monroe, W. W., Silva, M. K., Larson, L. L., Orr, Jr. F. M. Compositional Paths in Four-Component Systems: Effect of Dissolved Methane on 1-D CO_2 Flood Performance. SPE Res. Eng., 5 (3), 423–432, 1990.

Moritis, G. Special Report: EOR/Heavy Oil Survey. Oil & Gas J., 104 (17), 37–57, 2006.

Morrow, N. R. Interfacial Phenomena in Petroleum Recovery. Surfactant Science Series, Vol. 36, CRC Press, 1991.

Mungan, N. Carbon Dioxide Flooding–Fundamentals. J. Can. Pet. Technol., 20 (1), 87–92, 1981.

Naseri, A., GhareSheikhloo, A. A., Kamari, A., Hemmati–Sarapardeh, A., Mohammadi, A. H. Experimental Measurement of Equilibrium Interfacial Tension of Enriched Miscible Gas–Crude Oil Systems. J. Mol. Liq., 211 (11), 63–70, 2015.

Novosad, Z., Costain, T. G. New Interpretation of Recovery Mechanisms in Enriched Gas Drives. J. Can. Pet. Technol., 27 (2), 54–60, 1988.

Novosad, Z., Costain, T. G. Mechanisms of Miscibility Development in Hydrocarbon Gas Drive: New Interpretation. SPE Res. Eng., 4 (3), 341–347, 1989.

Orr, Jr. F. M., Jessen, K. An Analysis of the Vanishing Interfacial Tension Technique for Determining of Minimum Miscibility Pressure. Fluid Phase Equilib., 255 (2), 99–109, 2007.

Orr, Jr. F. M., Silva, M. K., Lien, C. L., Pelletier, M. T. Laboratory Experiments to

Evaluate Field Prospects for CO_2 Flooding. J. Pet. Technol., 34 (4), 888–898, 1982.

Peng, D. Y., Robinson, D. B. A New Two-Constant Equation of State. Ind. Eng. Chem. Fundam., 15 (1), 58–64, 1976.

Poettmann, F. H., Christiansen, R. L., Mihcakan, M. Discussion of Methodology for the Specification of Solvent Blends for Miscible Enriched-Gas Drives. SPE Res. Eng., 7 (1), 154–156, 1992.

Pyo, K., Damian-Diaz, N., Powell, M., van Nieuwkerk, J. CO_2 Flooding in Joffre Viking Pool. Paper CIPC 2003-109, presented at the Petroleum Society's Canadian International Petroleum Conference, Calgary, Alberta, June 10–12, 2003.

Randall, T. E., Bennion, D. B. Laboratory Factors Influencing Slim-Tube Test Results. J. Can. Pet. Technol., 28 (4), 60–70, 1989.

Rao, D. N. A New Technique of Vanishing Interfacial Tension for Miscibility Determination. Fluid Phase Equilib., 139 (1–2), 311–324, 1997.

Rao, D. N., Lee, J. I. Application of the New Vanishing Interfacial Tension Technique to Evaluate Miscibility Conditions for the Terra Nova Offshore Project. J. Pet. Sci. Eng., 35 (1), 247–262, 2002.

Rao, D. N., Lee, J. I. Determination of Gas–Oil Miscibility Conditions by Interfacial Tension Measurements. J Colloid Interface Sci., 262 (2), 474–482, 2003.

Shokrollahi, A., Arabloo, M., Gharagheizi, F., Mohammadi, A. H. Intelligent Model for Prediction of CO_2–Reservoir Oil Minimum Miscibility Pressure. Fuel, 112 (10), 375–384, 2013.

Sibbald, L. R., Novosad, Z., Costain, T. G. Methodology for the Specification of Solvent Blends for Miscible Enriched-Gas Drives. SPE Res. Eng., 6 (3), 373–378, 1991.

Simon, R., Graue, D. J. Generalized Correlations for Predicting Solubility, Swelling and Viscosity Behaviour of Crude Oil–CO_2 Systems. J. Pet. Technol., 17 (1), 102–106, 1965.

Srivastava, R. K., Huang, S. S. Technical Feasibility of CO_2 Flooding in Weyburn Reservoir–A Laboratory Investigation. J. Can. Pet. Technol., 36 (10), 48–55, 1997.

Srivastava, R. K., Huang, S. S. New Interpretation Technique for Determining Minimum Miscibility Pressure by Rising-Bubble Apparatus for Enriched-Gas Drives. Paper SPE 39566, presented at the SPE India Oil and Gas Conference and Exhibition, New Delhi, India, February 17−19, 1998.

Srivastava, R. K., Huang, S. S., Dong, M. Laboratory Investigation of Weyburn CO_2 Miscible Flooding. J. Can. Pet. Technol., 39 (2), 41–51, 2000.

Stalkup, F. I. Miscible Flooding, SPE Monograph Series, Vol. 8, SPE, Richardson, TX, 1983.

Teklu, T. W., Alharthy, N., Kazemi, H., Yin, X., Graves, R. M., AlSumaiti, A. M. Phase Behavior and Minimum Miscibility Pressure in Nanopores. SPE Res. Eval. & Eng., 17 (3), 396–403, 2014.

Thomas, F. B., Zhou, X. L., Bennion, D. B., Bennion, D. W. A Comparative Study of RBA, P–X, Multicontact and Slim-Tube Results. J. Can. Pet. Technol., 33 (2), 17–26, 1994.

Torabi, F., Firouz, A. Q., Kavousi, A., Asghari, K. Comparative Evaluation of Immiscible,

Near Miscible and Miscible CO_2 Huff-n-Puff to Enhance Oil Recovery from a Single Matrix–Fracture System (Experimental and Simulation Studies). Fuel, 93 (3), 443–453, 2012.

Wang, Y., Orr, Jr. F. M. Analytical Calculation of Minimum Miscibility Pressure. Fluid Phase Equilibr., 139 (1–2), 101–124, 1997.

Wang, X., Zhang, S., Gu, Y. Four Important Onset Pressures for Mutual Interactions between Each of Three Crude Oils and CO_2. J. Chem. Eng. Data, 55 (10), 4390–4398, 2010.

Watkins, G. C., Sharp, K. C. Enhanced Oil Recovery: Retrospect and Prospect. J. Can. Pet. Technol., 24 (1), 61–63, 1985.

Whitson, C. H., Brule, M. R. Phase Behaviour, SPE Monograph Series, Vol. 20, SPE, Richardson, TX, 2000.

Whittaker, S., White, D., Law, D., Chalaturnyk, R. IEA GHG Weyburn CO_2 Monitoring & Storage Project Summary Report 2000–2004, Petroleum Technology Research Centre, Regina, 2004.

Whorotn, L. P., Brownscombe, E. R. United States Patent No. 2623596, December 30, 1952.

Wu, R. S., Batycky, J. P. Evaluation of Miscibility from Slim Tube Tests. J. Can. Pet. Technol., 29 (6), 63–70, 1990.

Yang, D., Gu, Y. Interfacial Interactions between Crude Oil and CO_2 under Reservoir Conditions. Pet. Sci. Technol., 23 (9), 1099–1112, 2005.

Yellig, W. F., Metcalfe, R. S. Determination and Prediction of CO_2 Minimum Miscibility Pressures. J. Pet. Technol., 32 (1), 160–168, 1980.

Zhang, K., Gu, Y. Two Different Technical Criteria for Determining the Minimum Miscibility Pressures (MMPs) from the Slim-Tube and Coreflood Tests. Fuel, 161 (12), 146–156, 2015.

Zhang, K., Gu, Y. New Qualitative and Quantitative Technical Criteria for Determining the Minimum Miscibility Pressures (MMPs) with the Rising-Bubble Apparatus (RBA). Fuel, 175 (7), 172–181, 2016a.

Zhang, K., Gu, Y. Two New Quantitative Technical Criteria for Determining the Minimum Miscibility Pressures (MMPs) from the Vanishing Interfacial Tension (VIT) Technique. Fuel, MS ID: JFUE-D-16-00870, submitted on March 23, 2016b.

Zhang, S., She, Y., Gu, Y. Evaluation of Polymers as Direct Thickeners for CO_2 Enhanced Oil Recovery. J. Chem. Eng. Data, 56 (4), 1069–1079, 2011.

Zhou, D., Orr, Jr. F. M. An Analysis of Rising-Bubble Experiments to Determine Minimum Miscibility Pressures. SPE J., 3 (1), 19–25, 1998.

Zick, A. A. A Combined Condensing/Vapourzing Mechanism in the Displacement of Oil by Enriched Gases. Paper SPE 15493, presented at the SPE 61st Annual Technical Conference and Exhibition, New Orleans, LA, October 5–8, 1986.